HELSINKI UNIVERSITY OF TECHNOLOGY
Faculty of Electronics, Communications and Automation
Department of Radio Science and Engineering

Janne Ilvonen

Isolated antenna structures of mobile terminals

Thesis submitted in partial fulfillment for the degree of Master of Science
in Espoo _____.____,2009

Supervisor

Professor Pertti Vainikainen

Instructor

Lic.Sc. (Tech.) Jari Holopainen

HELSINKI UNIVERSITY OF TECHNOLOGY

ABSTRACT OF THE MASTER'S THESIS

Author:	Janne Ilvonen		
Name of the Thesis:	Isolated antenna structures of mobile terminals		
Date:	August 16, 2009	**Number of pages:**	98
Faculty:	Electronics, Communications and Automation		
Department:	Radio Science and Engineering		
Supervisor:	Professor Pertti Vainikainen		
Instructor:	Lic.Sc. (Tech.) Jari Holopainen		

In this master's thesis the feasibility of isolated antenna structures in the mobile terminal environment has been investigated. It has also been studied if the effect of the user could be reduced with the isolated antenna structures compared to the traditional antenna structures.

In today's mobile terminals with internal antenna elements the chassis or PCB of the mobile terminal is used as a radiator and the antenna element mainly creates the antenna resonance and couples currents to the chassis. Especially at lower UHF frequencies, below 1 GHz, a significant portion of the power is radiated by the chassis. In these structures the effect of the user's hand is remarkable since the hand of the user in the vicinity of the chassis changes the matching and decreases the radiation efficiency. One method to reduce the effect of the user might be to isolate the antenna from the chassis.

In this work, as the chassis of the mobile terminal is not used significantly as a radiator and the antenna structure should be as small as possible, we have to allow narrower impedance bandwidth than in traditional mobile terminals. In this thesis the bandwidth of ca. 2% is used as the bandwidth requirement for the isolated antenna structures and it is assumed that an efficient center frequency tuning method is available.

The feasibility of such isolated antenna structures has been studied by simulations at GSM 900 and 1800 bands. Also the specific absorption rate (SAR), hearing-aid compatibility (HAC) and the user effect on matching and radiation efficiency were simulated. Some promising isolated antenna structures, like a small bow-tie, have been found. Isolated antenna structures suit best for higher UHF frequencies, over 1.8 GHz, where the 2% bandwidth is easy to achieve and SAR values are lower. Here certain isolated structures are shown to increase the radiation efficiency with hand compared to the traditional antenna structures and the user effect on matching is very small in these cases. The isolated antenna structures can also be used to decrease the near field values on the HAC plane.

The drawbacks of the isolated antenna structures are associated with lower GSM frequencies; a large antenna structure is needed if multi-band operation is required and high SAR values are common. Here also the performance of the antenna can be deteriorated substantially if the user's fingers or palm cover the whole antenna structure.

Keywords: isolated antenna, mobile terminal antenna, bandwidth, specific absorption rate (SAR), hearing aid compatibility (HAC), effect of user

TEKNILLINEN KORKEAKOULU

DIPLOMITYÖN TIIVISTELMÄ

Tekijä:	Janne Ilvonen		
Työn nimi:	Matkapuhelimien isoloidut antennirakenteet		
Päivämäärä:	16. elokuuta 2009	**Sivumäärä:**	98
Tiedekunta:	Elektroniikan, tietoliikenteen ja automaation tiedekunta		
Laitos:	Radiotieteen ja -tekniikan laitos		
Työn valvoja:	Professori Pertti Vainikainen		
Työn ohjaaja:	TkL Jari Holopainen		

Tässä diplomityössä tutkittiin isoloitujen antennirakenteiden soveltuvuutta matkapuhelinympäristössä. Työssä tutkittiin myös voidaanko isoloiduilla antennirakenteilla pienentää käyttäjän vaikutusta verrattuna perinteisiin matkapuhelimen antennirakenteisiin.

Nykyisillä sisäisellä antennielementillä varustetuilla matkapuhelimilla runkoa tai piirilevyä käytetään säteilijänä ja antennielementillä luodaan resonanssitaajuus ja kytketään virtoja runkoon. Erityisesti matalilla, alle 1 GHz UHF-taajuuksilla, matkapuhelimen runko toimii pääsäteilijänä ja tällaisissa rakenteissa käyttäjän käden vaikutus on erityisen suuri. Käyttäjän käsi muuttaa antennin sovitusta ja laskee säteilyhyötysuhdetta. Eräs tapa pienentää käyttäjän vaikutusta saattaisi olla erottaa antennirakenne puhelimen rungosta.

Tässä työssä antennirakenteelta vaadittavaa kaistanleveyttä on pienennetty verrattuna perinteisiin antenneihin, koska isoloiduissa rakenteissa puhelimen runkoa ei käytetä merkittävästi hyväksi ja koska antennin tulisi olla mahdollisimman pieni. Työssä antennilta vaaditaan ainoastaan 2 %:n kaistanleveys ja oletetaan, että on olemassa tehokas menetelmä keskitaajuuden virittämiseen.

Antennirakenteiden soveltuvuutta matkapuhelimiin tutkittiin simuloinneilla. Myös ominaisabsorptionopeutta (SAR), kuulolaitteiden yhteensopivuutta (HAC) ja käyttäjän vaikutusta sovitukseen ja säteilyhyötysuhteeseen on tutkittu simuloinneilla. Joitakin lupaavia antennirakenteita, kuten pieni rusettiantenni, on löydetty. Työn tulokset osoittavat, että isoloidut antennirakenteet soveltuvat parhaiten korkeammille UHF-taajuuksille, jossa riittävä 2 % kaistanleveys on helppo saavuttaa ja SAR-arvot ovat pienemmät. Täällä useimmilla isoloiduilla rakenteilla säteilyhyötysuhde käden kanssa on suurempi ja käyttäjän vaikutus sovitukseen pienempi kuin perinteisillä matkapuhelinantenneilla. Isoloiduilla antenneilla voidaan myös pienentää huomattavasti lähikenttäarvoja kuulokkeen kohdalla ja siten parantaa HAC suoritusta.

Isoloitujen antennirakenteiden haitat tulevat esille matalilla GSM-taajuuksilla, jolloin antennirakenteista tulee isokokoisia, jos vaaditaan monikaistaista toimintaa ja SAR-arvot ovat korkeat. Täällä myös isoloidun antennin toiminta huononee merkittävästi jos käyttäjän sormet tai kämmen peittävät koko antennirakenteen.

Avainsanat: isoloitu antenni, matkapuhelinantenni, kaistanleveys, ominaisabsorptionopeus (SAR), kuulolaitteiden yhteensopivuus (HAC), käyttäjän vaikutus

Preface

This master's thesis has been prepared at the Department of Radio Science and Engineering of Helsinki University of Technology during January 2009 - July 2009.

At first, I would like to thank the supervisor of this thesis, professor Pertti Vainikainen for excellent ideas and guidance. I would also like to thank him for giving me an opportunity to work with this interesting thesis subject.

My special thanks belong to my instructor and workmate, Lic.Sc. (Tech.) Jari Holopainen, for his constructive comments and suggestions related to the thesis. He had always time for my questions concerned for example the quality factor or the simulation tools.

I would like to thank Risto Valkonen for his Matlab code and for helping me with the LaTeXword processing tool. Outi Kivekäs deserves special thanks for giving valuable comments and ideas. I would also like to thank Clemens Icheln for giving me help with the simulation tools. And of course I would like to thank the whole personnel in the Radio Laboratory for a comfortable working atmosphere.

My parents, Ritva and Jouko deserve thanks for supporting and encouraging my studies.

Finally, I would like to thank my loving and caring fiancée Katriina for her support and patience during the work. Also my children Maria and Heikki deserve a big hug.

Espoo, August 16, 2009

Janne Ilvonen

Contents

List of abbreviations

ANSI	American National Standards Institute
AWF	Articulation Weighting Factor
Balun	Balanced to unbalanced transformer
BBB	Blood-Brain Barrier
BW	Bandwidth
CCE	Capacitive Coupling Element
CDMA	Code Division Multiple Access
Ci(x)	Cosine integral function
DVB-H	Digital Video Broadcast - Handheld
E-GSM	Extended Global System of Mobile Communications
EMC	Electromagnetic Compatibility
FDTD	Finite Difference Time Domain method
FET	Field-Effect Transistor
GaAs	Gallium Arsenide
GPS	Global Positioning System
GSM	Global System of Mobile Communications
HAC	Hearing Aid Compatibility
ICNIRP	International Commission on Non-Ionizing Radiation Protection
IEEE	Institute of Electrical and Electronics Engineers
MEMS	Microelectromechanical Systems
MoM	Method of Moments
PCB	Printed Circuit Board
PEC	Perfect Electric Conductor
PIFA	Planar Inverted-F Antenna
RF	Radio Frequency
RMS	Root Mean Square
SAM	Standard Anthropomorphic Model
SAR	Specific Absorption Rate
SEM	Scanning Electron Microscopy

TDMA	Time Division Multiple Access
TKK	Helsinki University of Technology
TRx	Transceiver
UHF	Ultra High Frequency (300 - 3000 MHz)
UMTS	Universal Mobile Telephone System
VSWR	Voltage Standing Wave Ratio
WCDMA	Wideband Code Division Multiple Access
WLAN	Wireless Local Area Network

List of symbols

Symbol	Meaning
A	area of a loop
a	radius of a sphere
a_0	radius of a wire
B_r	relative impedance bandwidth
$B_{r,cc}$	relative impedance bandwidth with critically coupled antenna
$B_{r,oc}$	relative impedance bandwidth with optimally overcoupled antenna
BW	bandwidth
C_0	mutual capacitance
c	speed of light
D	largest dimension of an antenna
D_a	directivity of antenna
d	gap between two microstrip
E	electrical field strength
E_{rms}	root mean square value of the electric field strength
f_c	center frequency
f_{high}	upper limit of frequency band
f_{low}	lower limit of frequency band
f_r	resonant frequency
G	conductance
G_a	gain of antenna
$G_{realized}$	realized gain of antenna
H	magnetic field strength
I	current
j	imaginary unit
k	wave number
L	inductance
L_P	power loss
L_{refl}	reflection loss

L_{retn}	return loss
l	length of a chassis
P_{in}	accepted power
P_l	lost power
P_r	Radiated power
P_{rad}	radiated power
p	radiation power factor
Q	quality factor
Q_0	unloaded quality factor
Q_c	quality factor for conductivity losses
Q_d	quality factor for dielectric losses
Q_e	external quality factor
Q_l	loaded quality factor
Q_{rad}	radiation quality factor
$Q_{rad,min}$	fundamental lowest limit of radiation quality factor
R	resistance
R_a	resistive part of antenna impedance
R_{loss}	conduction and dielectric losses
R_r	radiation resistance
r_1	near field distance
r_2	far field distance
S	maximum allowed value of $VSWR$
S_{11}	reflection coefficient
SAR	specific absorption rate
T	coupling coefficient
T_{opt}	optimal value of coupling coefficient
TE	a transversal electric field wavemode
TM	a transversal magnetic field wavemode
V	voltage
$VSWR$	voltage standing wave ratio
W	energy
W_e	average stored electric energy
W_m	average stored magnetic energy
w_1	wide of microstrip line 1
w_2	wide of microstrip line 2
X_a	reactive part of antenna impedance
Y_0	characteristic admittance
Y_{in}	input admittance
Z_0	impedance of a feed line
Z_a	impedance of an antenna structure

Z_{in}	input impedance
Z_L	impedance of a load
Z_{out}	impedance at output
β	wave number
ϵ_0	permittivity in free space
ϵ_r	relative permittivity
η	efficiency
η_m	matching efficiency
η_{rad}	radiation efficiency
η_{tot}	total efficiency
η_{wave}	wave impedance in free space
λ	wavelength
λ_0	wavelength in free space
ω_r	angular resonant frequency
ρ	reflection coefficient
ρ_{in}	reflection coefficient at input
ρ_d	density of tissue
ρ_L	load reflection coefficient
σ	conductivity
σ_d	conductivity of tissue

CHAPTER 1

Introduction

Nowadays, a typical mobile terminal should operate in all existing mobile systems and thus quad-band functionality is required. There are also increasing amount of different radio systems, e.g. digital television (DVB-H), GPS, Bluetooth and WLAN, that should also be included in mobile terminals. In the near future, mobile terminals have probably still increasing amount of radio systems while the space reserved for the antennas is decreasing. This means that the evaluation of the effect of the user is becoming more and more important.

It is shown in [1] that, especially at lower UHF frequencies, below 1 GHz, a significant portion of the power is radiated by the chassis or PCB in today's mobile terminal with internal antenna element. The internal antenna element (e.g. PIFA) mainly creates the antenna resonance and couples currents to the chassis. In these structures the effect of the user is remarkable since the hand of the user located in the vicinity of the chassis changes the matching and decreases the radiation efficiency. One method to reduce the user effect may be to isolate the antenna from the chassis. The isolated antenna structure gives the possibility to shape the mobile terminal more freely since the chassis is not needed. This feature can also be used to design a general antenna element that can be included in several devices with a lower cost.

The goal of this work is to investigate the feasibility of such isolated antenna structures in the mobile terminal environment. Also in this work it is considered how the effect of the user can be reduced with isolated antenna structures compared to traditional unbalanced antenna structures. Two different isolated structures are investigated: 1) galvanically isolated structures where the chassis of the mobile terminal and the ground of the antenna structure are isolated and 2) balanced structures where antenna structures do not need a separate ground plane to work. The investigated antenna types are the following: wire antenna, helix antenna, bow-tie antenna and capacitive coupling element (CCE) antenna.

The chassis of the mobile terminal is not used significantly as a radiator and thus the isolated antenna structures are larger than traditional antenna elements (such as PIFAs or coupling elements) with a given bandwidth. Thus we have to allow narrower bandwidth to keep the size of the antenna structure small enough to fit inside a mobile terminal and therefore some tuning or switching method is needed. The small antenna has a strong correlation between the antenna size, efficiency and impedance bandwidth and it is not possible to maximize all of them at the same time. In this work the quality factor has a very significant role since when dealing with small antennas the quality factor defines the bandwidth of an antenna, and thus a comprehensive study is being made. We assume in this work that an efficient switching method is available and to mention some, the Micro-Electro-Mechanical-Systems (MEMS) is a promising technique to perform wideband tuning. In this work the bandwidth of 2% is used as the bandwidth requirement for the isolated antenna structures.

This thesis is organized as follows. The basic theory on small antennas and their most important performance parameters such as radiation efficiency, impedance bandwidth and quality factor are introduced in Chapter 2. Also some isolated antenna structures are discussed. In Chapter 3 the isolated antenna structures in the mobile terminals are studied. The achievable bandwidth potentials are studied using two different methods: 1) calculating first the quality factor of the antenna structure to get the bandwidth potential and 2) calculating all possible matching circuit topologies with a single resonant LC-circuit to get the bandwidth potential directly. Also the radiation patterns of the different balanced antenna structures are simulated. The most promising structures based on these results are studied further in Chapter 4. Chapter 4 concentrates on the user interaction of the isolated antenna structures. The effect of the user is studied and the specific absorption rate (SAR) and hearing-aid compatibility (HAC) have been simulated and compared to the requirements. Finally, Chapter 5 is for summary and conclusions.

CHAPTER 2

The available bandwidth and structures of small antennas

Any piece of conductive material works as an antenna at any frequency if the conductive material can be matched and coupled to a transceiver (TRx) . The available bandwidth of an antenna depends on its electrical size and thus in small antennas very good matching can be achieved only across a narrow impedance bandwidth. Inherently narrow bandwidth is one of the main features of small antennas and it is also one of the main aspects to be discussed in this chapter.

In the following, radiation regions, antenna parameters, and theoretical calculations related to the impedance bandwidth of small antennas are represented. Also some balanced antenna structures, such as a dipole, and bandwidth enhancement methods are discussed.

2.1 Basics of radiation regions

An antenna can be defined as a device that transmits electromagnetic field into the surrounding space or respectively receives an electromagnetic field from the surrounding space. For an electrically large antenna ($D > \lambda$) the generated field can be divided into three regions. These three regions are the reactive near field, the radiating near field and the far field, as shown in Figure 2.1. There are no strict distances where each region starts and ends and the distances depend on the structure and the electrical length of the antenna, [2], [3], [4].

The reactive near field is the region closest to the antenna, wherein the reactive field predominates. It is not possible to use approximate equations to calculate the E and

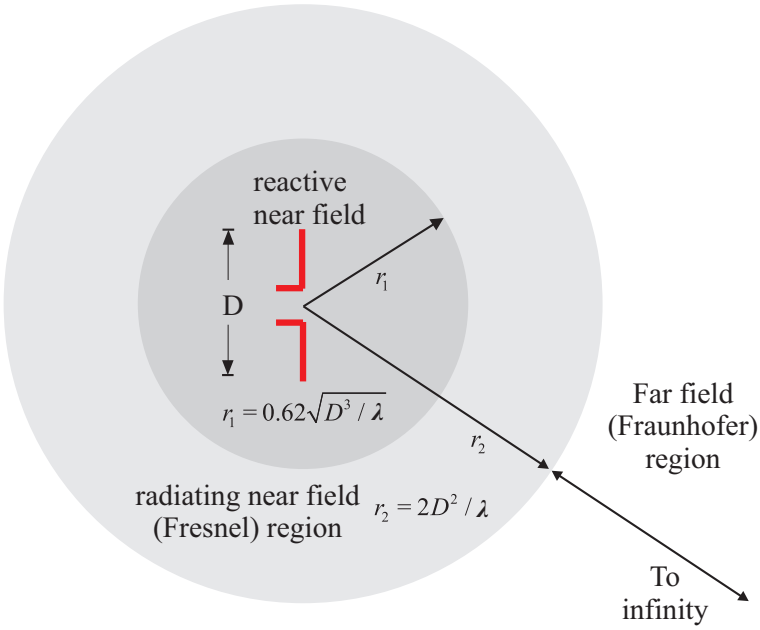

Figure 2.1: Radiation regions of an electrically large antenna [2].

the H fields. The reactive near fields need to be calculated based on the Maxwell's equations [4].

The reactive near field is not radiating but when moving away from the antenna at a certain distance r_1 the reactive and the radiating energies become equally strong. This distance r_1 determines the border of the reactive and the radiating near fields for most antennas [2], [4]:

$$r_1 < \sqrt{\frac{2D^3}{3\sqrt{3}\lambda}} \approx 0.62\sqrt{\frac{D^3}{\lambda}}, \tag{2.1}$$

where λ is the wavelength and D is the largest dimension of the antenna. In the radiating near field, also called the Fresnel region, the radiation fields predominate and the field pattern depends on the distance from the antenna. At a certain distance r_2 the angular field distribution is essentially independent of the distance from the antenna. This distance r_2 determines the border of the radiating near field and the far field, also called the Fraunhofer region [2], [4]:

$$r_2 = \frac{2D^2}{\lambda}. \tag{2.2}$$

These preceding definitions are valid when an antenna is electrically large ($D > \lambda$). When an antenna is electrically small, the approximate outer edge of the reactive near field is given by:

$$r_1 \leq \frac{\lambda}{2\pi}. \tag{2.3}$$

This is also the definition of an electrically small antenna, which means that the antenna can be enclosed inside a sphere of radius r_1 [5]. Later in this chapter, fundamental limitations of small antennas are discussed.

2.2 Small antenna as a resonator

A structure that has a natural capability to resonate and thus has a certain resonant frequency is called a resonator. The general definition of the quality factor is used to describe the ability of the resonator to store energy within one cycle and can be defined as [6], [7]

$$Q = \frac{\omega_r W}{P} = \frac{\omega_r (W_e + W_m)}{P}, \tag{2.4}$$

where $\omega_r = 2\pi f$ is angular resonant frequency, W is total time-average energy stored in the system, W_e is the time-average stored electric energy, W_m is the time-average stored magnetic energy, and P is the time-average of the dissipated power. In most applications of this definition, the Q is evaluated at the resonant frequency. In this case the Q can be expressed as [6]

$$Q = \frac{2\omega_r W_i}{P}, \tag{2.5}$$

where W_i is the time-average energy stored either in electric or magnetic field. At the resonance frequency, ω_r, there are equal amounts of stored electric and magnetic energy ($W_e = W_m$). This definition is equivalent to that of Equation (2.4) at the resonant frequency. For a non-resonant antenna, it is indirectly assumed that the antenna system should be tuned to the resonance. The resonance is achieved by adding a capacitive or inductive energy storage element depending on whether the stored energy is predominantly magnetic or electric. When an antenna is electrically small, according to the definition in Equation (2.3), the resonator theory can be applied to describe the performance of small antennas [8].

Different quality factors can be defined and next some important quality factors are presented when dealing with small antennas. The quality factor in (2.4) is a so-called unloaded quality factor Q_0 and it describes the internal power losses of the resonator. With most small antennas, the internal quality factor Q_0 can be divided into three

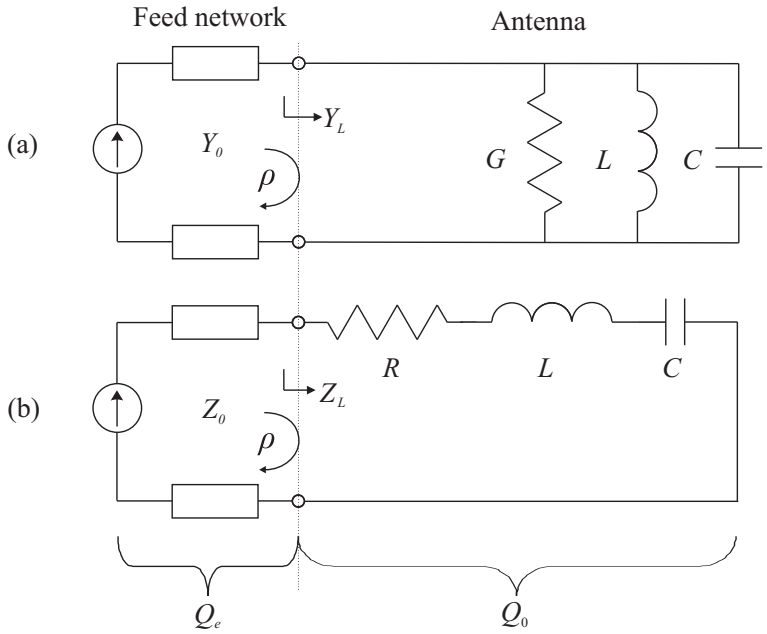

Figure 2.2: a) Equivalent circuit for a parallel resonator antenna. b) Equivalent circuit for a series resonator antenna.

quality factors that are the radiation guality factor Q_{rad}, conductor quality factor Q_c, and dielectric quality factor Q_d and they have a connection as follows [7]

$$\frac{1}{Q_0} = \frac{1}{Q_{rad}} + \frac{1}{Q_c} + \frac{1}{Q_d}. \tag{2.6}$$

When a resonator (here an antenna) is connected to the external circuit, e.g. to the transceiver (TRx), also the external circuit must be taken into consideration, as shown in Figure 2.2. The loaded quality factor can be written

$$\frac{1}{Q_l} = \frac{1}{Q_0} + \frac{1}{Q_e}, \tag{2.7}$$

where the external quality factor Q_e represents the losses of the circuit outside the resonator. It also means that the unloaded quality factor needs to be measured indirectly because a measurement cannot be done without connecting the resonator to an external network.

2.3 Antenna parameters

In general, the performance of the antennas is described by radiation quantities like gain and radiation pattern. The application defines which qualities are the most important [7].

For small antennas circuit characteristics are very important. These characteristics define the impedance bandwidth and total efficiency of the antenna. Also the dimensions of the antenna are very important when mobile terminal antennas are designed. Actually one has to make a compromise between the bandwidth, radiation efficiency, and size since they are interrelated. Next, some important antenna parameters are introduced.

2.3.1 Reflection coefficient and impedance bandwidth

An antenna can be seen as a load, whose impedance consists of resistive R and reactive X parts, according to Equation (2.8) and Figure 2.2 b). The reactance consists of capacitive and inductive parts and when those parts cancel each other, the antenna appears purely resistive and the antenna is said to be in resonance. At the resonant frequency, the antenna usually, but not always, accepts the largest amount of power and the resistance is a combination of the radiation resistance R_r and the loss resistance R_{loss} [4]. The capacitive and inductive reactances of the antenna are determined by its physical properties, like dimensions, and the environment where it is located.

$$Z_L = R + \mathrm{j}\omega L + \frac{1}{\mathrm{j}\omega C} = R + \mathrm{j}(\omega L - \frac{1}{\omega C}) = R + \mathrm{j}X. \tag{2.8}$$

$$R = R_r + R_{loss}. \tag{2.9}$$

In practice, the impedance Z_L of an antenna differs from the characteristic impedance Z_0 of the feed line, and a part of the voltage is reflected back from the load. The reflection coefficient ρ can be calculated from [7] (see Figure 2.2 b)):

$$\rho = \frac{Z_L - Z_0}{Z_L + Z_0}. \tag{2.10}$$

and it is often denoted equal with the scattering parameter S_{11}. The load is perfectly matched i.e $\rho = 0$, when Z_L and Z_0 are equal. Typically antennas are not perfectly matched and a slight mismatch needs to be accepted to get maximum impedance bandwidth [9].

The voltage standing wave ratio $VSWR$ defines the ratio between the maximum and the minimum voltages along a transmission line and it can be calculated from the absolute value of the reflection coefficient [7]

$$VSWR = \frac{1 + |\rho|}{1 - |\rho|}. \tag{2.11}$$

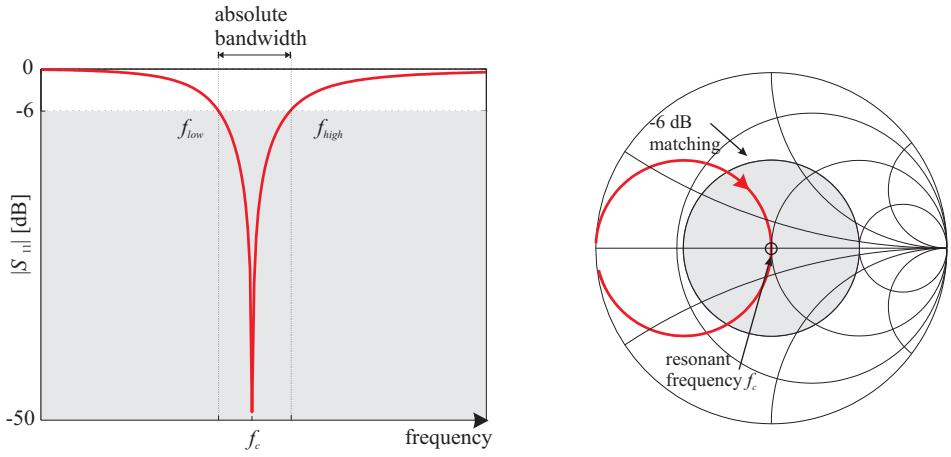

Figure 2.3: Impedance of an antenna a) in the Cartesian coordinate system and b) in the Smith chart. At the resonant frequency reactances cancel each other and the antenna is purely resistive.

The return loss describes the ratio between the incident and the reflected power in decibels [7]

$$L_{retn} = 10 \log \frac{1}{|\rho|^2}. \tag{2.12}$$

An often used matching criterion for mobile terminal antennas is to have return loss L_{retn} $\geq$ 6 dB [10] within the frequency band (presented in Figure 2.3). The corresponding values for the voltage standing wave ratio $VSWR \leq 3$ and the reflection coefficient $|\rho|$ = $|S_{11}| \leq$ -6 dB.

Above the absolute impedance bandwidth was discussed. The relative bandwidth can be determined as follows;

$$B_r = \frac{f_{high} - f_{low}}{f_c}, \tag{2.13}$$

where f_{high} - f_{low} defines the absolute impedance bandwidth, where a certain matching criterion $VSWR \leq S$ is valid, and f_c is the center frequency. The relative impedance bandwidth is often denoted as a percentage value. In Figure 2.3, the impedance bandwidth is defined according to the absolute value of the reflection coefficient.

For a resonator, the impedance bandwidth can be calculated also using the equivalent circuit model presented in Figure 2.2 a). It can be shown that the relative bandwidth B_r and the unloaded quality factor Q_0 have a relation [9]:

$$B_r = \frac{1}{Q_0}\sqrt{\frac{(TS-1)(S-T)}{S}}, \tag{2.14}$$

where $T = Y_0/G$ is the coupling factor for a parallel resonator antenna. The largest bandwidth is achieved when the coupling factor T is [9]

$$T_{opt} = \frac{1}{2}\left(S + \frac{1}{S}\right), \tag{2.15}$$

which is called the optimal overcoupling. The corresponding bandwidth $B_{r,oc}$ can be calculated from

$$B_{r,oc} = \frac{1}{2Q_0}\left(S - \frac{1}{S}\right). \tag{2.16}$$

When the antenna is perfectly matched, the coupling factor is $T = 1$ since $Y_L = Y_0$, and in that case the antenna is said to be critically coupled. The corresponding bandwidth $B_{r,cc}$ can be calculated from

$$B_{r,cc} = \frac{1}{Q_0}\frac{S-1}{\sqrt{S}}. \tag{2.17}$$

2.3.2 Efficiency, directivity and gain

The total antenna efficiency η_{tot} is a product of the radiation efficiency η_{rad} and the matching efficiency η_m [2], [3], [8].

$$\eta_{tot} = \eta_{rad}\eta_m, \tag{2.18}$$

where η_m can be calculated as follow η_m = 1-$|\rho|^2$. The antenna structure losses are caused by resistive losses. The antenna radiation efficiency can be calculated as

$$\eta_{rad} = \frac{R_r}{R_r + R_{loss}}, \tag{2.19}$$

where R_r represents the radiation losses and R_{loss} represents the ohmic losses in the antenna structure. The radiation efficiency can be also defined as the ratio between the radiated power P_{rad} and the power accepted by the antenna P_{in} and it is also related to the quality factors as follows:

$$\eta_{rad} = \frac{P_{rad}}{P_{in}} = \frac{Q_0}{Q_{rad}}. \tag{2.20}$$

It can be seen from Equation (2.14) that if T and S are fixed to some level, the relative bandwidth B_r can be increased by decreasing the unloaded quality factor Q_0. The quality factor can be decreased e.g. by increasing the internal losses of the antenna. As can be seen from Equation (2.20), if the unloaded quality factor Q_0 is decreased (Q_{rad} is constant), also the radiation efficiency η_{rad} decreases. The price paid for the increased bandwidth is the decreased efficiency.

The gain of an antenna depends on the directivity and the efficiency of an antenna [2]. In an ideal case, the antenna gain G_a and the directivity D_a are equal but in practice the dielectric and the conductive losses decrease the gain. The radiation efficiency η_{rad} of the antenna also determines the dependency of the antenna gain G_a and the directivity D_a as follows [7], [11]:

$$G_a = \eta_{rad} D_a. \tag{2.21}$$

In practice in small antennas, the matching losses are significant and thus they need to be taken into account. The realized gain $G_{realized}$ can be calculated from [11]:

$$G_{realized} = \eta_{tot} D_a = \eta_{rad} \eta_m D_a. \tag{2.22}$$

2.4 Theoretical calculation of quality factor

The quality factor has a very significant role when dealing with small antennas. In this thesis, a comprehensive study to the quality factor is made mainly because of two reasons: firstly because the quality factor gives a good tool to estimate the bandwidth of a small antenna and therefore needs to be introduced properly. Secondly it is over 60 years when Wheeler published the first theoretical attempt to describe the fundamental limit of the electrically small antennas. There has been some progress until these days to describe the fundamental limit of $Q_{rad,min}$ and therefore it is important to sum up the present stage of the fundamental limit of the quality factor. First in this section the historical aspects of the quality factor are discussed and finally some latest approximation methods to estimate the quality factor are introduced.

2.4.1 History of quality factor

One of the first theoretical attempts to quantify small antennas was made by Harold A. Wheeler in 1947. Wheeler's definition for a small antenna was: "the small antenna to be considered is one whose maximum dimension is less than the radianlength", where the radianlength is $1/2\pi$ wavelength. This is the same definition as given earlier in Equation (2.3). Wheeler introduced the term "radiation power factor", defined as [5]

$$p = \frac{1}{6\pi}\frac{\text{volume of antenna}}{\text{radianlength}^3} \approx \frac{\text{radiation resistance of antenna}}{\text{reactance of antenna}}. \tag{2.23}$$

Wheeler defined that the radiation power factor p is the fundamental limitation for the bandwidth and the practical efficiency of a small antenna. The radiation power factor p depends only on the ratio of the volumes of the antenna and that of the cube defined by the radianlength, so it depends only on the frequency and the dimensions of an antenna.

The radiation power factor p can be expressed also in a more common way using the radiation quality factor Q_{rad} and the wave number $k_0 = 2\pi/\lambda_0$, where the radianlength is $1/k_0$:

$$Q_{rad}^{-1} = p = \frac{4\pi^2}{3\lambda^3} \cdot Vol, \tag{2.24}$$

where Vol is the cylindrical volume occupied by the antenna [1].

Wheeler showed that when the size of the antenna decreases, the radiation resistance decreases relative to the ohmic losses in both the antenna and the matching circuit and therefore decreases the overall system efficiency as well. Wheeler demonstrated that the matching of a small antenna can be done efficiently for a narrow impedance bandwidth but a wider bandwidth requires the decrease of the total efficiency.

A year later, in 1948 Chu derived an approximate lower limit for the radiation quality factor of an electrically small antenna [12]. He defined the minimum radiation $Q_{rad,min}$ that can be obtained for an omni-directional antenna that fits inside a sphere of radius $a = \lambda_0/2\pi$:

$$Q_{rad,min} = \text{Larger of}\left\{\frac{2\omega W_e}{P_{rad}}, \frac{2\omega W_m}{P_{rad}}\right\}, \tag{2.25}$$

where W_e and W_m are the time average, nonpropagating, stored electric and magnetic energies beyond the input terminals, ω is the radian frequency, and P_{rad} represents the

[1] Wheeler used the cylindrical volume instead of the spherical volume because that is the only shape that can alternatively be occupied by either a capacitor or an inductor. The antenna is assumed to operate as a lumped circuit element.

total radiated power of the antenna. Chu concluded that an antenna which generates a field outside the sphere corresponding to the infinitesimally small dipole has the smallest Q of all antennas.

Much later in 1960, Harrington continued Chu's work and made a theoretical analysis of the effects of antenna size on parameters such as gain, bandwidth, and efficiency [13]. The Chu-Harrington's limit of $Q_{rad,min}$ for linearly polarized waves can be written:

$$Q_{rad,min} = \frac{1 + 3k^2a^2}{k^3a^3(1 + k^2a^2)}. \tag{2.26}$$

When both a TM mode and a TE mode are equally excited, the value of Q_{rad} is halved. An electrically small dipole antenna exhibits the TM mode whereas an electrically small loop antenna exhibits the TE mode. The approximation for Equation (2.26) when $ka << 1$ can be written:

$$Q_{rad,min} \approx \frac{1}{k^3a^3}. \tag{2.27}$$

In 1964, Collin published a general method to evaluate the Q of an antenna. The $Q_{rad,min}$ of the antenna is calculated by subtracting the energy density of the radiating field from the energy density of the total field [14]. The first spherical mode of Q_{rad}, can be written for the linearly polarized waves as:

$$Q_{rad,min} \approx \frac{1}{k^3a^3} + \frac{1}{ka}. \tag{2.28}$$

The result in Equation (2.28) was different than Chu-Harrington's limit in Equation (2.26). The problem in evaluating the Q_{rad} of an antenna exists when calculating the field radiated by the antenna. That field consists of the radiating field carrying the power to infinity and the localized reactive near field, as shown in Figure 2.1. It is not possible to treat those fields as separate fields and the approximate results depend on how the above-mentioned difficulties are solved.

McLean derived in 1996 an exact method, which was more straightforward than those previously published [15]. McLean wanted to re-examine the fundamental limit of $Q_{rad,min}$ with a different concept than the other. McLean calculated the radiation Q_{rad} directly from the fields of the TM_{01} spherical mode and showed that the electric and magnetic energies can be calculated independently of each other. McLean found an algebraic error from the Chu's limit of Q_{rad} in Equation (2.26)[2]. McLean assumed like

[2] The Chu-Harrington's limit corrected later by McLean [15]: $Q_{rad} = \frac{1+2k^2a^2}{k^3a^3(1+k^2a^2)}$;

The original uncorrected Chu-Harrington's limit [13]: $Q_{rad} = \frac{1+3k^2a^2}{k^3a^3(1+k^2a^2)}$.

Chu, that the antenna radiates only one mode, in this case the $n = 1$ spherical mode. An exact expression for Q_{rad} and the linearly polarized waves can be written as:

$$Q_{rad,min} = \frac{1 + 2k^2a^2}{k^3a^3(1 + k^2a^2)} = \frac{1}{k^3a^3} + \frac{1}{ka(1 + k^2a^2)}. \tag{2.29}$$

If $ka << 1$ this can be approximated

$$Q_{rad,min} \approx \frac{1}{k^3a^3} + \frac{1}{ka}. \tag{2.30}$$

The minimum Q_{rad} for the case when both a TM mode and a TE mode are excited can be written as:

$$Q_{rad,min} = \frac{1}{2}\left[\frac{1}{k^3a^3} + \frac{2}{ka}\right]. \tag{2.31}$$

Equation (2.30) is exactly the same as the Collin's limit in Equation (2.28) but calculated in a different way.

McLean's definition gives the fundamental limit of $Q_{rad,min}$ and it is not possible to reach that limit in practice. There are several reasons why it is so. For example: 1) the definition of $Q_{rad,min}$ does not take into account the energy stored inside the sphere and 2) the entire spherical volume is not utilized by the antenna. Next some latest attempts to reach the fundamental limit of $Q_{rad,min}$ are discussed.

2.4.2 Today's methods to approximate quality factor

Thiele investigated in 2003 the limit of Q_{rad} by taking into account also the energy stored inside the sphere. Thiele's method is based on the calculation of the far field pattern and it relies on the concept of superdirectivity. Small antennas can be considered to be superdirective, since they have more directivity than their small size warrants [16]. Figure 2.4 shows the curve (far field Q) based on the Thiele's method. Thiele gives also some results for a linear dipole, a bow-tie and an end-loaded dipole to illustrate the validity of the lower bound of Q_{rad}, see Figure 2.4. In Figure 2.4 the top two curves with different wire radii are calculated using Equations (2.23) and (2.24) ($Q = X/R$). The bottom curve is calculated using the McLean's Equation (2.30). The far field Q_{rad}, the solid line curve, is the lower bound for a sinusoidal current dipole and is calculated using the Thiele's method. The bow-tie and the end-loaded dipole data points are determined using $Q = X/R$.

Wen Geyi investigated also in 2003 the case when the energy inside the sphere is taken

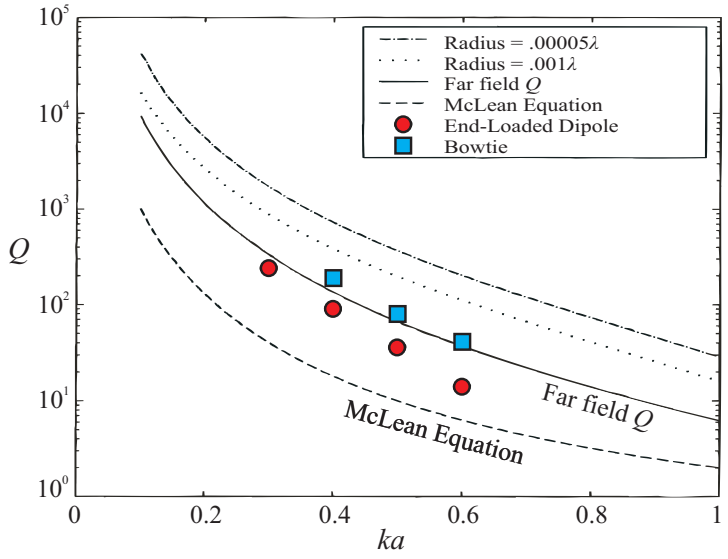

Figure 2.4: The Thiele's limit and Q of some antenna structures [16].

into account [14]. He defined the limit of Q_{rad} by using the Poynting theorem in both frequency and time domain. He calculated Q_{rad} for different antenna structures, like a small dipole and a small loop antenna. For a small dipole, the approximate value of Q_{rad} can be written [17]:

$$Q_{rad,min} \approx \frac{6\left[\ln\left(\frac{a}{a_0}\right) - 1\right]}{k^3 a^3}. \tag{2.32}$$

where a is the radius of a sphere and a_0 is the radius of a wire, as shown in Figure 2.5 b). Geyi formula is based on a triangular current distribution, so Equation (2.32) is valid only when $ka < 1$. Geyi calculated also the Q_0 of a small antenna using the Foster reactance theorem and the Q_0 can be determined directly by the antenna input impedance as follows [18]:

$$Q_{0,Geyi} = \frac{\omega \frac{\partial X_a}{\partial \omega} \pm X_a}{2R_a^{rad}}, \tag{2.33}$$

where R_a and X_a are the real and the imaginary part of the antenna input impedance. In Equation (2.33) either the - or + sign is chosen depending on which one gives the highest Q. It is good to note that this formula is not sufficiently accurate to calculate the Q factor especially at the antiresonant frequency ranges[3].

[3]The frequency ω_0, at which $X_0(\omega_0) = 0$, $\begin{cases} \text{defines a } \textit{resonant} \text{ frequency of the antenna if } X_0' > 0; \\ \text{defines an } \textit{antiresonant} \text{ frequency of the antenna if } X_0' < 0. \end{cases}$

Arthur Yaghjian and Steven Best published also in 2003 how to define a useful and accurate approximate expression for Q and its relationship to the bandwidth [19], [20], [21], [22]. They proved and showed that the quality factor of the antenna can be determined very accurately using the following approximate expression [19]:

$$Q_Z(\omega_0) = \frac{\omega_0}{2R(\omega_0)} \left| Z^{'}(\omega_0) \right| \tag{2.34}$$

$$= \frac{\omega_0}{2R(\omega_0)} \sqrt{\left[R'(\omega_0)\right]^2 + \left[X'(\omega_0) + \left|X(\omega_0)\right| / \omega_0\right]^2} \tag{2.35}$$

where $Z^{'}(\omega_0)$, $R^{'}(\omega_0)$ and $X^{'}(\omega_0)$ are the frequency derivatives of the untuned antenna impedance, resistance, and reactance, respectively. Equation (2.34) is valid when the tuned or self-resonant antenna exhibits a single impedance resonance within its defined operating bandwidth. If the small antenna is designed so that it exhibits multiple resonances the approximation may not be valid anymore [23].

Geyi derived an approximate expression for Q similar to (2.34), but with $|Z_0^{'}(\omega_0)|$ replaced by $|X_0^{'}(\omega_0)|$. Such an expression would not produce an accurate approximation to Q in the antiresonant frequency ranges.

Steven Best investigated in 2005 electrically small spherical dipole antennas that fill the entire volume of the sphere [24]. He found out that the quality factor of the linearly polarized 4-arm folded spherical helix dipole is within 1.52 times the fundamental limit (2.30) of Q_{rad} for an electric dipole when $ka \approx 0.263$. The quality factor of the elliptically polarized 4-arm folded spherical helix dipole is within 2 times the fundamental limit (2.31) of Q_{rad} for a dual-mode antenna. As a result it is possible to get quite close to the fundamental limit by utilizing the whole spherical volume.

2.4.3 Comparison of different methods to estimate quality factor

In this section different methods to estimate the Q-factor and the achievable bandwidth potentials are briefly discussed.

As an example, a small dipole of size $a = 13.5$ mm having a $\lambda/2$ resonance at 5.6 GHz and $a_0 = 0.1$ mm is here simulated with IE3D [25], which is an electromagnetic simulator based on the method of moments. In Figure 2.5 a) the limit of Q of a dipole is calculated by different methods. It is good to notice that the antenna is not electrically small when $ka >> 1$ and McLean's and Geyi's equations do not necessarily give a good approximation when $ka > 1$. The bottom curve is calculated using the McLean's

Equation (2.30). The blue-dotted solid line is calculated using the Geyi's method in Equation (2.32). The red solid line is calculated from simulated small dipole results (IE3D) using the Equation (2.34). The dotted line is calculated using Equation (2.33). The quality factors $Q_{0,Geyi}$ and Q_Z are calculated using simulated input impedance results. When comparing these results, good agreement between the simulated input impedance results and the Geyi Equation (2.32) is achieved when the antenna is small enough ($ka < 1.5$). The Geyi's results calculated with (2.33) using simulated input impedance results give wrong values when $1.5 \leq ka \leq 3.5$ because the antiresonant mode is dominating and thus the frequency derivative of the input reactance of the antenna is less dominant and $R_0'(\omega_0)$ can be significant.

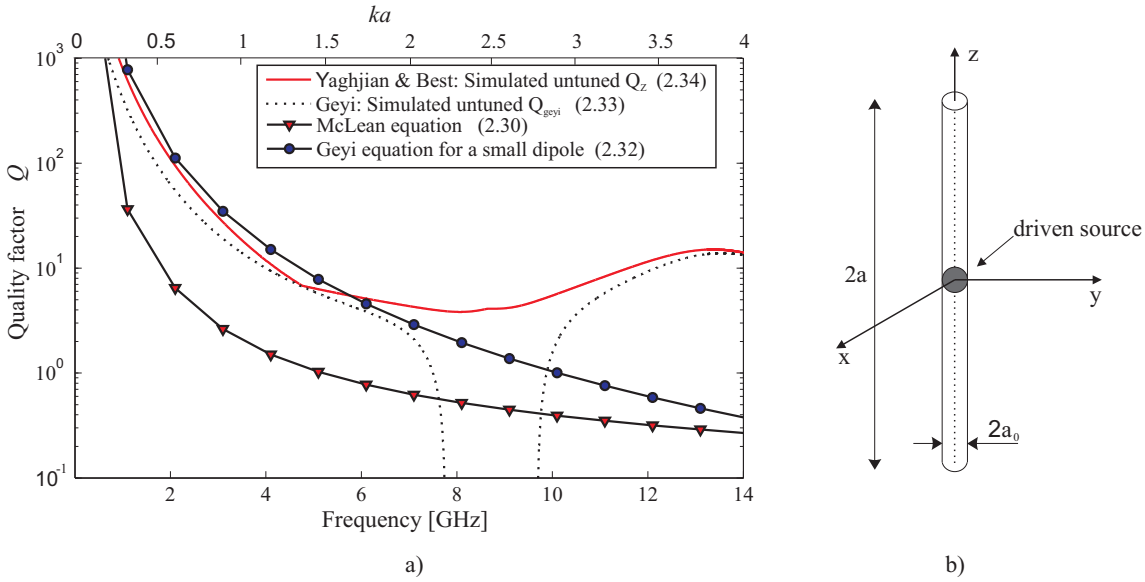

Figure 2.5: a) Quality factor Q is represented with respect to frequency and ka, b) dipole antenna used in simulations.

In Figure 2.6 a) and b), the quality factor Q_0 and the achievable bandwidth are calculated using simulated input impedance results. Figure 2.6 c) presents the used PIFA antenna structure. In both cases the values are calculated with two different methods. The black lines are calculated using a Matlab code[4]. The Matlab code calculates all possible matching circuit topologies with a single resonant LC-circuit and then it chooses the option which gives the largest bandwidth [26]. The used matching criterion is return loss $L_{retn} \geq 6$ dB ($S = 3$) and the antenna is perfectly matched at the matching frequency (critical coupling). The relation between the quality factor Q and the bandwidth can be calculated using Equation (2.17)[5]. The frequency range is from 800 MHz to 1.8 GHz. The red lines are calculated using Equation (2.34). It can be seen that there are big differences between the methods especially at 1.2 GHz, where the chassis $\lambda/2$ wavemode

[4]The Matlab code used in these simulations was programmed by Mr. Risto Valkonen at the Department of Radio Science and Engineering of Helsinki University of Technology

[5]Equation (2.34) is valid only when the pure single-resonance is achieved

is present. It is obvious that the difference between these two methods is related to the fact that the L-section matching network is a single resonant circuit and when multiple resonances are present Equation (2.34) gives a wrong quality factor Q. It is reasonable to use both methods at the same time because this way it is possible to discover the multiple resonance cases which in some cases are very difficult to notice otherwise.

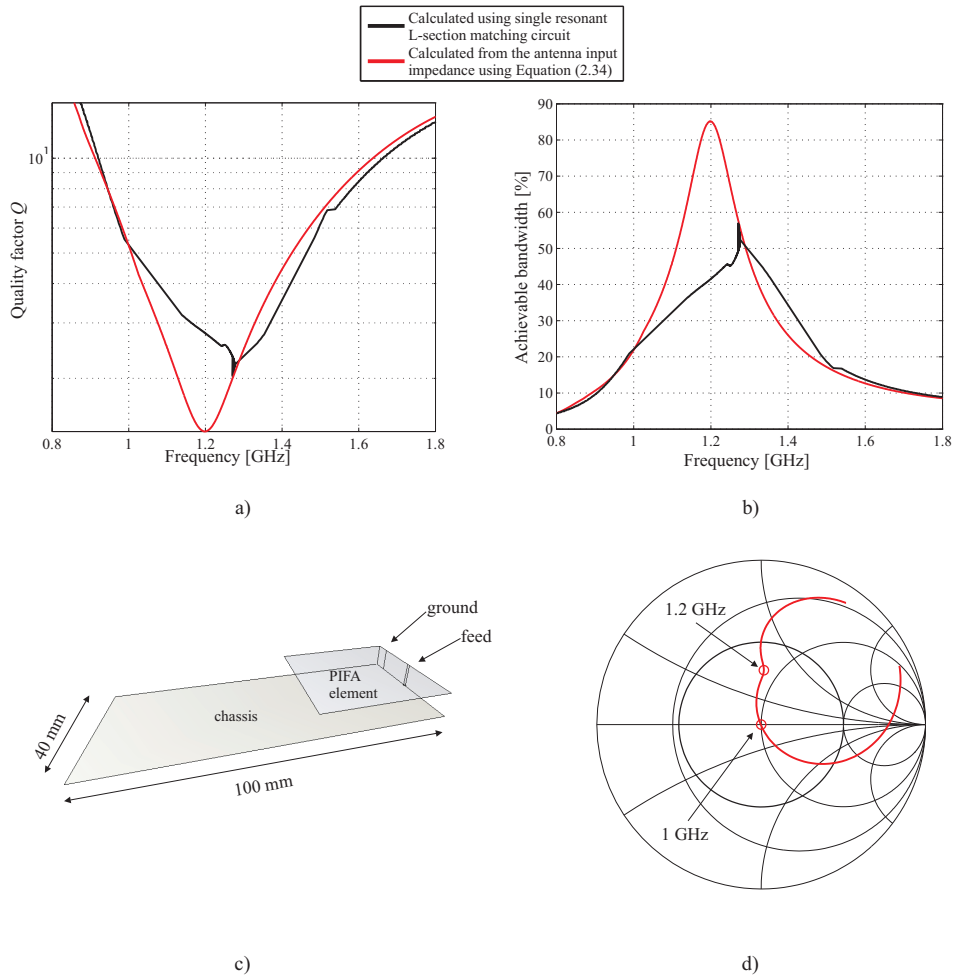

Figure 2.6: a) Quality factor Q of PIFA antenna, b) achievable bandwidth of PIFA antenna, c) PIFA element on a finite chassis and d) reflection coefficient of PIFA antenna on the Smith chart

2.5 Bandwidth enhancement methods

As discussed earlier in this work, the chassis of the mobile terminal is not used significantly as a radiator and as presented earlier the size of the antenna and the achievable bandwidth potential have a close relation; the smaller the antenna the smaller the bandwidth. Thus the isolated antenna structures are larger than the traditional antenna elements, like a PIFA or a coupling element with a given bandwidth. Thus we have to

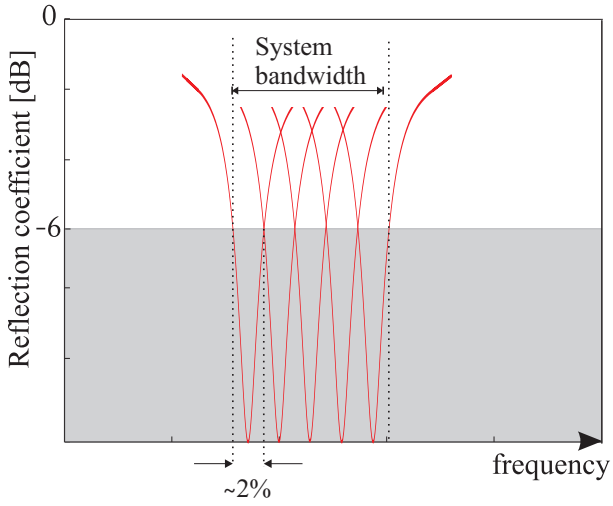

Figure 2.7: Bandwidth requirement of a cellular system and the required ca. 2% bandwidth of the isolated antenna structure.

allow narrower bandwidth to keep the size of the antenna structure small enough to fit inside a mobile terminal and therefore some switching method or additional resonators are needed to cover the required frequency band, see Table 2.1 and Figure 2.7.

In this work the bandwidth of ca. 2% is used as the bandwidth requirement for the isolated antenna structures. The bandwidth requirement of ca. 2% is chosen because it gives a good compromize between the size of the antenna and the feasibility of the tuning circuit. The required bandwidth depends on the used system. In Table 2.1 the cellular systems used in the mobile terminals and their bandwidth requirements are represented. It is needed to increase the 2% bandwidth by 4 to 7 times to fulfill the requirement, as can be seen in Table 2.1.

Table 2.1: Frequency bands of certain cellular systems used in the mobile terminals.

System	Center frequency [MHz]	Absolute bandwidth [MHz]	Relative bandwidth [%]
GSM 850	859	70	8.1
E-GSM 900	920	80	8.7
GSM 1800	1795	170	9.5
GSM 1900	1920	140	7.3
WCDMA2100	2035	270	13.3

2.5.1 Multiple resonances

Earlier, only the single resonant matching circuits and antennas have been discussed. However, it is well known that a very good method to increase the impedance bandwidth is to have additional resonators. In Figure 2.8, the theoretical maximum relative bandwidth B_r is represented as a function of the return loss criterion [10]. It can be

seen that with one additional resonators ($n = 2$), the impedance bandwidth can be approximately doubled (100%) compared to the single-resonant operation. With two additional resonators ($n = 3$) the enhancement is approximately 150% and after a couple of additional resonators the improvement in bandwidth saturates rapidly towards the Bode-Fano criterion ($n = \infty$), which gives the theoretical maximum limit for the impedance bandwidth that can be obtained with a matching circuit containing an infinite number of reactive components. It can be calculated from [27], [28], [29]:

$$B_{r,max} = \frac{\pi}{Q_0 \ln(\frac{S+1}{S-1})}, \tag{2.37}$$

where S is the $VSWR$ impedance matching criterion.

According to Equations (2.16) and (2.37), the theoretical maximum bandwidth enhancement with infinity additional resonator is about 240% and thus this method cannot be used in this work. For example, an optimally-coupled single-resonant antenna having the relative bandwidth of 2%, has the quality factor $Q_0 \approx 66.7$. By adding infinity additional optimally-coupled resonators, the bandwidth can be increased to 6.8%.

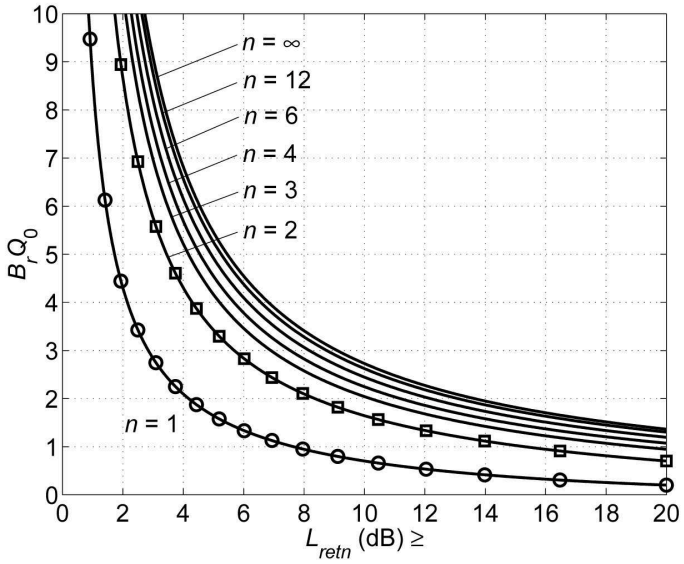

Figure 2.8: Theoretical maximum relative impedance bandwidth of a resonant antenna having a certain Q_0 with $n-1$ additional resonators as a function of the minimum allowed return loss L_{retn} [10].

2.5.2 Switchable center frequency

Microelectromechanical systems (MEMS) switches can be used to select the appropriate matching circuit, as shown in Figure 2.9 b). The frequency band is divided into several

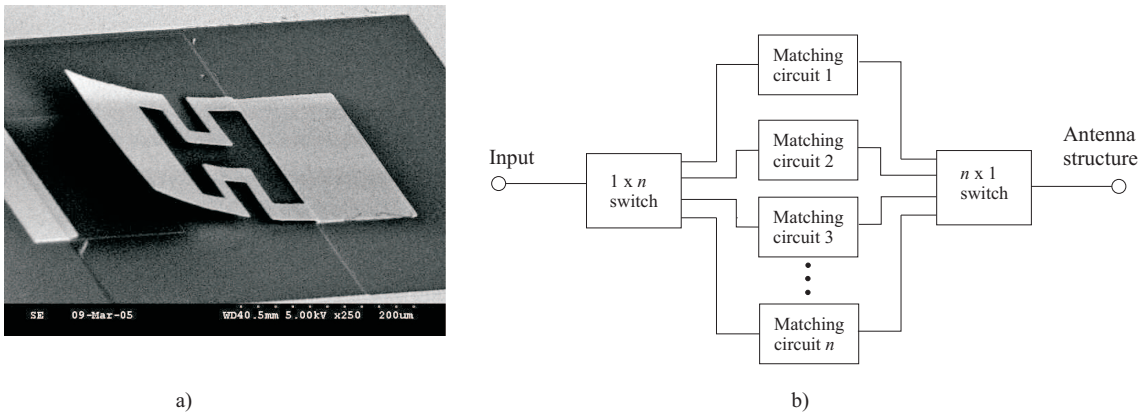

Figure 2.9: a) SEM photo of a fabricated RF MEMS switch [30], b) a block diagram of a parallel matching circuit topology.

sub-bands and each sub-band has its own matching circuit. It is possible to cover e.g. 10% system bandwidth with 5 sub-bands each having 2% bandwidth and thus this is the method that can be used to increase the bandwidth in this work.

MEMS is a promising method to integrate mechanical systems, like switches, to silicon substrate through micromachining technology (see Figure 2.9 a)). RF MEMS switches have overwhelming advantages over traditional pin diodes and GaAs FETs [30], [31]. They can be used to build RF circuits with very low power consumption, resistance, and capacitance. Drawbacks are the limited lifetime (ca. 100 billion cycles) and high development costs. There are also some unresolved problems of developing suitable fabrication techniques [31].

2.6 Isolated antenna structures

In this section isolated antenna structures are introduced. The isolation in this case means that the chassis of the mobile terminal and the whole antenna structure are separated either galvanically or by using balanced structures, like a dipole or a loop antenna. The balanced antenna structures are isolated from the chassis by their nature and those structures do not need a separate ground plane to work.

2.6.1 Galvanically isolated antenna structures

In galvanically isolated structures the isolation among the antenna structure and the chassis of the mobile terminal depends on the coupling between these objects and the frequency. When there are strong electric fields between the antenna structure and the chassis of the mobile terminal, the capacitive coupling is dominating over the inductive coupling. Whereas when strong currents are concentrated between the antenna structure

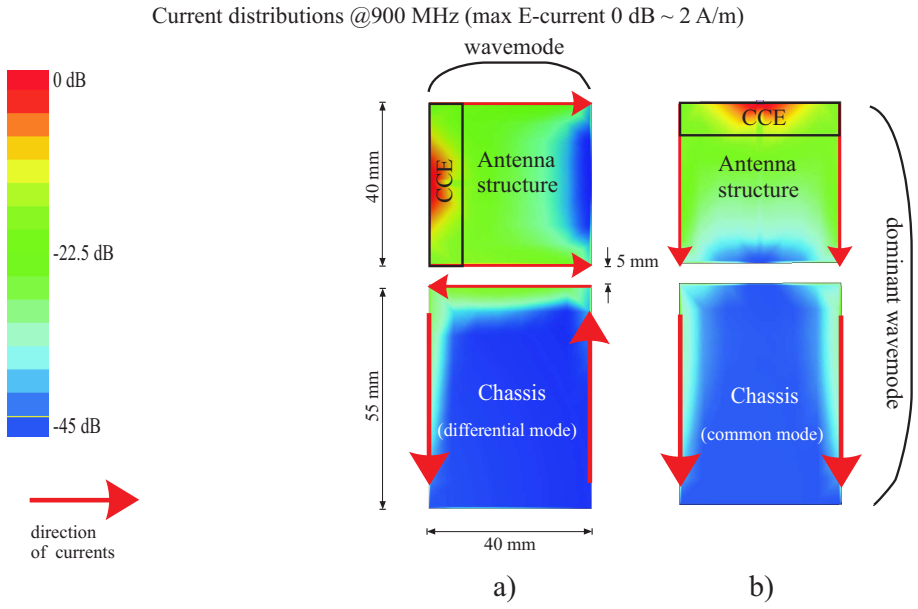

Figure 2.10: Current distributions of two different isolated antenna structures: a) CCE is placed on the side, b) CCE is placed on the top.

and the chassis, the inductive coupling is dominating. In Figure 2.10 a) it is quite obvious that the inductive coupling is dominant and in Figure 2.10 b) the capacitive coupling is dominant.

One method to increase the isolation between the antenna structure and the chassis is to increase the gap between them. It is possible to estimate the isolation by adding another capacitive coupling element (CCE) to the bottom end of the chassis and measure the S_{21} parameter. In this case both coupling elements are unmatched and those results can be used only to estimate the effect of the gap. The simulated S_{21} parameters do not give the actual isolation between the antenna structure and the chassis. In Figure 2.11, simulated $|S_{21}|$ parameters are represented as a function of the gap. The total length of the antenna structure remains the same and when increasing the gap the chassis become shorter. The S_{21} parameters are simulated with IE3D. Firstly it can be seen that when the CCE is placed on the side it is possible to get larger isolation compared to the situation when the CCE is placed to the top. Secondly, increased gap between the chassis and the antenna structure is not a very efficient way to increase the isolation.

One can also see that an effective way to reduce the effect of the induced current on the chassis is to make an antenna structure which creates differential currents to the chassis. These differential currents do not radiate as effectively as common mode currents since a part of the radiation is cancelled in the far field. An example of this kind of structure is shown in Figure 2.10 a). It can be seen that the currents of the chassis have different directions and obviously there is better isolation when the currents cancel each other like in Figure 2.10 a). That can be seen also in Figure 2.11 when comparing the S_{21}

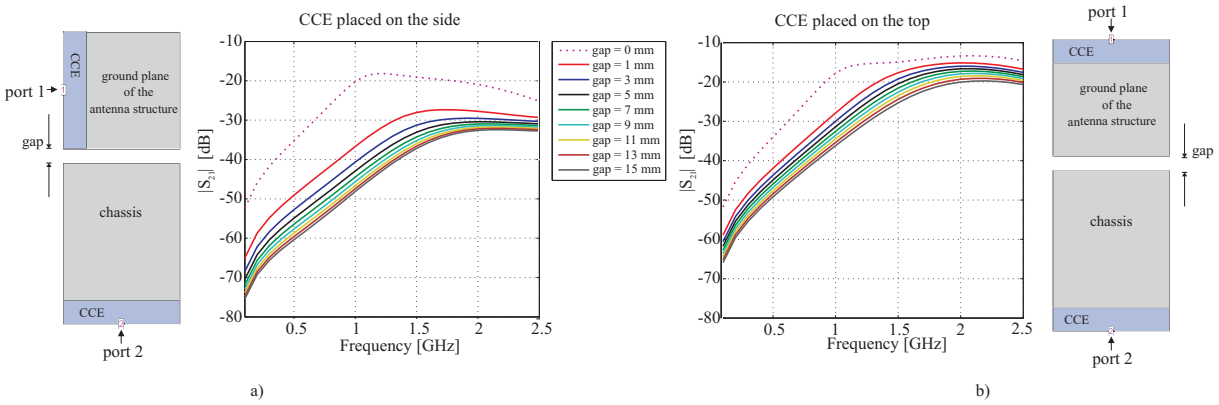

Figure 2.11: Isolation S_{21} as a function of gap between the antenna structure and the chassis when a) CCE is placed on the side, b) when CCE is placed on the top.

parameters.

2.6.2 Balanced antenna structures

In this section four different balanced antenna structures are introduced; 1) wire antennas, 2) loop antennas 3) helix antennas, and 4) bow-tie antennas.

Wire antennas

Wire antennas are the oldest and the simplest antenna structures. When the feed is positioned symmetrically in the middle of the wire, the antenna is called a dipole-type wire antenna [2]. The symmetric positioning is not actually necessary but it is usually the most convenient.

First, infinitesimal dipoles, also known as a Hertzian dipole or a short dipole, ($l << \lambda$) are represented because more complex geometries can be considered to be consisting of Hertzian dipoles [4]. The current distribution of the infinitesimal dipole is constant along the wire, as shown in Figure 2.12 a), and the radiation resistance can be estimated from [2]:

$$R_r = \frac{2P_{rad}}{|I_0|^2} = 80\pi^2 \left(\frac{l}{\lambda}\right)^2. \tag{2.38}$$

For the infinitesimal dipoles the near field region is valid when $r < \lambda/2\pi$ and the far field region when $r >> \lambda/2\pi$.

When the length l of the dipole is short ($\lambda/50 < l \leq \lambda/10$) compared to the wavelength λ, the antenna is said to be a small dipole [2]. The current distribution of a small dipole

can be approximated by a triangular current distribution shown in Figure 2.12 b). The radiation resistance of the antenna can be estimated from [2]:

$$R_r = \frac{2P_{rad}}{|I_0|^2} = 20\pi^2 \left(\frac{l}{\lambda}\right)^2. \tag{2.39}$$

It can be seen that for the small dipole the radiation resistance is one-fourth of R_r in (2.38). The directivity of a lossless infinitesimal and a small dipole is $D = 1.5 \approx 1.76$ dBi.

When the length of the dipole increases the triangular current distribution approximation is no more accurate. A better approximation for a linear dipole of any length is a sinusoidal current distribution, shown in Figure 2.12 c). The derivation of the resistance expression comes quite complicated because of sine and cosine integral functions. For the approximation of the radiation resistance of a lossless $\lambda/2$ dipole we get [2]:

$$R_r \approx \frac{\eta_{wave}}{4\pi}\mathrm{Ci}(2\pi) \approx 73\ \Omega, \tag{2.40}$$

where $\mathrm{Ci}(x)$ is the cosine integral function and η_{wave} is wave impedance in free space ($\eta_{wave} \approx 377\ \Omega$). The directivity of the $\lambda/2$ dipole is $D \approx 1.64 \approx 2.15$ dBi.

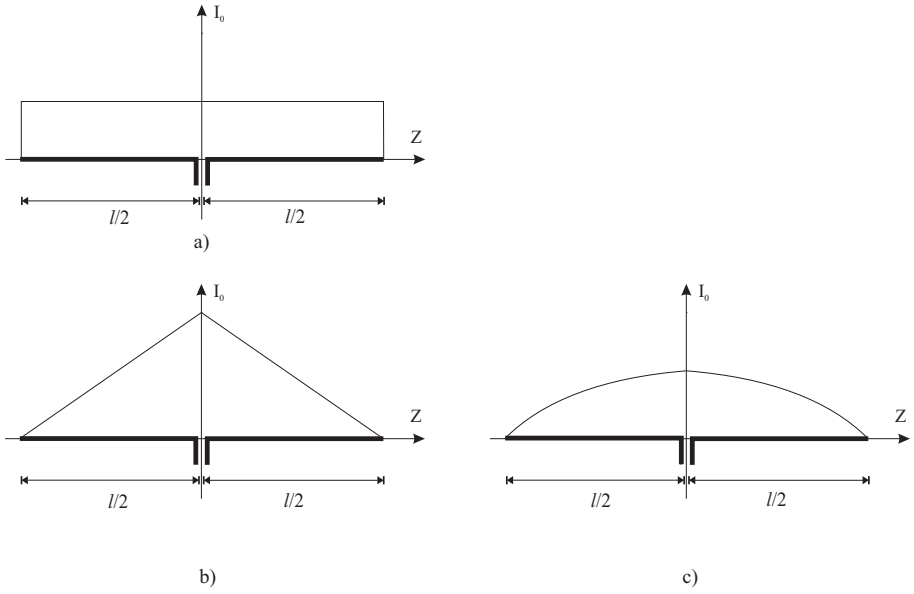

Figure 2.12: a) Constant current distribution of a infinitesimal dipole, b) triangular current distribution of a small dipole, c) sinusoidal current distribution of a dipole ($l = \lambda/2$).

The radiation resistance of a thin $\lambda/2$ dipole is $R_r \approx 73\ \Omega$ and the resistance decreases when the radius of the wire increases. The infinitesimal dipoles (Herzian dipoles or short dipoles) are not practical since the radiation resistance of the infinitesimal dipole having the length of $\lambda/50$ is about 0.3 Ω and it will lead to very large mismatch or low radiation

efficiency when connected to practical transmission lines. Often dipole antennas are fed by using coaxial feed lines which are not symmetric and therefore a balun[6] is needed [4].

Different wire antenna structures

A traditional wire antenna does not fill the spherical volume effectively and thus the radiation quality factor Q_{rad} is rather high. By utilizing the spherical volume better it is possible to reduce the radiation quality factor Q_{rad} [24].

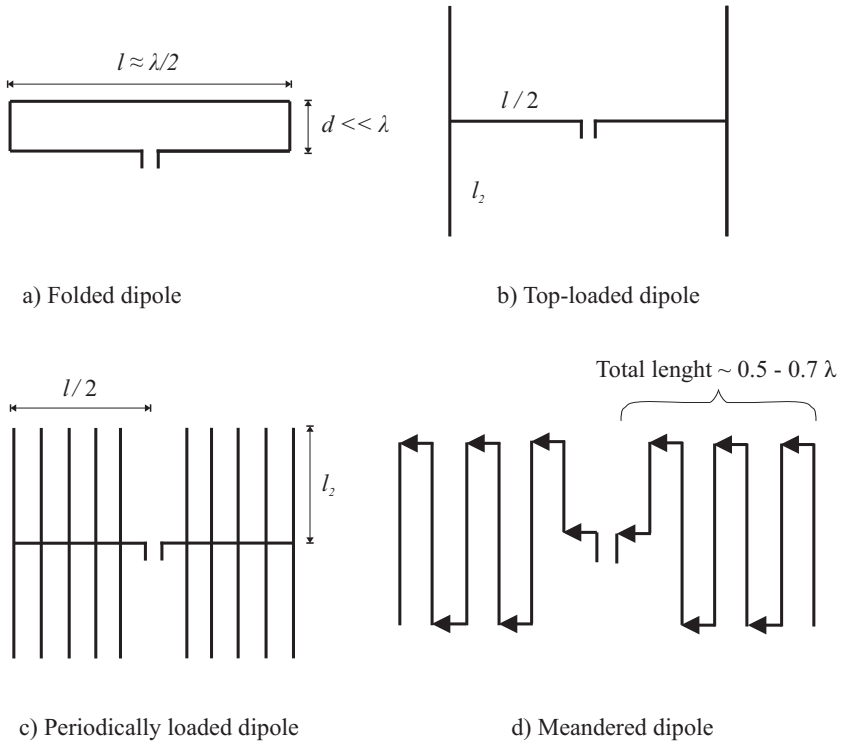

Figure 2.13: a) Folded dipole, b) top-loaded dipole, c) periodically loaded dipole, d) meandered dipole.

A folded dipole antenna has a narrow loop, $d << \lambda$, whose length is $l \approx \lambda/2$ at the operating frequency, showed in Figure 2.13 a). The folded dipole antenna can be decomposed into common and differential modes of the antenna when unbalanced feeding is used. The common mode is achieved when $l = \lambda/4$ and the differential mode when $l = \lambda/2$. Thus the mode depends on the frequency. By using the folded dipoles it is possible to isolate the antenna structure from the chassis even though the antenna is unbalanced [2], [4].

When $l \approx \lambda/2$, the radiation resistance of the folded dipole can be calculated from [2]:

$$Z_{in} = 4Z_a, \tag{2.41}$$

[6]Balun is an electrical transformer that can convert balanced feed to unbalanced and vice versa

where Z_a is the radiation resistance of the $\lambda/2$-dipole (Equation (2.40)).

When tuning the large capacitive reactance of the small wire dipole, usually a large inductance is needed and that causes normally high losses and decreases the total realized gain. It is possible to reduce matching losses significantly by achieving a self-resonance. One method to decrease the resonance frequency of the small wire antenna is to use top-loading that increases the self-capacitance [8], as shown in Figures 2.13 b) and c). Another method is to use meandered structures to increase the self-inductance and thus decrease the resonant frequency, as shown in Figure 2.13 d) [32]. The meandered wire dipole has a vector current alignment where the dominant current vectors are in-phase and in the same direction and thus increase the self-inductance.

Loop antennas

Loop antennas are simple and widely used antenna structures as well as wire dipoles. The loop can have many different shapes like a rectangle, square, circle, or ellipse. Loop antennas are classified as electrically small (circumference $< \lambda/10$) and electrically large antennas (circumference $\approx \lambda$) [2].

A small circular loop (radius $<< \lambda$, area A) has a similar far field radiation pattern as an infinitesimal magnetic dipole and the radiation resistance of the small circular loop is calculated simply by multiplying Equation (2.38) by the factor $(kA/l)^2$ [2], [4]:

$$R_r = 320\pi^4 \left(N^2 \frac{A^2}{\lambda^4} \right) \Omega, \tag{2.42}$$

where N is the number of turns of an arbitrary shaped small loop. A small loop antenna has a very low radiation resistance and inductive reactance. The inductive reactance of the small loop can be tuned to zero using a low loss capacitor which has usually smaller losses than the inductor used to match a small wire dipole.

Helical antennas

A helix antenna consists of N turns, diameter D, and spacing S between each turn, as shown in Figure 2.14 a). The helix antenna can operate in many modes but usually the main modes are the normal (broadside) and the axial (endfire) modes [2], [8].

In the normal mode operation ($\pi D << \lambda$) the power pattern of the antenna is almost the same as for a straight wire, as shown in Figure 2.14 c), though the polarization is not linear. In this mode the helix can be considered to consist of N small loops and N short dipoles connected together in series as shown in Figure 2.14 b). The total field is the superposition of the fields of the small radiators.

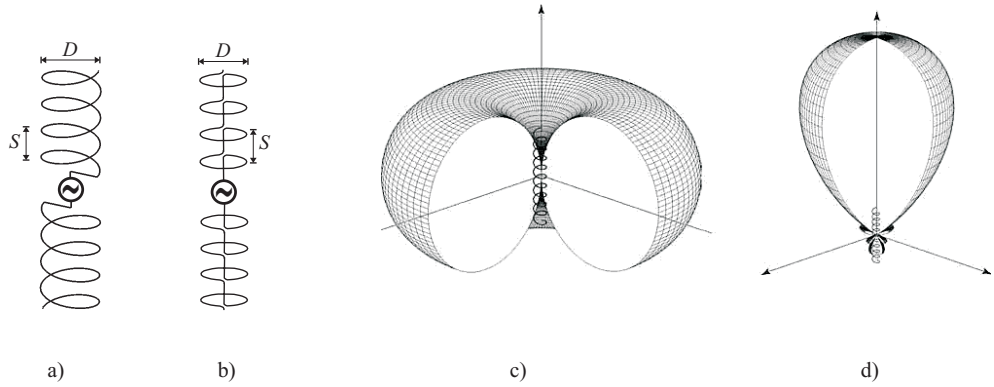

Figure 2.14: a) Helical antenna, b) helical antenna and its equivalent consisting of small loops and short dipoles, c) normal (broadside) mode [2] ,d) axial (endfire) mode [2].

Table 2.2: Comparison of a small helix dipole and a small wire dipole with the same length 0.05λ [8].

Antenna structure	Input impedance [Ω]	η_{rad} [%] at feed point	η_{tot}[%] matched to 50Ω
small helix dipole	11.7 +j00	80	75
small wire dipole	0.49 -j900	91	18

If the circumference πD is near the wavelength λ the antenna works in the axial mode, as shown in Figure 2.14 d), and circular polarization is achieved. However, this mode is impractical to realize in the mobile terminals because the structure gets too big.

As an example, a small wire dipole with a matching circuit and a small helix dipole that is in self-resonance are compared. The total length of both antennas is 0.05λ. Table 2.2 shows the comparison of those antennas.

As a conclusion the small helix has much better efficiency when matched to 50 Ω than the small dipole. There are some reasons why the small helix has better efficiency, e.g. 1) the spherical volume is utilized better by the helix and thus the radiation quality factor Q_{rad} is lower and 2) the electrical size of the small helix is much larger than that of the small dipole and thus the small helix has larger radiation resistance than the small dipole. But it is good to note that the achievable bandwidth range of the small helix is not very wide because of the self-resonance [8]. When the small helix is not in self-resonance, an additional matching circuit is needed and that limits the achievable bandwidth and decreases the efficiency.

Bow-tie antennas

Bow-tie antennas are triangle-shaped broadband antennas that have a certain spread angle α, as shown in Figure 2.15 a) [33]. The input impedance is very sensitive to the feeding technique and therefore the feeding needs extra consideration. The simplest

feeding technique is to use a balun and feed the bow-tie antenna like a dipole. If the antenna is broadband the bandwidth of the balun can limit the achievable bandwidth of the antenna.

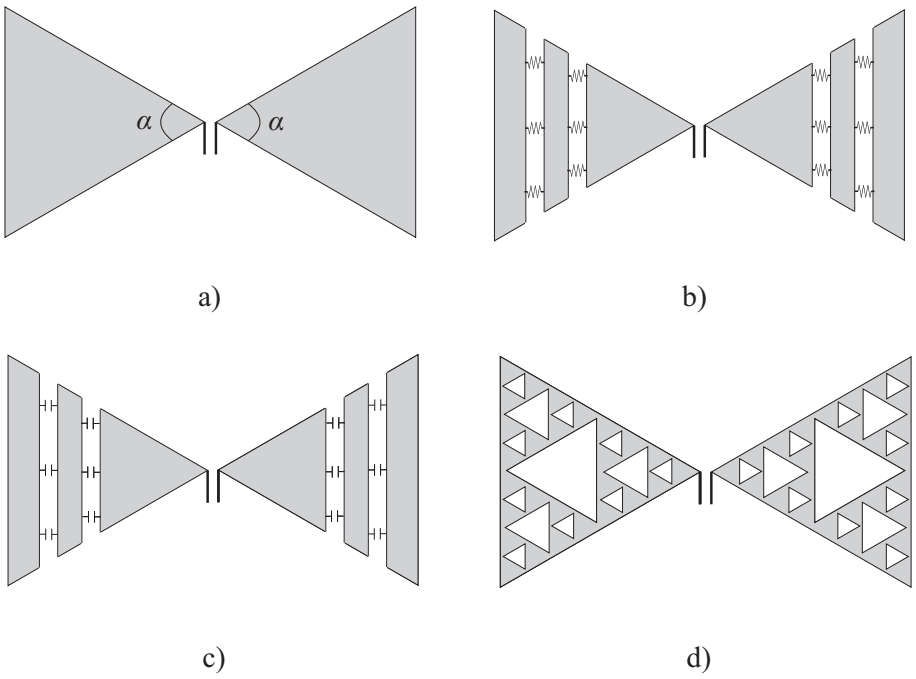

Figure 2.15: a) Bow-tie antenna, b) bow-tie antenna with resistive loading, c) bow-tie antenna with capacitive loading ,d) fractal Sierpinski bow-tie antenna .

It is possible to increase the impedance bandwidth of a bow-tie antenna by reducing the internal reflections. One method to reduce the reflections and the ringing effects[7] at the feed point is to load the antenna. The loading can be done e.g. resistively or capacitively, as shown in Figure 2.15 b) and c). The resistive loading is the most effective way to reduce the ringing effect but it reduces also the radiation efficiency of the antenna. The capacitive loading does not decrease the efficiency and thus the combination of resistive and capacitive loading may be a good compromise [34], [35] .

Fractal geometries can be used also in bow-tie antennas to decrease the size of the antenna structure [36]. Fractals are geometries that repeat themselves and are self-similar. The fractal bow-tie antenna is made by using several triangular slots on the surface of the conventional bow-tie antenna. The repetition might be in combination with rotations and translations. Figure 2.15 d) shows first three iterations of a Sierpinski fractal bow-tie antenna. The fractals reduce the electrical size of the antenna and decrease the resonant frequency, maintaining the same directivity [36].

[7]Ringing effect is caused mainly by multiple reflections between the antenna open ends and the feed point

CHAPTER 3

Isolated antenna structures in mobile terminals

This chapter is focused on studying the feasibility of isolated antenna structures in the mobile terminal environment. The chassis may deteriorate in some cases the performance of the antenna structure and thus the effect of the chassis is also studied. At first in Section 3.1 isolated antenna structures and their bandwidth potentials are investigated. The summary of the achievable bandwidth potentials are discussed in Section 3.2. In Section 3.3 the radiation patterns of those antenna structures are represented.

3.1 Bandwidth potentials of isolated structures

In this section bandwidth potentials of isolated antenna structures are simulated. First different balanced antenna structures and in the end galvanically isolated antenna structures are handled. The bandwidth potentials are simulated with and without the chassis of the mobile terminal to study the effect of the chassis. The distance between the antenna structure and the chassis is fixed to 5 mm in all cases when the chassis is present. The size of the antenna structure is defined from the required bandwidth potential, which is fixed to ca. 2%. The maximum allowed dimensions of the chassis are 100 mm x 40 mm [length x width] with 7 mm thickness and the maximum allowed dimensions of the isolated antenna structure are 40 mm x 40 mm x 7 mm [length x width x thickness].

All the presented simulation results in this section are based on Method of Moments (MoM)-based software Zeland IE3D [25]. The achievable bandwidth potentials are calculated from the simulated S_{11} at each simulated frequency using two different methods, presented earlier in Section 2.4.3. The used matching criterion is return loss $L_{retn} \geq 6$ dB and the antenna is perfectly matched at the matching frequency (critical coupling). All

results are compared to the reference antenna which is the capacitive coupling element antenna (CCE) [1].

3.1.1 The reference antenna

The used reference antenna structure is the capacitive coupling element (CCE) with the chassis having dimensions 100 mm x 40 mm [length x width], see Figure 3.1 a). In this structure the coupling element is used to couple the currents to the chassis and the antenna resonance is created with a separate matching circuitry. This makes it possible to use a very simple and small antenna structure compared to the more traditional PIFA structure where the antenna element is also used to create the antenna resonance.

As can be seen in Figure 3.1 b), the bandwidth potentials at 900 MHz and 1800 MHz are about 8% which is almost enough to fulfill the E-GSM 900 and GSM 1800 bandwidth requirements shown in Table 2.1. The bandwidth potentials are calculated when the antenna is perfectly matched at the matching frequency but when using the optimal overcoupling it is possible to increase the bandwidth potential about 15% and both bandwidth requirements would be then fulfilled.

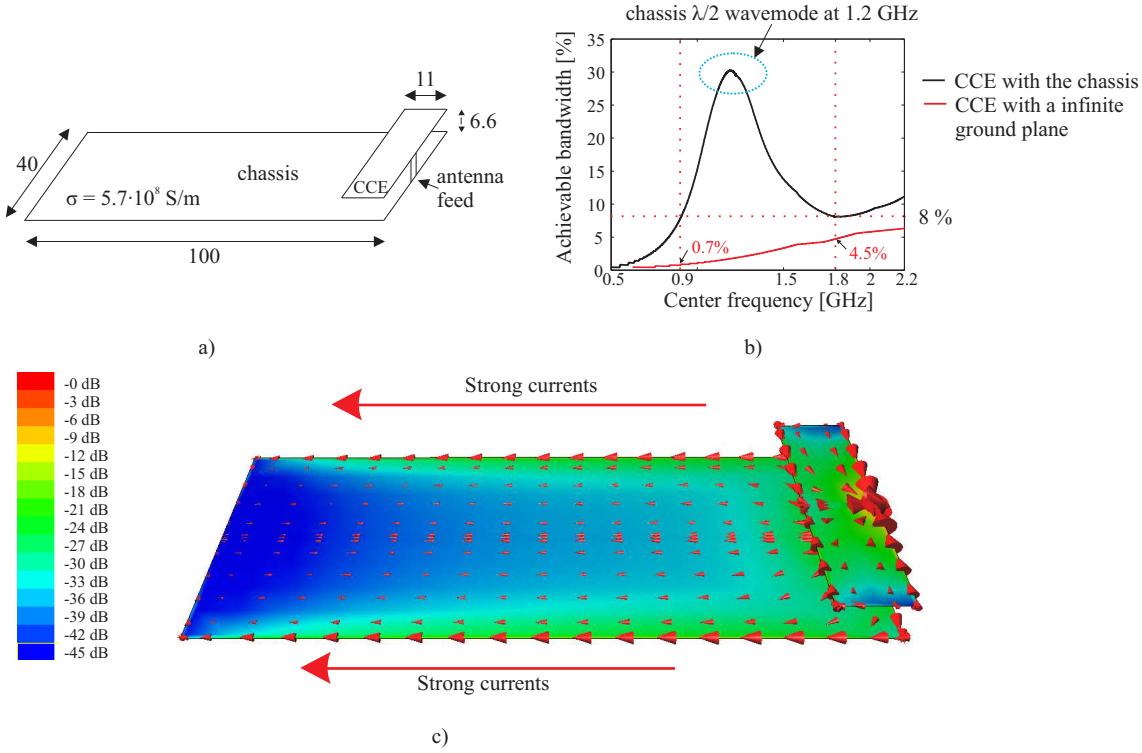

Figure 3.1: a) CCE structure with chassis (dimensions in mm). b) Achievable bandwidth as a function of the matching frequency and c) the current distribution of the CCE and the chassis at 900 MHz (max E-current = 10 A/m).

Figure 3.1 c) shows the current distribution of the reference antenna at 900 MHz and

it can be clearly seen that there are rather strong currents along the long edges of the chassis and thus the chassis is the main radiator [1]. Based on this, the radiated power of the CCE can be estimated by calculating the ratio of the bandwidths when the CCE is placed on an infinite ground plane and on the chassis [1]. At 900 MHz ca. 91% of the radiated power is contributed by the chassis and at 1800 MHz about 44% of the radiated power is contributed by the chassis . It is obvious that when the hand of the user is close to the chassis, the hand interacts with the strong edge currents and changes the matching and decreases the radiation efficiency.

3.1.2 Wire antennas

As discussed earlier, a simple wire antenna does not fill the spherical volume effectively and thus the radiation quality factor Q_{rad} is rather high. Simulation results show that at lower UHF frequencies, below 1 GHz, these simple wire antennas are either too large or do not fulfill the 2% bandwidth requirement (shown later in Table 3.1). By utilizing the spherical volume more effectively it is possible to reduce the radiation quality factor Q_{rad} and thus increase the achievable bandwidth. First in this section top-loaded dipoles are handled and in the end some meandered wire dipoles are presented.

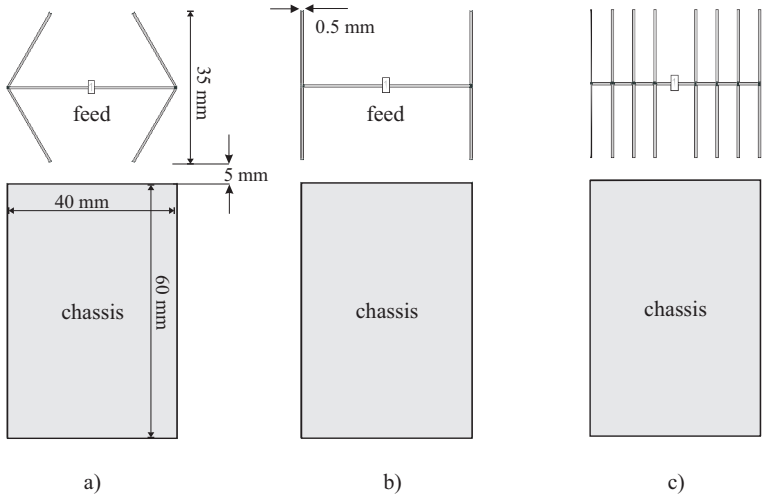

Figure 3.2: Different top-loaded wire dipole structures: a) top-loaded wire dipole (case #1), b) top-loaded wire dipole (case #2), c) periodically loaded wire dipole (case #3).

By top-loading the wire dipole it is possible to increase the self-capacitance and thus decrease the resonance frequency [8]. Three different top-loaded wire dipole structures are investigated, as shown in Figure 3.2. The diameter of the wire is 0.5 mm in all cases. Top-loaded wires are folded 60 degrees in case #1 presented in Figure 3.2 a) to fill the spherical volume more efficiently. When placing the antenna inside a real mobile terminal, a rectangular shape can often fill the volume better and make it possible to use larger antenna structures to get smaller radiation Q, like in case #2 shown in Figure

3.2 b). It is possible to increase even more the self-capacitance by periodically loading the wire dipole, like in case #3 shown in Figure 3.2 c). All these three structures are designed so that the best structure (case #3) fulfills the 2% bandwidth requirement at 1 GHz with the chassis. This gives a good knowledge of the capacity of each structure and it is easy to compare the structures. The dotted lines are calculated using Equation (2.34) and the solid lines are obtained using the Matlab code that calculates the L-section matching circuit automatically [26].

The simulated achievable bandwidth potentials with and without the chassis are presented in Figure 3.3. The both cases are investigated to discover the whole capacity of each structure and to see the effect of the chassis.

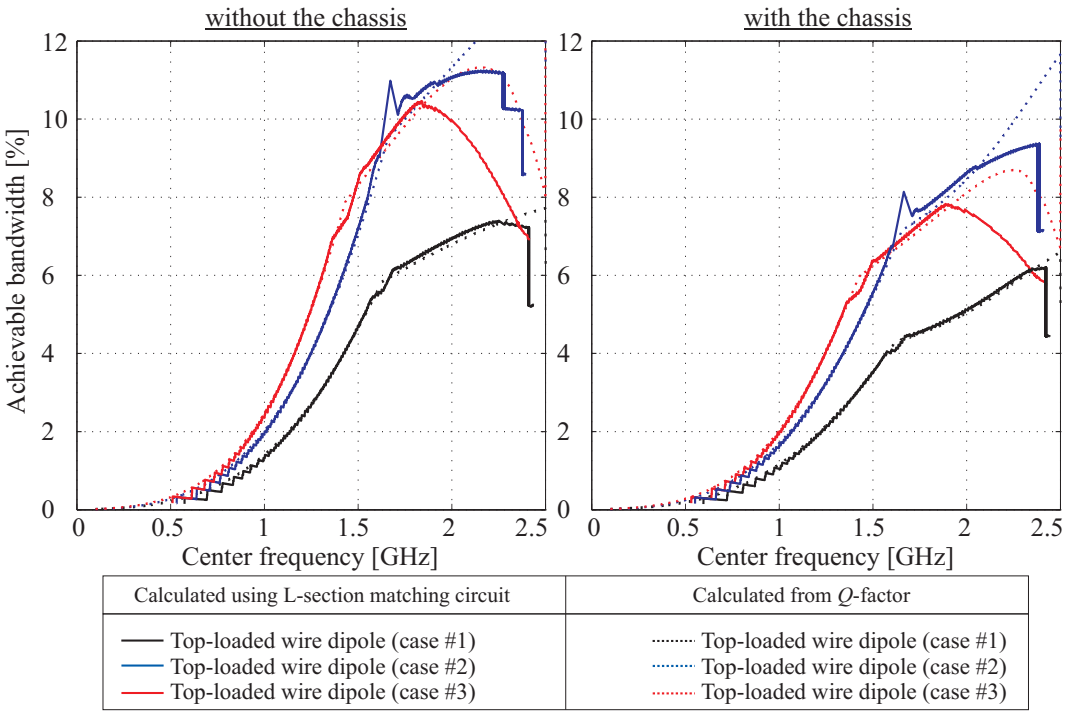

Figure 3.3: Achievable bandwidth potentials of different loaded wire dipole structures with and without the chassis.

According to Figure 3.3, one can see that in case #3 the chassis decreases the achievable bandwidth potential at 1 GHz ca. 19% and at 1.8 GHz ca. 27%. This is due to the fact that most balanced antenna structures work best in free space and, vice versa, perform worst when placed in the vicinity of other conductors, like the chassis of the mobile terminal. At 1 GHz the radiation resistance is decreased from 6 Ω to 4.9 Ω (ca. -18%) and the reactance is almost the same (-152 Ω versus -149 Ω) without and with the chassis. This can be roughly explained so that in the low-loss case the reactance describes the near fields and the radiation resistance describes the far fields. When the chassis is in the vicinity of the antenna structure, coupling between these structures creates currents that are in the opposite directions and cancel a part of the radiation in the far field

and therefore decrease the radiation resistance. The achievable bandwidth maximum is located near 1.8 GHz and the relative bandwidth at 1.8 GHz is ca. 7.6% with the chassis and thus almost fulfills the bandwidth requirement of the GSM1800 cellular system.

Next some meandered wire dipole structures are presented. Meandering of the wire dipole increases the self-inductance and thus decreases the resonance frequency [32]. It is possible to meander the wire structure in many ways. In this work two different cases are inspected. These two cases are shown in Figures 3.4 a) and b). In case #4, shown in Figure 3.4 a), the purpose is to modify the meandered wire antenna structure with decreased coupling between the wires having opposite current vectors and with increased coupling between the wires having reinforcing current vectors. In case #5, shown in Figure 3.4 b), the purpose is to make as dense fitting as possible to maximize the total wire length. In case #6 the occupied size of the antenna structure is increased to be comparable to the top-loaded wire dipole structures and in case #7 there are also two additional elements to fill the occupied area more efficiently.

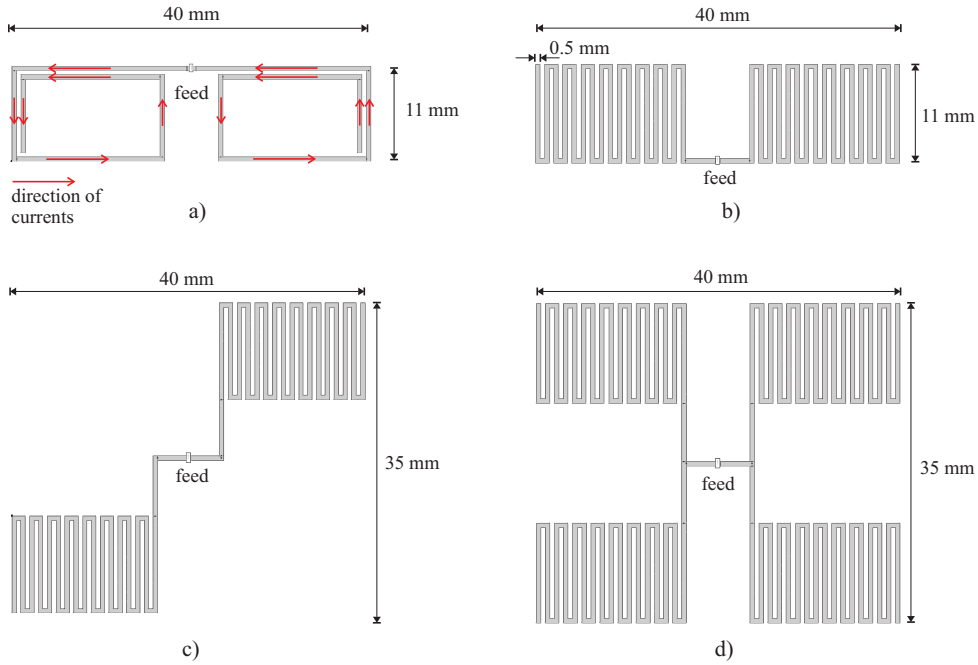

Figure 3.4: Different meandered wire dipole structures: a) meandered wire dipole (2 elements, case #4), b) meandered wire dipole (2 elements, case #5), c) meandered wire dipole (2 elements, case #6), and d) meandered wire dipole (4 elements, case #7).

According to Figure 3.5, one can see that the chassis decreases the bandwidth potential by about the same amount than for top-loaded wire dipoles except in cases #6 and #7. In case #6 the bandwidth potential is increased at 1GHz when the chassis is present. In case #7 there is strong coupling between the antenna structure and the chassis that causes decreased bandwidth potential at 1GHz. It is good to note that case #4 does not

fulfill the bandwidth requirement at lower frequencies. Case #5 fulfills the 2% bandwidth requirement at 1 GHz and cases #6 and #7 are even better. At higher frequencies, over 1.8 GHz, case #4 gives better bandwidth potential than the others.

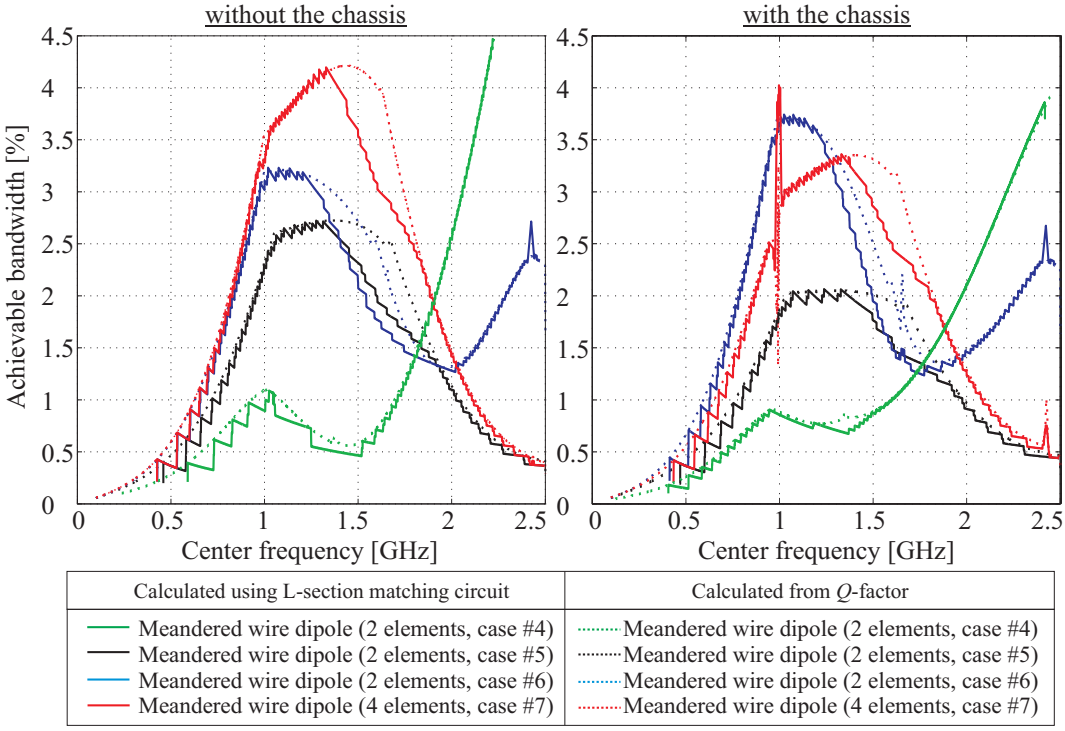

Figure 3.5: Achievable bandwidth potentials of different meandered structures with and without the chassis.

Conclusions of the wire antennas

Different wire antennas were simulated in the previous section. It was shown that by loading or meandering the wire antenna structures it is possible to decrease the radiation quality factor Q_{rad}. Table 3.1 shows the comparison of different wire antennas. One can see that the small wire dipole (total length 40 mm) is a very poor radiator at lower frequencies. The most promising wire antenna structure seems to be the meandered dipole case #6 where the 2 elements are placed in the opposing corners and the size of the structure is 35 mm x 40 mm [length x width]. This structure gives ca. 3.7% relative bandwidth at 1 GHz. Although the bandwidth is sufficient, the structure is large. Consequently, the meandered wire dipole case #5 is chosen to be the most promising isolated wire antenna structure. The loaded dipole case #3 gives practically the same bandwidth potential but is much larger.

According to Table 3.1, one can see that the meandered wire dipole case #4 gives about the same resonant frequency as the other meandered structures but the used total wire length is much smaller. This is caused by the fact that when the wires are closely coupled

Table 3.1: Comparison of the resonant performance properties of the antenna structures with the chassis.

Antenna structure	Resonant frequency [MHz]	Total wire length per element [mm]	Input impedance at 1 GHz [Ω]	Quality factor Q at 1 GHz
Small wire dipole – Fig 2.5b	3530	20	1.8 -j1095	636
Loaded dipole #1 – Fig 3.2a	1625	60	5.33 -j340	99.2
Loaded dipole #2 – Fig 3.2b	1660	55	8.4 -j378	67.8
Loaded dipole #3 – Fig 3.2c	1445	160	4.9 -j149	56.9
Meandered dipole #4 – Fig 3.4a	960	82	7.5 +j75	147
Meandered dipole #5 – Fig 3.4b	1040	198	9.2 -j43	61.7
Meandered dipole #6 – Fig 3.4c	980	204.5	21.1 +j18	31.3
Meandered dipole #7 – Fig 3.4d	990	204.5	10.5 +j3.9	41.7

and at the same time the currents flow into the same direction, like in case #4, the self-inductance is strong and short wire length is achieved [32], [37]. The longer wire length seems to decrease the gradient of the reactive part of the input impedance, e.g. in case #5. The derivative of the reactive part defines the quality factor Q and the lower the gradient the lower the Q, see Equations (2.33) and (2.35). Looking at Table 3.1, one might conclude that the decrease in the quality factor Q can be directly attributed to the increase in radiation resistance, but this is not the case. The similarity in some results is coincidental.

3.1.3 Helical antennas

The helical antennas fill the spherical volume more efficiently than the wire antennas and are normally tuned to be in self-resonance at the operating frequency and thus the radiation quality factor Q_{rad} is lower than the wire antennas having the same size, as discussed in Section 2.5.2. The dimensions of the dipole helix used in the simulations are: total length of the single element = 16 mm, distance between the feed and the helix structure = 2 mm, distance between the helix and the chassis = 5 mm, diameter of the helix = 4 mm, radius of the wire = 0.04 mm and 9 turns, as shown in Figure 3.6 a). Helix is fed symmetrically like a dipole and it is tuned to be in self-resonance at 900 MHz.

From Figure 3.6 b) one can see that there is a very little effect of the chassis on the bandwidth potential at the self-resonance. At higher frequencies the coupling between the antenna structure and the chassis increases and thus the bandwidth potential decreases. The achievable bandwidth at 900 MHz is ca. 2.3% and decreases rapidly towards 1% bandwidth potential. The drawback is that the helix structure works well only near the self-resonance. Dual-band operation can be achieved by using a dual-band helix. The dual-band helix can be made e.g. by changing the pitch angle of the helix [38]. In this

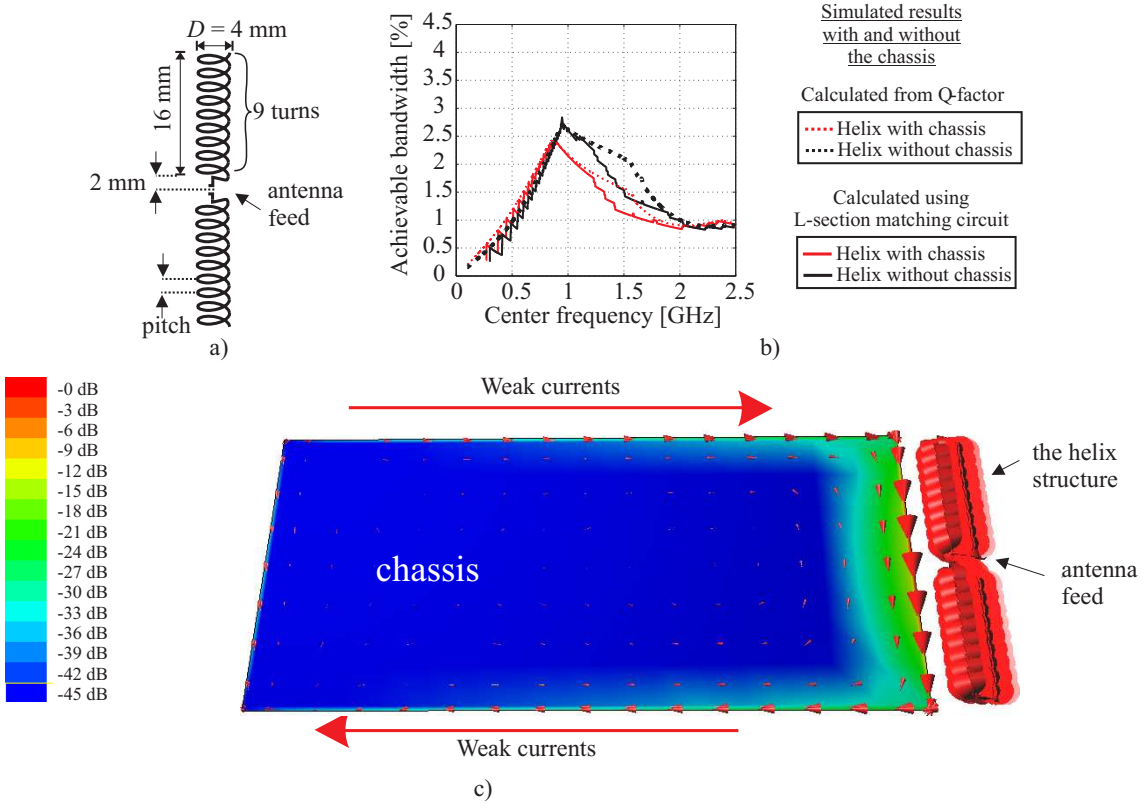

Figure 3.6: a) The helix structure and the dimensions. b) Achievable bandwidth with and without the chassis as a function of the matching frequency and c) the current distribution of the helix and the chassis at 900 MHz (max E-current = 10 A/m).

thesis only the single-band helix having self-resonance at 900 MHz is studied.

As can be seen in Figure 3.6 c), there are very weak differential currents along the long edges of the chassis and thus low coupling to the chassis at 900 MHz. The structure is also very small compared to the top-loaded wire dipole structures. When comparing the helix structure to the meandered wire dipole structures one can see a close relation between them. The helix has a 3D structure and thus it fills the spherical volume better achieving lower radiation quality factor Q_{rad} than the meandered wire dipole of the same size.

In Table 3.2 the helix structure and the best flat wire antenna structure are compared to each other. As can be seen the helix structure gives lower quality factor with shorter total wire length even though the helix has the self-resonance at 925 MHz and the meandered wire dipole case #5 has the self-resonance at 1040 MHz[1]. The volume occupied by the antenna structures is almost the same in both cases: Helix has the volume 0.45 cm^3 and the meandered wire dipole #2 has the volume 0.44 cm^3 (with fictitious 1 mm thickness). The helix has lower Q since it fulfills the spherical volume more efficiently compared to

[1]If the self-resonance of the meandered wire dipole would be tuned to 925 MHz the quality factor Q would be even larger.

the meandered wire dipole, as shown earlier.

Table 3.2: Comparison of the resonant performance properties of the antenna structures with the chassis.

Antenna structure	Resonant frequency [MHz]	Total wire length per element [mm]	Input impedance [Ω]	Quality factor Q
Helix – Fig 3.6c	925	116	18.9 -j57 at 0.9 GHz	48.8 at 0.9 GHz
Meandered dipole case #5 – Fig 3.4b	1040	198	9.2 -j43 at 1 GHz	61.7 at 1 GHz

3.1.4 Bow-tie antennas

The bow-tie antennas are not based on the self-resonance at lower frequencies like the previous wire dipole structures and the helix. Consequently, the bow-tie structures are bigger at lower frequencies compared to the structures based on the self-resonance when a certain bandwidth is required. On the other hand, the bow-tie structures can achieve broadband operation at higher frequencies. Two differently sized bow-tie structures are investigated, one for the lower frequencies (case #2) and one for the higher frequencies (case #1). In Figure 3.7 these two structures are presented.

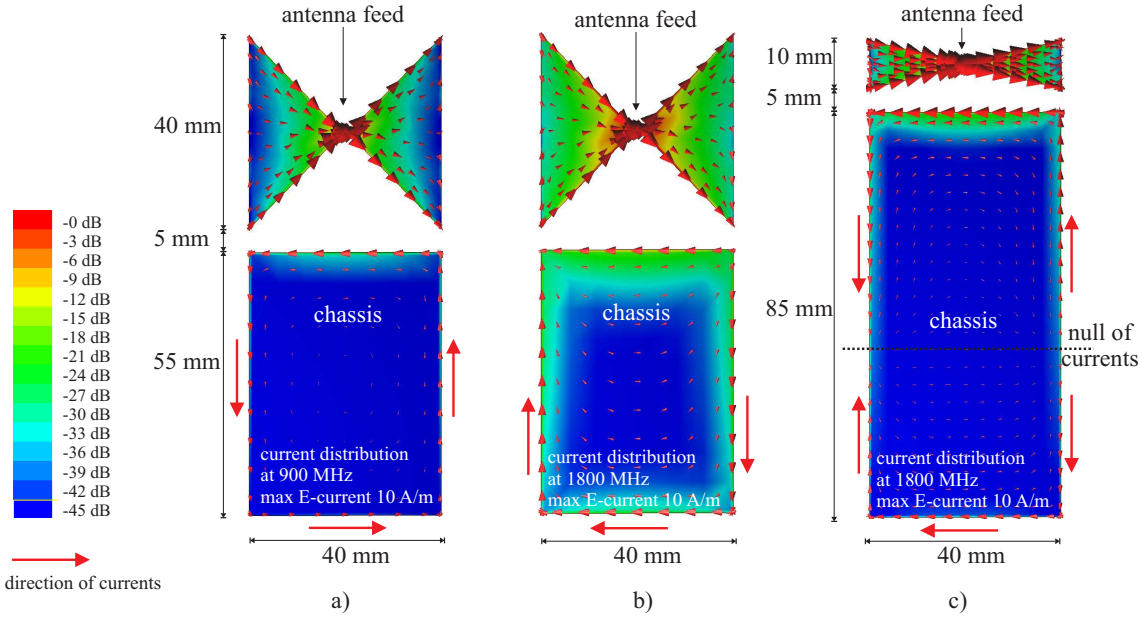

Figure 3.7: a) Bow-tie structure case #2 at 900 MHz. b) Bow-tie structure for case #2 at 1800 MHz. c) Bow-tie structure case #1 at 1800 MHz. (max E-current = 10 A/m).

According to Figure 3.7, one can see that there are differential currents along the long edges of the chassis. The chassis decreases the bandwidth potential more at higher frequencies and thus the effect of the chassis is clearly larger at higher frequencies as

can be seen when comparing Figure 3.8. It can be seen in Figure 3.7 c) that some characteristic wavemodes of the chassis are excited. The characteristic wavemodes are excitation independent and thus they depend only the shape and size of the chassis and frequency. Those wavemodes get probably more significant at higher frequencies and deteriorate the isolation between the chassis and the antenna structure.

The bandwidth potential at 900 MHz in the bow-tie case #2 with the chassis is ca. 1.7% and the chassis decreases the bandwidth potential ca. 15%. At 1800 MHz the bandwidth potential with the chassis is ca. 13.6% and the chassis decreases the bandwidth potential ca. 32%. The size of the bow-tie case #1 is comparable to the meandered wire dipoles cases #4 and #5 but at 900 MHz the achievable bandwidth is only ca. 0.5% with the chassis (see Figure 3.8). At 1800 MHz the achievable bandwidth increases to ca. 4% whereas the achievable bandwidth of the meandered wire dipole case #5 with the chassis is only ca. 1.3%.

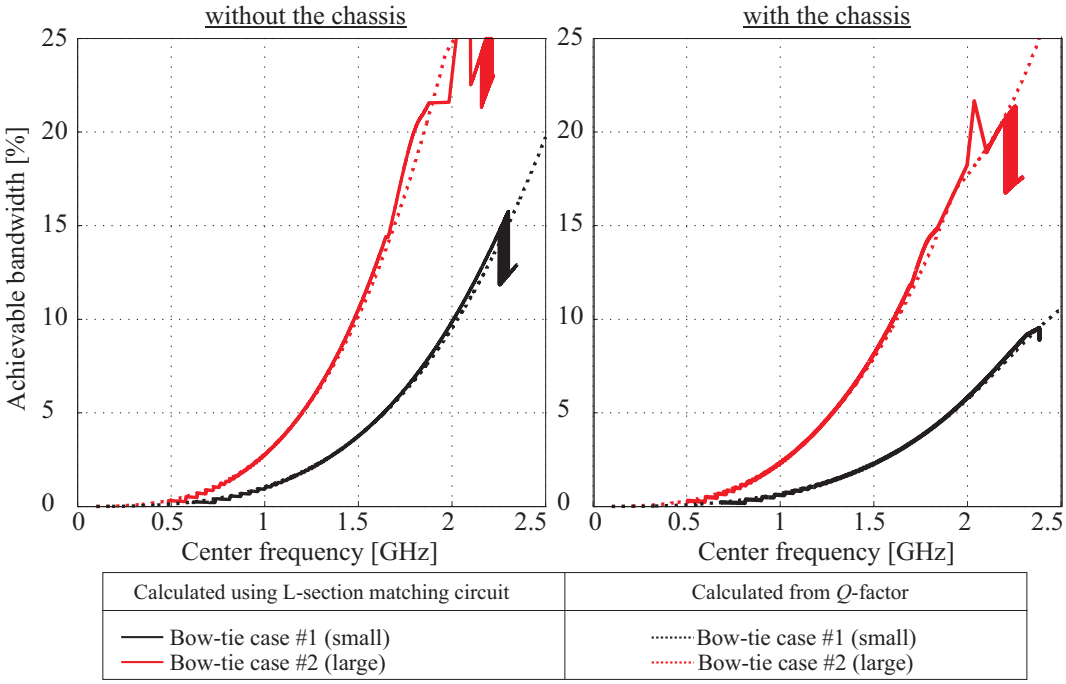

Figure 3.8: Achievable bandwidth potentials of different bow-tie structures with and without the chassis.

In Table 3.3 the bow-tie antenna structures and the helix are compared to each other. One can see that the helix gives good bandwidth performance at lower frequencies but at higher frequencies the bow-tie structures are better. One should note that the poor performance of the helix structure at higher frequencies is due to the self-resonance only at 900 MHz. One can tune the self-resonance of the helix at 1800 MHz to get good performance at higher frequencies, too. In the bow-tie structures, the problem is that the self-resonance is achieved above 2 GHz, if the maximum allowed size is fixed to only 40 mm x 40 mm [length x width]. It might be possible to lower the self-resonance by

Table 3.3: Comparison of the resonant performance properties of the antenna structures with the chassis.

Antenna structure	Self-resonance frequency [MHz]	Total wire length per element [mm]	Input impedance [Ω]	Quality factor Q
Bow-tie case #1	2720	–	2.6 -j536 at 0.9 GHz	230 at 0.9 GHz
Bow-tie case #2	2050	–	3.8 -j223 at 0.9 GHz	67.4 at 0.9 GHz
Helix – Fig 3.6c	925	116	18.9 -j57 at 0.9 GHz	48.8 at 0.9 GHz
Bow-tie case #1	2720	–	10.8 -j177 at 1.8 GHz	27.8 at 1.8 GHz
Bow-tie case #2	2050	–	15.9 -j26 at 1.8 GHz	8 at 1.8 GHz
Helix – Fig 3.6c	925	116	62.8 -j1602 at 1.8 GHz	102 at 1.8 GHz

loading the antenna structure either resistively or capacitively, as shown earlier in Figure 2.15 b) and c), respectively [34], [35].

3.1.5 Capacitive coupling element antennas

As presented earlier in Section 2.5.1, in galvanically isolated antenna structures the capacitive coupling element, later called CCE, is used to couple currents to the surface of the chassis and the antenna resonance is created with a separate matching circuitry outside the coupling element. The ground plane of the antenna structure is galvanically isolated from the chassis of the mobile terminal and the isolation between these objects depends on the coupling and the frequency. The gap between the antenna structure and the chassis of the mobile terminal is fixed to 5 mm. Two different CCE positions are investigated: 1) CCE placed on the top, and 2) CCE placed on the side of the mobile terminal. The purpose is to study the coupling mechanism. Both the solid ground plane and the meandered ground plane are investigated with two different CCE positions.

The self-resonance of the structure with solid ground plane is around 2.5 GHz and the bandwidth potential at 900 MHz with the chassis is only ca. 0.6% when the CCE is placed on the side and ca. 0.9% when the CCE is placed at the top, respectively. It is possible to increase the bandwidth potential by decreasing the self-resonance by meandering the ground plane. In Figure 3.9, the dimensions of the meandered ground plane that has a self-resonance at 860 MHz are presented. The bandwidth potentials with the chassis of the antenna structure with the meandered ground plane at 900 MHz is ca. 1.8% when the CCE is placed on the side and ca. 3.4% when the CCE is placed at the top, as shown in Figure 3.11.

According to Figure 3.10, one can see that when the CCE is placed at the top, there are common mode currents along the long edges of the chassis and the antenna structure and thus create the wavemode which increases the bandwidth potential, as can also be

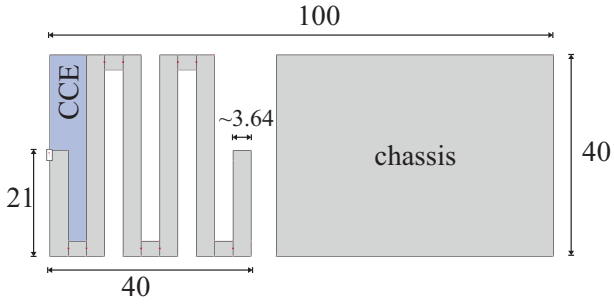

Figure 3.9: The meandered ground plane of the galvanically isolated antenna structure (Dimensions are in mm).

seen in Figure 3.11. When the CCE is placed on the side, there are differential mode currents along the short edges of the chassis and they cancel a part of the radiation in the far field decreasing the bandwidth potential.

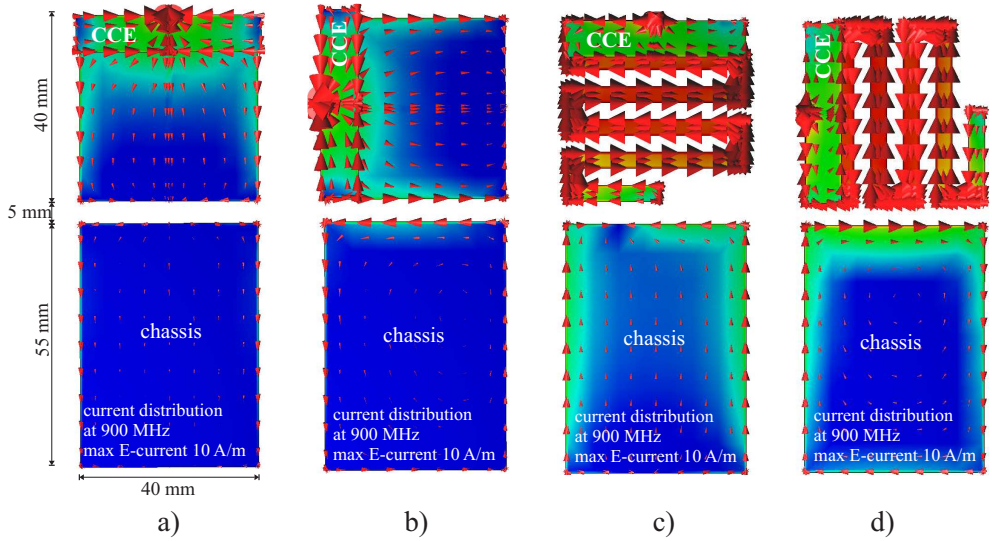

Figure 3.10: The current distributions of the isolated antenna structures at 900 MHz: a) solid ground and the CCE is placed on the top, b) solid ground and the CCE is placed on the side, c) meandered ground and the CCE is placed of the top, d) meandered ground and the CCE is placed of the side.

Table 3.4: Comparison of the resonant performance properties of the antenna structures with the chassis. Input impedances are presented without matching circuit.

Antenna structure	Self-resonance frequency [MHz]	Input impedance at 900 MHz [Ω]	Quality factor Q at 900 MHz
Solid ground + CCE top – Fig 3.10a	2610	0.62 -j100	127
Solid ground + CCE left – Fig 3.10b	2688	0.98 -j100	201
Meandered ground + CCE top – Fig 3.10c	847	39.7 +j107	33.4
Meandered ground + CCE left – Fig 3.10d	852	17.6 +j92	63.7

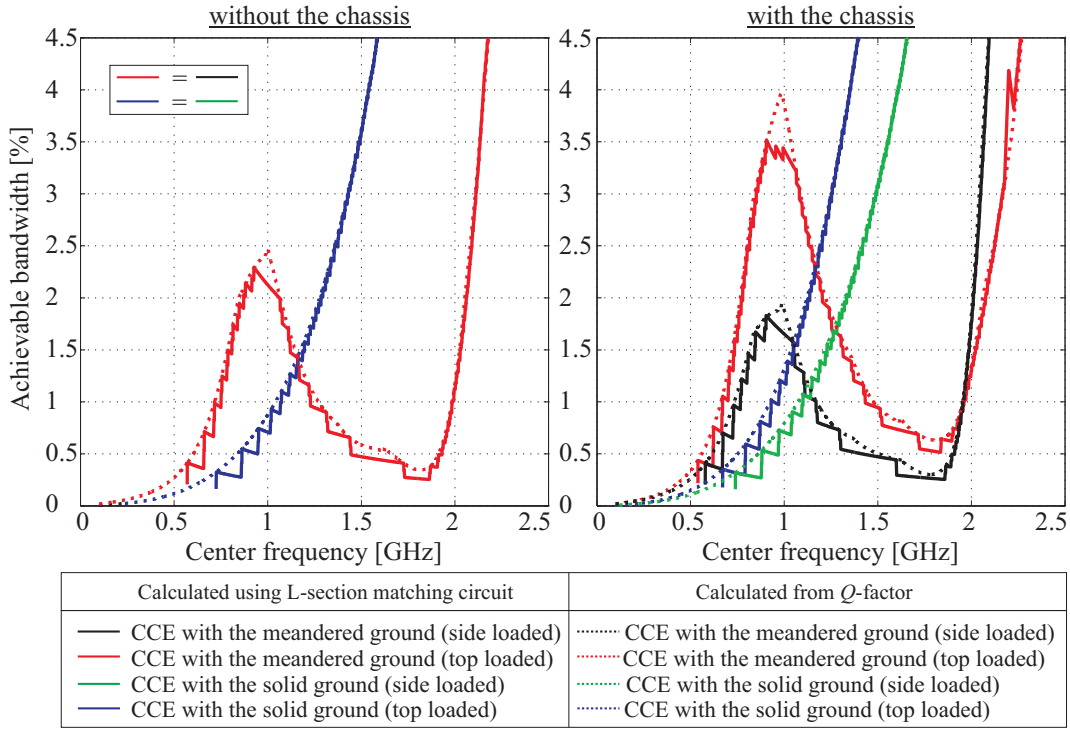

Figure 3.11: Achievable bandwidth potentials of different galvanically isolated antenna structures with and without the chassis. (Please note: The side and top loaded cases are the same in the case without the chassis).

3.2 Summary of the achievable bandwidth potential results

According to Table 3.5, one can see that it is quite difficult to fulfill the bandwidth requirement of ca. 2% at the lower and higher frequency bands at the same time. It can be done but a large antenna structure is needed, like the loaded dipole case #3 or bow-tie case #2. Using small antenna structures, like the helix or the bow-tie case #1 can fulfill the bandwidth requirement only at either lower or higher frequency band.

One has to choose which parameter is the most important when a certain bandwidth is required. The requirement of a small antenna structure gives two options 1) the helix for the lower frequency band or 2) the small bow-tie #1 for the higher frequency band. The requirement of dual-band operation gives two reasonable options 1) the periodically loaded dipole case #3 or the large bow-tie #2. The large bow-tie structure is a little larger than the periodically loaded dipole #3 but gives much larger bandwidth potential at higher frequencies.

The achievable bandwidth potentials, shown in Table 3.5, are calculated using an L-section matching circuit. Simulated frequencies are chosen to correspond the center frequencies of the popular cellular systems, shown in Table 2.1. The results are simulated

Table 3.5: Comparison of the achievable bandwidth potentials of the isolated antenna structures with the chassis.

Structure	Achievable bandwidth potentials with the chassis [%] Center frequency [MHz] 859	920	1795	1920	2035
Reference antenna	5.9	8.9	8.0	8.4	9.4
Small wire dipole – Fig 2.5b	0.2	0.2	3.0	3.7	4.6
Loaded dipole #1 – Fig 3.2a	0.7	0.9	4.6	4.9	5.2
Loaded dipole #2 – Fig 3.2b	1.0	1.3	7.8	8.3	8.7
Loaded dipole #3 – Fig 3.2c	1.2	1.5	7.5	7.7	7.5
Meandered dipole #4 – Fig 3.4a	0.6	0.8	1.2	1.5	1.9
Meandered dipole #5 – Fig 3.4b	1.3	1.5	1.3	1.1	0.9
Meandered dipole #6 – Fig 3.4c	2.0	2.5	2.1	1.7	1.1
Meandered dipole #7 – Fig 3.4d	2.7	3.5	1.3	1.3	1.5
Helix – Fig 3.6c	2.2	2.4	1.1	1.0	0.9
Bow-tie #1 small – Fig 3.7a	0.4	0.5	4.1	5.1	6.2
Bow-tie #2 large – Fig 3.7b	1.5	1.8	14.3	18.0	21.7
Solid ground + CCE top – Fig 3.10a	0.7	1.0	8.6	8.2	8.2
Solid ground + CCE left – Fig 3.10b	0.4	0.5	6.1	7.2	8.5
Meandered ground + CCE top – Fig 3.10c	3.2	3.5	0.6	0.8	1.6
Meandered ground + CCE left – Fig 3.10d	1.7	1.8	0.3	0.7	2.6

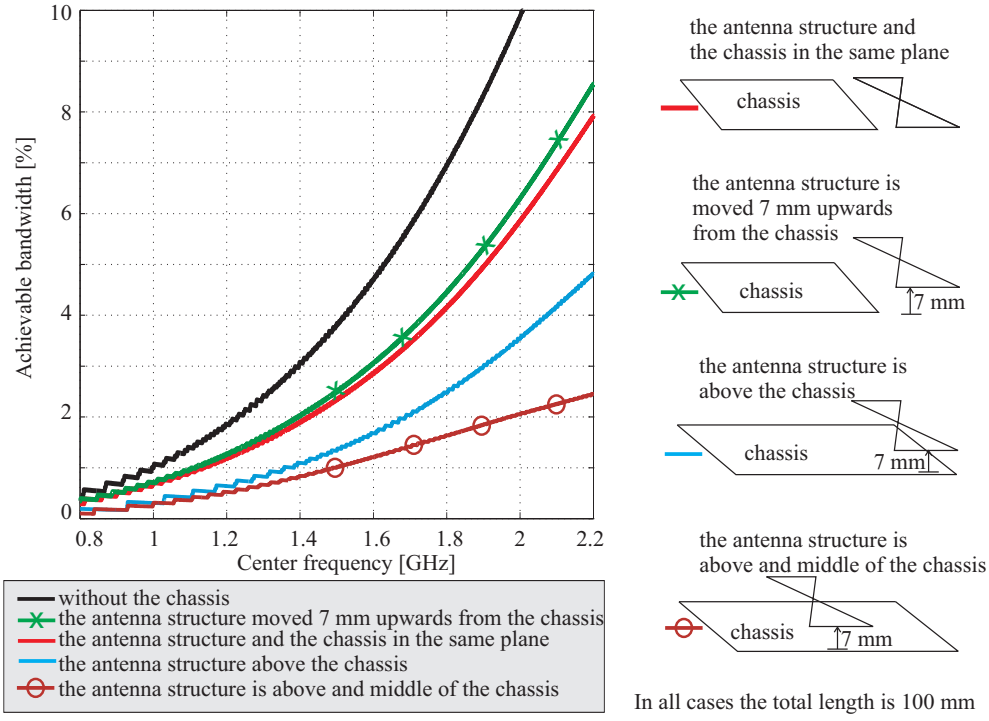

Figure 3.12: Achievable bandwidth potentials of the small bow-tie #1 structure in different antenna structure positions.

with the chassis in the same plane as the antenna structure but the planar balanced antenna structure gives the possibility to move antenna structure 7 mm upwards from the chassis. There is a comparison of the effect of moving the small bow-tie #1 antenna structure upwards from the chassis in Figure 3.12. One can see, that the effect of the moving the antenna structure further from the chassis is quite small on the bandwidth potential but might be significant e.g. on specific absorption rate (SAR) and therefore these different positions for the antenna structures are used later when e.g. the effect of the user and the SAR are investigated.

One can also ask, what happens if the antenna structure is placed above the chassis. In Figure 3.12 this is investigated. As can be seen, the achievable bandwidth potential collapses when the antenna element is placed above the 100-mm-long chassis and it can also be seen that the bandwidth potential will decrease even more if the antenna structure is moved toward the center of the chassis. The benefits of this placement might be the lower SAR hence the chassis acts as a shielding and decrease the field values on the other side.

3.3 Far field distributions of certain isolated antenna structures

In this section the radiation patterns of the reference antenna and one promising balanced structure (the small bow-tie) are handled. The radiation patterns are simulated in free space without the hand. Also the cases with and without the chassis are investigated to see the effect of the chassis. The radiation patterns are plotted at 920 MHz and 1795 MHz frequencies which correspond the center frequencies of GSM 900 and 1800 systems, respectively. The radiation patterns are normalized to the maximum of 0 dB gain.

The simulated radiation patterns of the reference antenna and small bow-tie case #1 are shown in Figures 3.13 and 3.14. As can be seen these two antenna structures behave quite differently. The reference antenna has a good omnidirectional radiation in the azimuthal plane ($x-y$ plane) at both frequencies whereas the small bow-tie case #1 has a good omnidirectional radiation in the elevation plane ($x-z$ plane). In Figure 3.14 can be seen that the chassis changes the radiation pattern compared to the case without the chassis. The radiation pattern without the chassis is very similar to the typical radiation pattern of a dipole antenna and thus is shaped as a doughnut. The minimum of the radiation pattern is achieved on y-axis. When the chassis is present the doughnut shape is changed and in the azimuthal plane ($x-y$ plane) a little cross-polar component is created. The cross-polar component increases at higher frequencies and thus the effect of the chassis is getting more significant though it is still much smaller than in the reference antenna case. All the balanced antenna structures behave in a similar way. In Appendix

A, all the radiation patterns of the balanced antenna structures are presented.

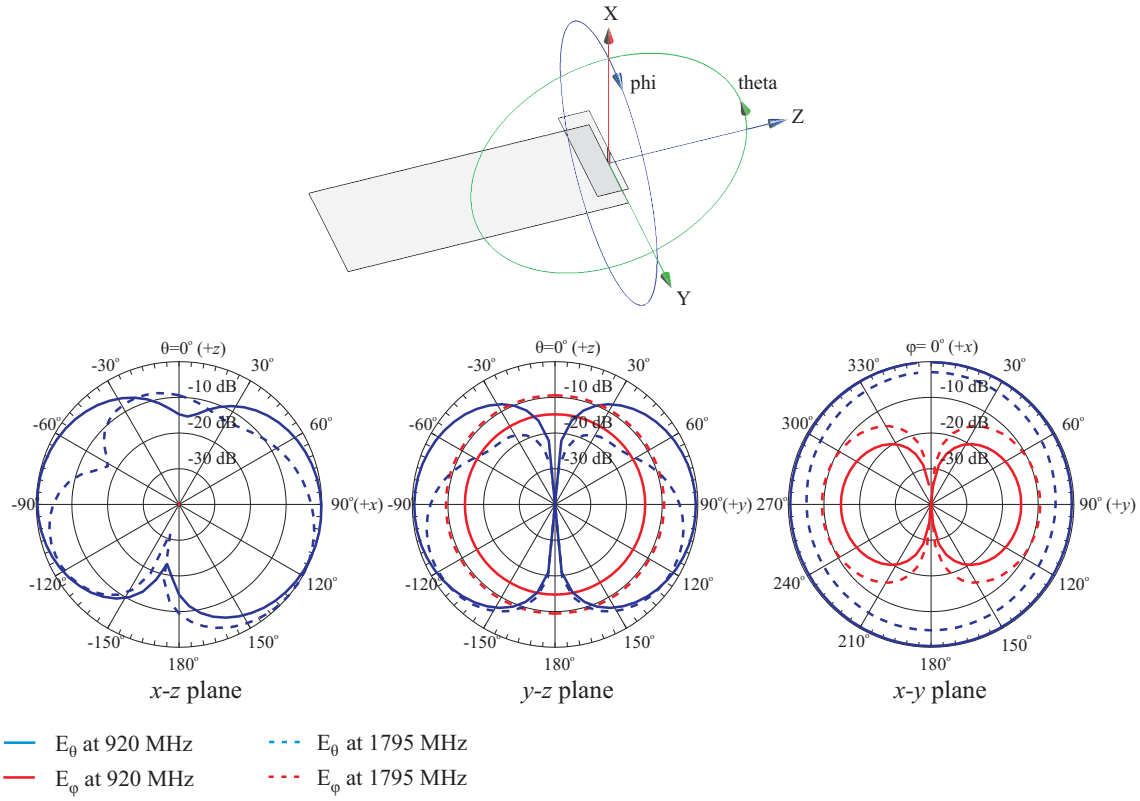

Figure 3.13: Simulated radiation patterns at 920 MHz and 1795 MHz of the reference antenna.

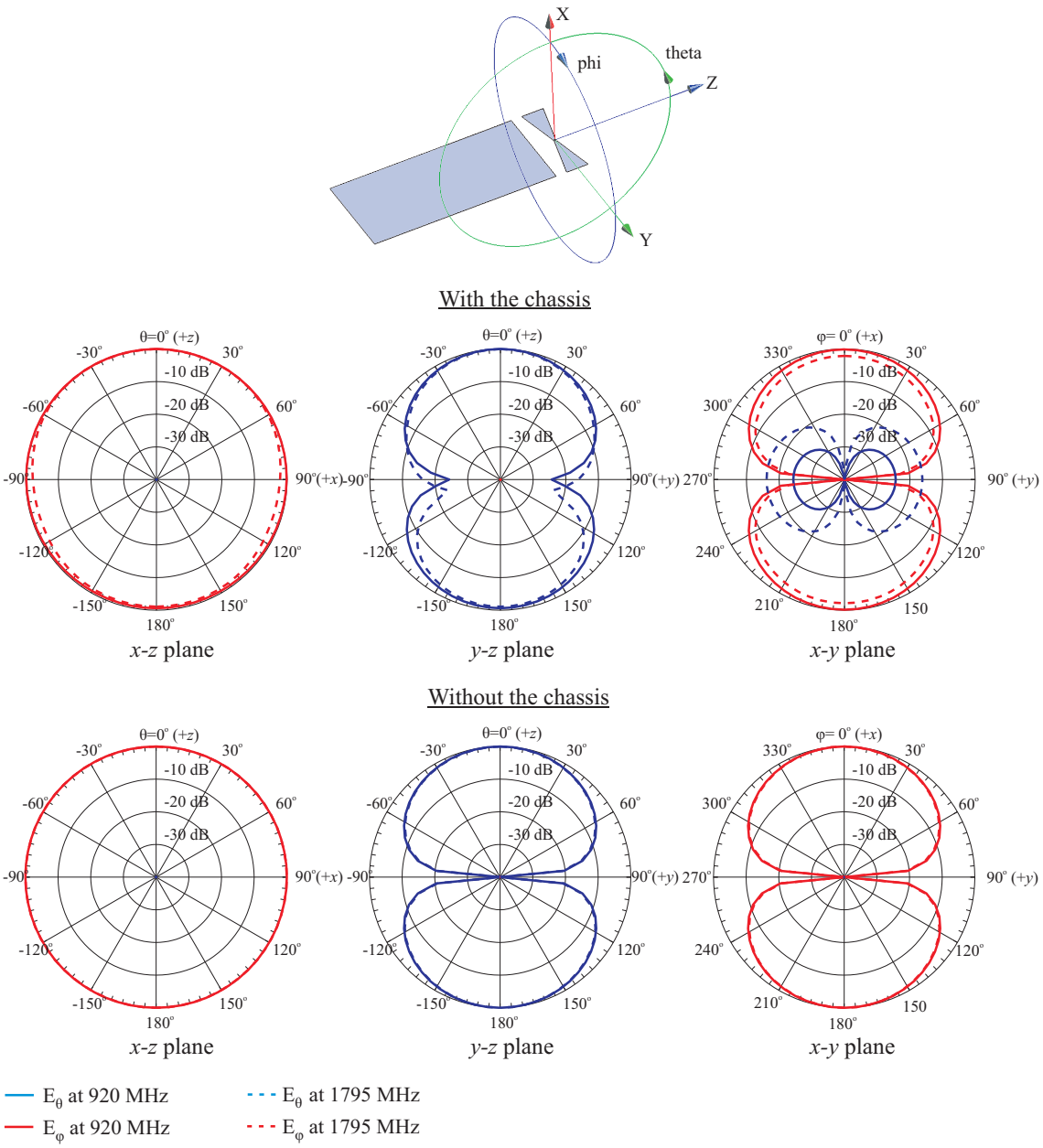

Figure 3.14: Simulated radiation patterns at 920 MHz and 1795 MHz of the small bow-tie #1 with and without the chassis.

CHAPTER 4

User interaction of the isolated antenna structures

This chapter handles possible benefits and drawbacks of the isolated antenna structures in mobile terminals. In the previous chapter the feasibility of the isolated antenna structures was investigated concerning mainly the bandwidth potential and in this chapter the most promising structures are studied further. When the current distribution is highly concentrated on the antenna structure there are obviously some benefits and drawbacks on the performance of the mobile terminal antenna. At first in Section 4.1 the effect of the user on matching and radiation efficiencies is investigated. In Sections 4.2 and 4.3 specific absorption rate (SAR) and hearing-aid compatibility (HAC) values are simulated and discussed.

4.1 Effect of the user on matching and radiation efficiency

Mobile terminals must work properly with and without the effect of the user. In the vicinity of the user, the antenna parameters, like the impedance matching, radiation efficiency and radiation pattern change compared to the free space -case and might thus complicate the operation of the antenna or even make it impossible to work properly. To avoid these problems the effect of the user must be taken into consideration when the mobile terminals are designed. As mentioned earlier, especially at lower UHF frequencies, below 1 GHz, a significant portion of the power is radiated by the chassis and thus the effect of the user is significant because the hand of the user changes the matching and decreases the radiation efficiency as well as changes the radiation pattern. At higher GSM frequencies (over 1.8 GHz) the antenna element is increasingly the main radiator and thus the hand of the user might deteriorate the operation of the antenna if the antenna element is close to the hand.

In this thesis one of the goals is to study if the effect of the user can be reduced by isolating the antenna structure from the chassis. First hand model and simulation setup are introduced and in the end simulation results of some promising isolated antenna structures are presented.

4.1.1 Hand model and simulation setup

The effect of the user is studied by comparing the results from free space simulations with results when the antenna structure is held in hand. All the simulations are made with finite-difference time-domain (FDTD) based electromagnetic simulator SEMCAD X [39]. The maximum FDTD-mesh cell size in the antenna structure and hand model is $\Delta x = \Delta y = \Delta z = 1.0$ mm. The smallest wavelength in the hand tissue at 1800 MHz is 29.2 mm and the maximum diagonal of the cell is $\Delta x \cdot \sqrt{3} = 1.73$ mm so that there are at least 16 cells per wavelength. In the free space the maximum cell size is 10 mm at 900 MHz and 5 mm at 1800 MHz. That was found to be a good compromise between the simulation accuracy and a reasonable simulation time.

The effect of the user on matching is investigated by broadband simulation. In the broadband simulation a Gaussian sine waveform is used as the excitation of the simulation and it is defined as follows: center frequency $f_c = 1450$ MHz and bandwidth $BW = 2$ GHz. The dielectric material of the hand is modelled having electrical properties at center frequency 1450 MHz so a small error is made and the error is largest at the edges. The effect of the user on radiation efficiency is investigated by using harmonic simulation. In the harmonic simulation a sinusoidal waveform is used as excitation of the simulation and the frequencies are excited at 900 MHz and 1800 MHz frequencies. Tissue equivalent material parameters for the homogeneous hand models used in these simulations are calculated by C. Gabriel and are listed in Table 4.1 [40].

Table 4.1: Standardized dielectric parameters of the hand phantom [40].

	Frequency [MHz]		
	900	1450	1800
permittivity $\epsilon_r^{'}$	36.2	33.8	32.6
conductivity σ_d [S/m]	0.79	1.07	1.26

The used hand model is based on ongoing standardization work of the hand phantom and the hand model is made from homogeneous material and thus bones are excluded [41]. There are different handgrips available and it depends on the used mobile terminal which hand model suites best. In this work a mono-block grip is used. The mono-block grip suites best for 'candybar' style mobile terminal and in this hand model the index finger is touching the upper part of the enclosure of the mobile terminal, as shown in Figure 4.1 b). The mono-block grip is designed based on the grip study findings and this grip

is used when the mobile terminal is held in the talking position [41].

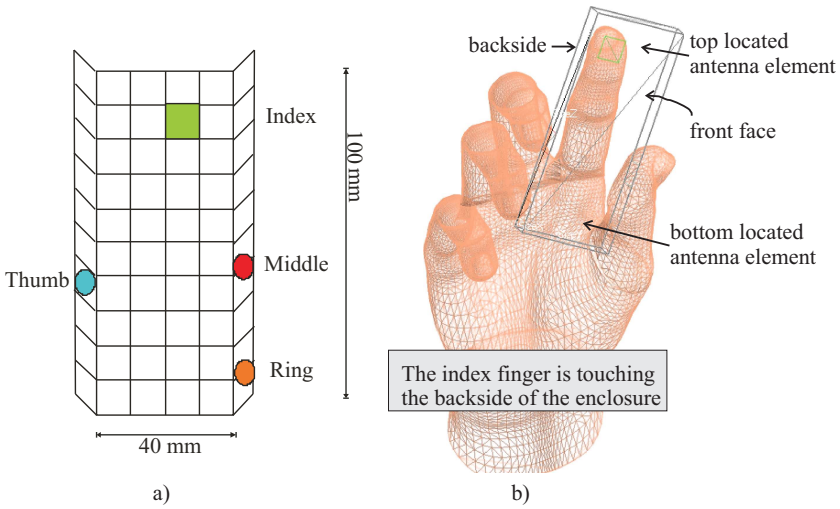

Figure 4.1: a) The places of the fingers and b)monoblock grip of the hand phantom used in simulations (talk position).

The antenna structure with chassis is placed inside a virtual enclosure of dimensions 102 mm x 42 mm x 9 mm [length x width x thickness]. The enclosure is modelled here to help placing the antenna structure in the correct place and it is not taken into consideration in the simulations. The places of the fingers are shown in Figure 4.1 a) and the fingers are touching the enclosure (except the pinky is not touching the enclosure) so that there is at least 1 mm gap between the antenna structure and the fingers.

The metal parts are modeled as perfect electric conductors (PEC) and hence all the losses are caused by the hand. In that case the interpretation of the results is easier and the effect of the hand can be seen clearly.

Two different positions for the planar balanced antenna elements are used: 1) front position where the antenna element is in the front face of the mobile terminal (the chassis and the antenna structure are in the same plane) and 2) back position where the antenna structure is in the backside of the mobile terminal. In this case the antenna structure is moved 7 mm upwards from the chassis and thus the antenna element is close to the index finger, as shown in Figure 4.2.

Two different locations are investigated for the antenna element: 1) top located antenna element, and 2) bottom located antenna element, as shown in Figure 4.1 b). In both of these locations also two different positions for the planar balanced antenna elements are used.

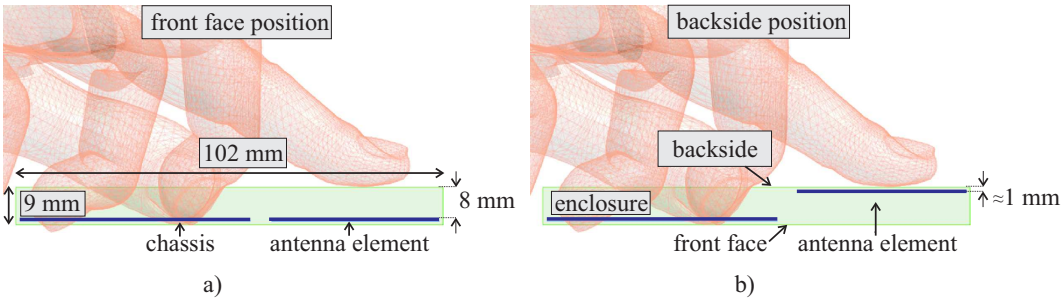

Figure 4.2: Two different positions for the planar balanced antenna structures. a) front position and b) back position.

4.1.2 Simulation results

The simulations are done so that first the antenna structure is simulated with SEMCAD in the free space without the hand. The matching circuits are not included in the SEMCAD simulations and thus the effect of the external matching circuits is added later with APLAC circuit simulator [42]. The used matching circuits are shown in Figure 4.3. To be able to see the change of the resonance frequency the same matching circuit is used also in the cases when the hand model is present.

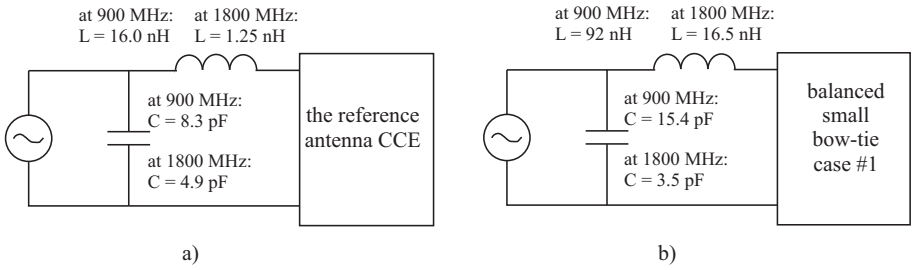

Figure 4.3: Matching circuits used for the a) reference antenna and b) small bow-tie case#1.

Here only the small bow-tie case #1 is handled thoroughly. In Figure 4.4 the reflection coefficient of the reference antenna and the small bow-tie case #1 are presented in the Cartesian coordinate system and on the Smith chart. The reflection coefficient is presented in free space and when the antenna structure is held with hand at the top or bottom locations. As can be seen from Figure 4.4 a) and c) the hand decreases the resonant frequency of the antenna at both frequency bands more in the reference antenna case than in the small bow-tie antenna case except at 1.8 GHz when the small bow-tie is bottom located. The top located antenna element decreases the resonant frequency more than the bottom located antenna element in the reference antenna case whereas the small bow-tie the situation is the other way. As can be seen in Figure 4.4 d), the coupling loop is much smaller for the small bow-tie than for the reference antenna when the antenna element is bottom located (red line). This indicates that the losses caused by the hand are increased, as can be seen in Table 4.3.

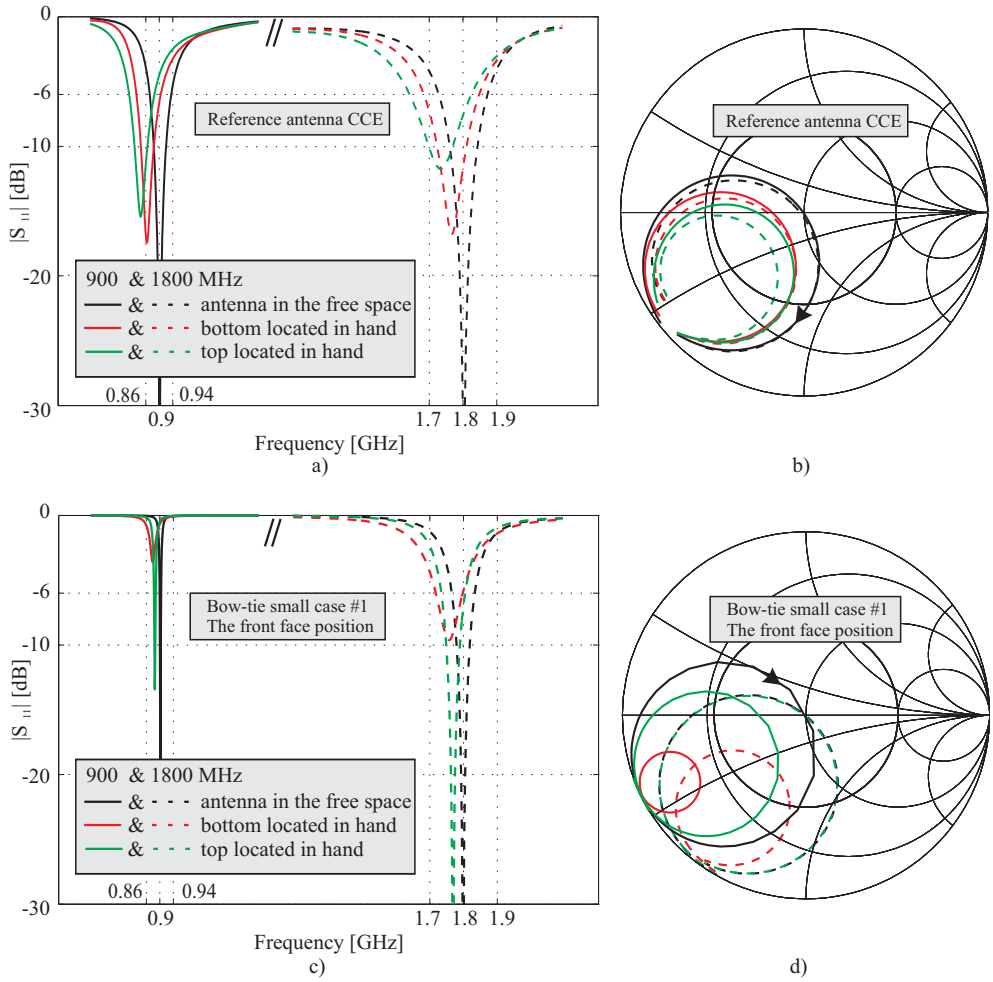

Figure 4.4: The effect of the user on matching of the reference antenna a) in the Cartesian coordinate system and b) on the Smith chart. The effect of the user on matching of the small bow-tie antenna c) in the Cartesian coordinate system and d) on the Smith chart.

In Tables 4.2 and 4.3 all the simulation results of the user effect on the matching and radiation efficiency η_{rad} are presented. All the antenna structures are matched at 900 MHz and 1800 MHz in the free space and then the effect of the hand is investigated when the antenna element is either top or bottom located. In Table 4.2, the resonant frequency with the hand and then the difference of the resonant frequency to the free space case are shown. In Table 4.3 the radiation efficiency η_{rad} is presented in the percentage and decibels values. Also the two different positions for the planar balanced antenna elements are studied in both tables.

As can be seen in Tables 4.2 and 4.3, there are couple of trends: 1) The big balanced antenna structures, like the large bow-tie case #2 or periodically loaded dipole case #3 perform well when the antenna element is far from the index finger (antenna element in the front face) but when the index finger is close the resonant frequency decrease substantially much. 2) The small antenna structures, like the small bow-tie, are quite

Table 4.2: The effect of the user on matching.

	The effect of the hand on matching							
	900 MHz				1800 MHz			
	antenna element top		antenna element bottom		antenna element top		antenna element bottom	
Structure	f_r [MHz]	Δf_r [%]	f_r [MHz]	Δf_r [%]	f_r [MHz]	Δf_r [%]	f_r [MHz]	Δf_r [%]
Reference antenna	848	-5.8	863	-4.1	1735	-3.6	1768	-1.8
Periodically loaded dipole case #3 (front)	891	-1.0	860	-4.4	1791	-0.5	1740	-3.3
Periodically loaded dipole case #3 (back)	841	-6.6	832	-7.6	1760	-2.2	1675	-6.9
Meandered dipole case #5 (front)	899	-0.1	872	-3.1	1808	+0.4	1774	-1.4
Meandered dipole case #5 (back)	892	-0.9	860	-4.4	1790	-0.6	1759	-2.3
Helix	896	-0.4	865	-3.9	1799	0	1796	-0.2
Bow-tie small #1 (front)	885	-1.7	879	-2.3	1770	-1.7	1757	-2.4
Bow-tie small #1 (back)	884	-1.8	871	-3.2	1771	-1.6	1736	-3.6
Bow-tie large #2 (front)	890	-1.1	848	-5.8	1819	+1.1	1748	-2.9
Bow-tie large #2 (back)	808	-10.2	809	-10.1	1735	-3.6	1648	-8.4
Meandered ground + CCE top (back)	880	-2.2	872	-3.1	1791	-0.5	1787	-0.7
Meandered ground + CCE side (back)	876	-2.7	832	-7.6	1790	-0.6	1791	-0.5

f_r is the resonant frequency with the hand phantom.
Δf_r is the difference of the resonant frequency to the free space case.
green color means better performance compared to the reference antenna
red color means deteriorated performance compared to the reference antenna

robust to the distance between the index finger and the antenna element. In the all balanced antenna structures the top location is better. When the antenna element is bottom located, the palm decreases the resonant frequency and absorbs the power more compared to the top located case, as can also be seen in Table 4.3. If we compare the frequency shift (Δf_r) results to the reference antenna we see that the balanced antenna structures perform especially well at lower 900 MHz frequency but at higher frequencies the advantage is almost lost, especially if the antenna element is bottom located as it is in many mobile terminals nowadays. When comparing the radiation efficiencies, shown in Table 4.3, one can see that the balanced antenna structures have almost constant radiation efficiencies at both frequencies when the antenna elements are bottom located. The helix seems to be very good at 1800 MHz frequency but the available bandwidth is only ca. 1% and there is an anti-resonance and thus the antenna is not radiating well. Galvanically isolated antenna structures perform very well compared to the reference

Table 4.3: The effect of the user on radiation efficiency.

Structure	The effect of the hand on radiation efficiency 900 MHz antenna element top η_{rad} [%]	[dB]	900 MHz antenna element bottom η_{rad} [%]	[dB]	1800 MHz antenna element top η_{rad} [%]	[dB]	1800 MHz antenna element bottom η_{rad} [%]	[dB]
Reference antenna	46	-3.4	48	-3.2	36	-4.4	53	-2.8
Periodically loaded dipole case #3 (front)	63	-2.0	37	-4.3	69	-1.6	57	-2.4
Periodically loaded dipole case #3 (back)	41	-3.9	35	-4.6	54	-2.7	52	-2.8
Meandered dipole case #5 (front)	64	-1.9	35	-4.6	-	-	-	-
Meandered dipole case #5 (back)	46	-3.4	32	-4.9	-	-	-	-
Helix	77	-1.1	33	-4.8	-	-	-	-
Bow-tie small #1 (front)	77	-1.1	35	-4.6	80	-0.9	53	-2.8
Bow-tie small #1 (back)	53	-2.8	32	-4.9	67	-1.7	48	-3.2
Bow-tie large #2 (front)	61	-2.1	36	-4.4	69	-1.6	59	-2.3
Bow-tie large #2 (back)	38	-4.2	35	-4.6	52	-2.8	56	-2.5
Meandered ground + CCE top (back)	69	-1.6	44	-3.6	27	-5.7	40	-4.0
Meandered ground + CCE side (back)	54	-2.7	34	-4.7	33	-4.8	27	-5.7
Solid ground + CCE top (back)	52	-2.8	41	-3.9	52	-2.8	50	-3.0
Solid ground + CCE side (back)	34	-4.7	43	-3.7	52	-2.8	57	-2.4

green color means better performance compared to the reference antenna
red color means deteriorated performance compared to the reference antenna

antenna and the effect of the user on matching is very small in many cases.

4.2 Specific absorption rate

During the recent years, the use of mobile phones has increased rapidly. At the same time the concern on electromagnetic radiation that mobile phones emit has also increased. According to the current knowledge, the main influence that electromagnetic radiation (UHF) has on humans is the rise in the tissue temperature and the temperature rise on the surface of the brain is shown to be not more than $0.2 - 0.3°C$ [43], [44]. As a comparison, the normal fluctuation of body temperature is around $\pm 1°C$, and in

exhausting physical exercise even a temperature rise of 2°C is quite common. Thus we can assume that the effect of the temperature rise caused by electromagnetic radiation is very small.

Disadvantages of the electromagnetic radiation of the mobile phones are investigated in order to determine the safety factors of the electromagnetic radiation. The safety factors are based on the scientific and experimental studies and the safety margin is very large. At UHF frequencies the safety margin is designed to protect against adverse health effects resulting from tissue heating [43]. However, according to the latest research results the electromagnetic radiation could cause temporary changes, for example, in the functions of cells. It has been observed that electromagnetic radiation can accelerate production of protein in the cells. The activator for these changes is unknown but it is known that this phenomenon is not the result of excessive heating of tissues [45].

In [46] the possibility that electromagnetic radiation can open a significant leakage of albumin through the blood-brain barrier (BBB) is investigated. Rats were exposed for 2 hours to electromagnetic radiation of a GSM mobile phone of different strengths. In that research, highly significant evidence is found for neuronal damage in both the cortex, the hippocampus and the basal ganglia in the brains of exposed rats and these changes are caused by nonthermal microwave exposure [46].

The problems with these research studies (e.g. [45] and [46]) are related to the repeatability of low-level effects.

In order to estimate the influence of the electromagnetic radiation, measurement standard has been developed. The Specific Absorption Rate (SAR) is a measure of the rate of radio energy absorption in body tissue. The SAR is defined as the power absorbed per mass of tissue and has units of watts per kilogram (W/kg) [47]:

$$SAR = \frac{\Delta P}{\Delta m} = \sigma_d \frac{|E_{rms}|^2}{\rho_d}, \tag{4.1}$$

where σ_d is the effective conductivity of the tissue (S/m), E_{rms} is the root mean square (rms) value of the electric field strength (V/m) in the tissue , and ρ_d is the mass density of the tissue (kg/m^3). The maximum local SAR is averaged over a specified volume or mass of tissue in the shape of a cube (IEEE) or any shape of tissue (ICNIRP). There are at least two different recommendations used for the SAR; in Europe the ICNIRP recommendations [48] are widely followed and in the United States the IEEE C95.1 1999 Edition is used. The IEEE C95.1, 1999 Edition [47] safety limits are stricter than the ICNIRP limits for the averaged mass (1 g vs. 10 g) and for the localized SAR in the head (1.6 W/kg vs. 2 W/kg). The safety limits of SAR are presented in Table 4.4.

According to the latest simulation and measurement results the absorption of the RF

Table 4.4: Basic restrictions for SAR values set by IEEE and ICNIRP.

Standard	Whole-body average SAR [W/kg]	Localized SAR (in head) [W/kg]	Localized SAR (e.g. hands, wrist) [W/kg]	Averaged mass of tissue [g]
IEEE Std C95.1 1999 Edition [47]	0.08	1.6	4	1
IEEE Std C95.1 2005 Edition [43]	0.08	2	4	10
ICNIRP [48]	0.08	2	4	10

energy requires a mass of tissue rather than a (partially empty) geometric volume [43]. Therefore the IEEE C95.1, 2005 Edition safety limits have been changed to correspond the averaging 10 g mass of tissue. However, according to the author's knowledge the current safety limits (year 2009) in the United States are based on the IEEE C95.1, 1999 Edition.

The SAM head phantom used in SAR measurement has been developed by the IEEE Standards Coordinating Committee (SCC34/SC2/WG1). The outer part of the SAM head phantom is made of a lossless plastic shell with an ear spacer [49]. The SAM shell is filled with a homogeneous fluid having the electrical properties of head tissue at the test frequency, see Table 4.5. Here the used SAM head phantom is provided by SEMCAD.

4.2.1 SAR simulation setup

The studied antenna structures are bottom located in all cases and the distance between the ear of the SAM head phantom and the antenna structure is 6 mm, as shown in Figure 4.5 a). The used antenna position is cheek/touch position, see Appendix B (Figure B.1). The antenna structures are bottom located because otherwise it is not possible to fulfill the HAC requirement (to be shown later) and because many mobile terminals available today have a bottom located antenna element, like Nokia 5800 XpressMusic or Apple iPhone 3G.

Two different positions for the planar balanced antenna structures are used: 1) front position where the antenna element is on the front face of the mobile terminal (the chassis and the antenna structure are in the same plane) and 2) back position where the antenna structure is on the backside of the mobile terminal. In this case the antenna structure is moved 7 mm upwards from the chassis and the distance of the chassis from the head is still 3 mm, as shown in Figure 4.5 b).

The localized SARs are calculated with two different averaging masses of tissue (1 g and 10 g) and the simulations are done for the E-GSM900 and GSM1800 frequencies which are 915 MHz and 1730 MHz, respectively. The simulated SAR values are normalized to

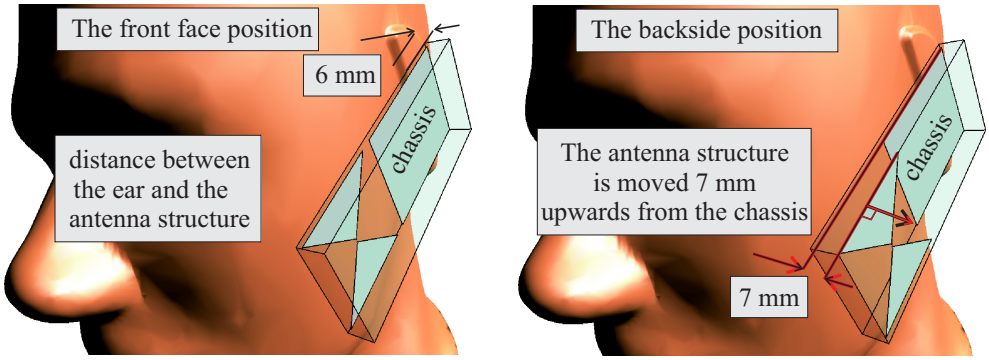

Figure 4.5: a) The antenna structure is in the same plane as the chassis, and b) the antenna structure is moved 7 mm upwards. In both cases the antenna structures are bottom located.

250 mW and 125 mW which are the maximum mean (rms) radiated powers of E-GSM900 and GSM1800 systems, respectively. The radiation efficiencies take into account only the losses of the head; the chassis and antenna are lossless.

The SAR values are simulated with finite-difference time-domain (FDTD) based electromagnetic simulator SEMCAD X [39]. The used dielectric parameters of the head phantom are listed in Table 4.5.

Table 4.5: Standardized dielectric parameters of the head phantom [49].

	Frequency [MHz]	
	900	1800 - 2000
ϵ_r'	41.50	40.0
σ_d [S/m]	0.97	1.4

4.2.2 SAR results

First the SAR values and the SAR distributions of the reference antenna are introduced. Figure 4.6 shows the SAR distribution and it is clearly seen that the SAR distribution is smooth since the whole chassis radiates. The red dot shows the location of the maximum SAR. The reference antenna also fulfills the ICNIRP SAR limit at both frequency bands even though a simple metal prototype structure is used, as can be seen in Table 4.6.

Next the SAR values of the isolated antenna structures are handled. There are two different positions for the planar balanced antenna structures and one position for the balanced helix and the galvanically isolated structures. The results of the SAR simulations for the front face positions are listed in Table 4.6 and the results for the backside positions are listed in Table 4.7.

Figure 4.7 shows the SAR distribution of the periodically loaded dipole case #3 and

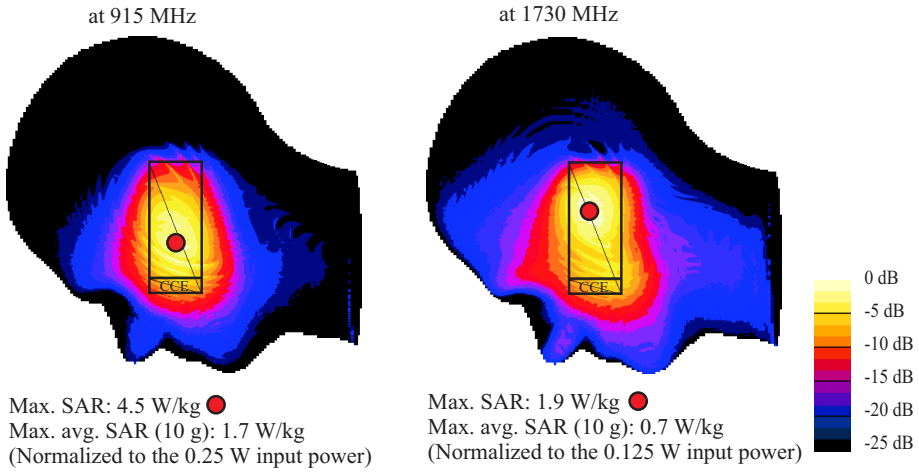

Figure 4.6: SAR distribution [dB] of the reference antenna on the surface of the head at 915 MHz and 1730 MHz.

Table 4.6: SAR values [kg/W] in the head with different averaging masses and frequencies. In all cases the antenna structures are bottom located and the antenna elements are in the front face position except the galvanically isolated structures, where the antenna elements are in the backside position.

Close position (gap 3 mm) Structure	at 915 MHz 1 g [W/kg]	10 g [W/kg]	η_{rad} [%]	at 1730 MHz 1 g [W/kg]	10 g [W/kg]	η_{rad} [%]
Reference antenna CCE (gap 9.6 mm)	2.4	1.7	30	1.2	0.7	47
Periodically loaded dipole case #3	8.5	4.9	8	6.5	3.2	22
Meandered dipole case #5	6.5	3.8	17	3.3	1.8	19
Helix	4.5	2.6	20	-	-	-
Bow-tie case #1 (small)	6.9	3.9	14	4.2	2.2	39
Bow-tie case #2 (large)	8.4	4.9	7	7.1	3.5	22
Solid ground + CCE top	1.4	1.0	52	1.1	0.7	56
Solid ground + CCE left	3.4	2.0	37	2.7	1.5	42
Meandered ground + CCE top	4.6	3.0	23	6.5	2.8	12
Meandered ground + CCE side	6.9	4.4	9	7.8	2.7	15

at 915 MHz SAR values are normalized to 0.25 mW input power
at 1730 MHz SAR values are normalized to 0.125 mW input power
green color means that the SAR values are under the safety limits
red color means very high SAR values (over 4 W/kg)

it can be clearly seen that the SAR distribution is highly concentrated near the antenna structure and this is because all the power is radiated directly by the antenna structure and the chassis is not used as a radiator. All the isolated antenna structures behave basically in the same way. The periodically loaded dipole case #3 is investigated here thoroughly because it fulfills the bandwidth requirement of ca. 2% at lower and higher frequency bands. The SAR value of this prototype structure is below EU SAR-

Table 4.7: SAR values [kg/W] in the head averaged to the 10 g mass of tissue at 915 MHz and 1730 MHz. In all cases the antenna structures are bottom located and the antenna elements are in the backside position.

Far position (gap 10 mm)	at 915 MHz			at 1730 MHz		
Structure	Avg. 10 g [W/kg]	difference to the front position [%]	η_{rad} [%]	Avg. 10 g [W/kg]	difference to the front position [%]	η_{rad} [%]
Reference antenna CCE (gap 9.6 mm)	2.4	-	30	1.2	-	47
Periodically loaded dipole case #3	3.5	-29%	20	1.6	-50%	47
Bow-tie case #1 (small)	2.7	-31%	38	0.9	-59%	61
Bow-tie case #2 (large)	3.8	-22%	16	1.9	-46%	43

at 915 MHz SAR values are normalized to 0.25 mW input power
at 1730 MHz SAR values are normalized to 0.125 mW input power
green color means that the SAR values are under the safety limits

requirement only at 1730 MHz when the antenna structure is in the backside position, as can be seen in Table 4.7.

As can be seen in Table 4.6 the SAR values are very high for the isolated antenna structures, also when compared to the reference antenna and it is not possible to fulfill the SAR requirements. The only exceptions are the galvanically isolated structures with the solid ground planes but those structures do not fulfill the bandwidth requirements at 900 MHz. From Table 4.7 one can see that when moving the antenna structure 7 mm upwards (to the backside position) it is possible to decrease the SAR values ca. 27% at 915 MHz and ca. 52% at 1730 MHz. As a result the SAR requirement is fulfilled at the higher 1730 MHz frequency band, when the antenna structure is in the backside position. Moving the antenna structure further also increases the radiation efficiency.

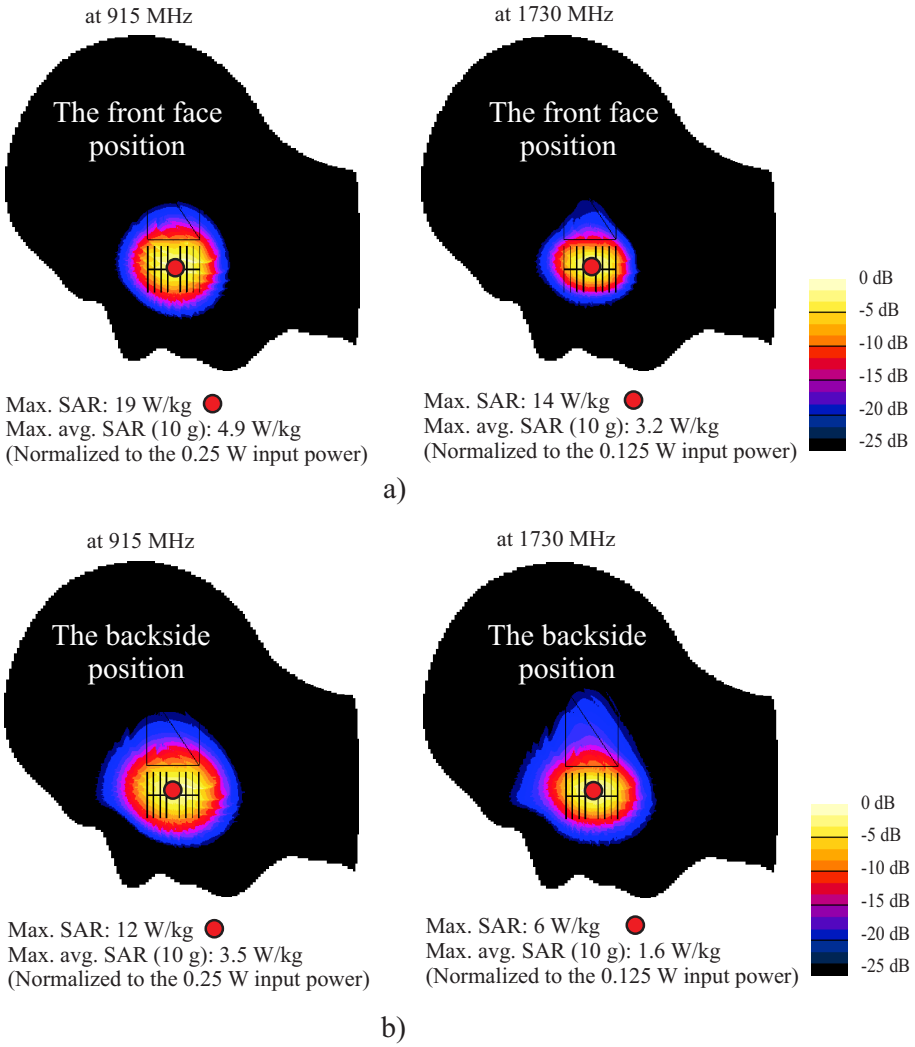

Figure 4.7: The SAR distribution [dB] of the periodically loaded dipole case 3 on the surface of the head at 915 MHz and 1730 MHz. a) Antenna structure in the front face position, and b) in the backside position.

4.3 Hearing aid compatibility

A hearing-aid is an electroacoustic device which typically fits in or behind the wearer's ear, and is designed to amplify and modulate sounds for the wearer. When a mobile terminal is held near the user's ear strong near fields of the mobile terminal may cause problems on the operation of a hearing-aid. To avoid these problems, a hearing-aid standard for the compatibility of hearing-aids and mobile terminals was introduced in the USA recently [50].

Hearing aid compatibility (HAC) is an area of growing importance because the average age of the population of many countries increases and thus the demand for the hearing-aid compatible devices increases. The standard will obviously get more widely introduced

around the world in the near future; in the EU it has been discussed and in China the standard is already valid.

4.3.1 Hearing aid compatibility standard

The hearing aid compatibility simulations are somewhat similar to the SAR simulation process. Both HAC and SAR involve near field simulations over the face of a mobile terminal except that the HAC simulations are made in free space without the user. The HAC simulation also requires separate results for electric (E) and magnetic (H) fields. Simulations are made over a square HAC plane, 50 mm x 50 mm [length x width], where the centre of the square is aligned with the earpiece. The HAC plane is placed at a 15 mm distance from the surface of the mobile terminal. The HAC plane is divided into nine evenly-sized blocks or sub-grids and for each block the maximums of the electric and magnetic fields are simulated and calculated. It is allowed to exclude tree adjacent blocks for both electric and magnetic fields except the center block. One of the excluded blocks has to be the same for both electric and magnetic fields. In the remaining six blocks the electric and magnetic field strengths have to be below the given limits in order to fulfill the hearing aid compatibility standard. Near field limits of the hearing-aid compatibility standard M3 are given in Table 4.8. In Appendix C (Figure C.1), simulation setup of the hearing aid compatibility is presented.

Table 4.8: Near field limits of the hearing-aid compatibility standard M3 (root mean square (rms) field values) [50].

Category		Telephone RF parameters			
		<960 MHz		>960 MHz	
Near field	AWF	E-field	H-field	E-field	H-field
Category M3	0 dB	250.9 V/m	0.76 A/m	79.3 V/m	0.24 A/m
	-5 dB	188.2 V/m	0.57 A/m	59.5 V/m	0.18 A/m

The articulation weighting factor (AWF) depends on the used transmission protocol. For CDMA, TDMA and UMTS (WCDMA) systems AWF=0 dB and for GSM systems AWF= -5 dB. In this work the stricter AWF=-5 dB standard is used. As can be seen in Table 4.8, the specified field values are much stricter above 960 MHz. Thus, it is assumed that it is more difficult to fulfill the standard at the upper GSM frequencies.

4.3.2 HAC results

First the HAC performance of the reference antenna is introduced. The simulated HAC field values are normalized to 2 W and 1 W which are the the maximum transmitted powers for handsets in GSM850 and GSM1900, respectively. Figure 4.8 shows the (rms) field values of the reference antenna. As can be seen, the simulated electric (E) and

magnetic (H) field values for this rather ideal antenna structure do not fulfill the specifications given in Table 4.8, not even closely. This is related to the fact that the two lowest order wavemodes of the chassis have a zero of the electrical current in the open end of the chassis and the electric field maxima occur at the same place as the current minima. Thus, in the vicinity of the open end of the chassis, i.e. on the HAC plane, there exist strong electric fields, as can be seen in Figure 4.8.

According to the reference antenna case and earlier studies by SMARAD[1], the near field values are rather high with traditional antenna structures and it is challenging to fulfill the hearing-aid compatibility standard especially at lower GSM frequencies. One method to decrease the field values of the reference antenna at 1880 MHz and thus fulfill the specification is to use top inverted wavetraps [51]. The wavetraps operate in a similar way as a balun, in which a high-impedance location is created with a short-circuited quarter-wavelength-long transmission line. One can then create a high-impedance location on the chassis and thus create a new chassis wavemode and especially avoid the zero of the electric currents in the open end of the chassis.

Next, the HAC field values of the small bow-tie case #1 are introduced. There are two different positions for the antenna structure like in the SAR simulations; the front face and backside positions. Figures 4.9 and 4.10 show the (rms) field values of the small bow-tie #1 antenna. In Appendix C (see Figures C.2 - C.11), all the near field distributions are presented. When moving the antenna structure 7 mm away from the chassis (backside position) there is a huge decrease in the field values on the HAC plane 2, which also decreases the SAR values as shown earlier. The field values on the HAC plane 1 are almost the same because when moving the antenna structure away is not a very effective way to decrease the coupling between the antenna structure and chassis, as shown in Chapter 2. Thus, later the HAC field values are calculated only at the front face position except the galvanically isolated structures which are calculated at the back side position. The results of the HAC simulations are listed in Table 4.9.

As can be seen in Table 4.9, all the balanced antenna structures fulfill the HAC specification at lower 836 MHz frequency which is the problematic frequency for the reference antenna as the wavetraps do not work efficiently at 836 MHz [51]. Balanced structures do not fulfill the stricter HAC limits at higher 1880 MHz frequency but by using the wavetraps it is possible to decrease the field values on the HAC plane 1 [51]. To demonstrate the operation of the wavetraps in the small bow-tie #1 structure, the wavetraps are placed at the top of the chassis and the field values are decreased ca. 37% compared to the case without the wavetraps, as shown in Table 4.9.

[1]Centre of Excellence in Smart Radios and Wireless Research at TKK - SMARAD

Table 4.9: HAC mean (rms) field values on the plane 1.

Structure	Electric [V/m] at 836 MHz	Electric [V/m] at 1880 MHz	Magnetic [A/m] at 836 MHz	Magnetic [A/m] at 1880 MHz
HAC specification field limits M3 (AWB = -5 dB)	< 188.2	< 59.5	< 0.57	< 0.18
Reference antenna CCE	552	264	0.89	0.75
Reference antenna CCE with wavetraps	551	63	0.90	0.18
Periodically loaded dipole case #3	139	121	0.41	0.27
Meandered dipole case #5	103	386	0.33	0.91
Helix	99		0.33	
Bow-tie case #1 (small)	105	106	0.33	0.24
Bow-tie case #1 (small) with wavetraps	111	67	0.37	0.15
Bow-tie case #2 (large)	148	128	0.42	0.28
Solid ground + CCE top	322	175	0.46	0.45
Solid ground + CCE side	155	110	0.43	0.28
Meandered ground + CCE top	366	209	0.46	0.62
Meandered ground + CCE side	148	120	0.52	0.38

at 836 MHz field values are normalized to 2 W input power
at 1880 MHz field values are normalized to 1 W input power

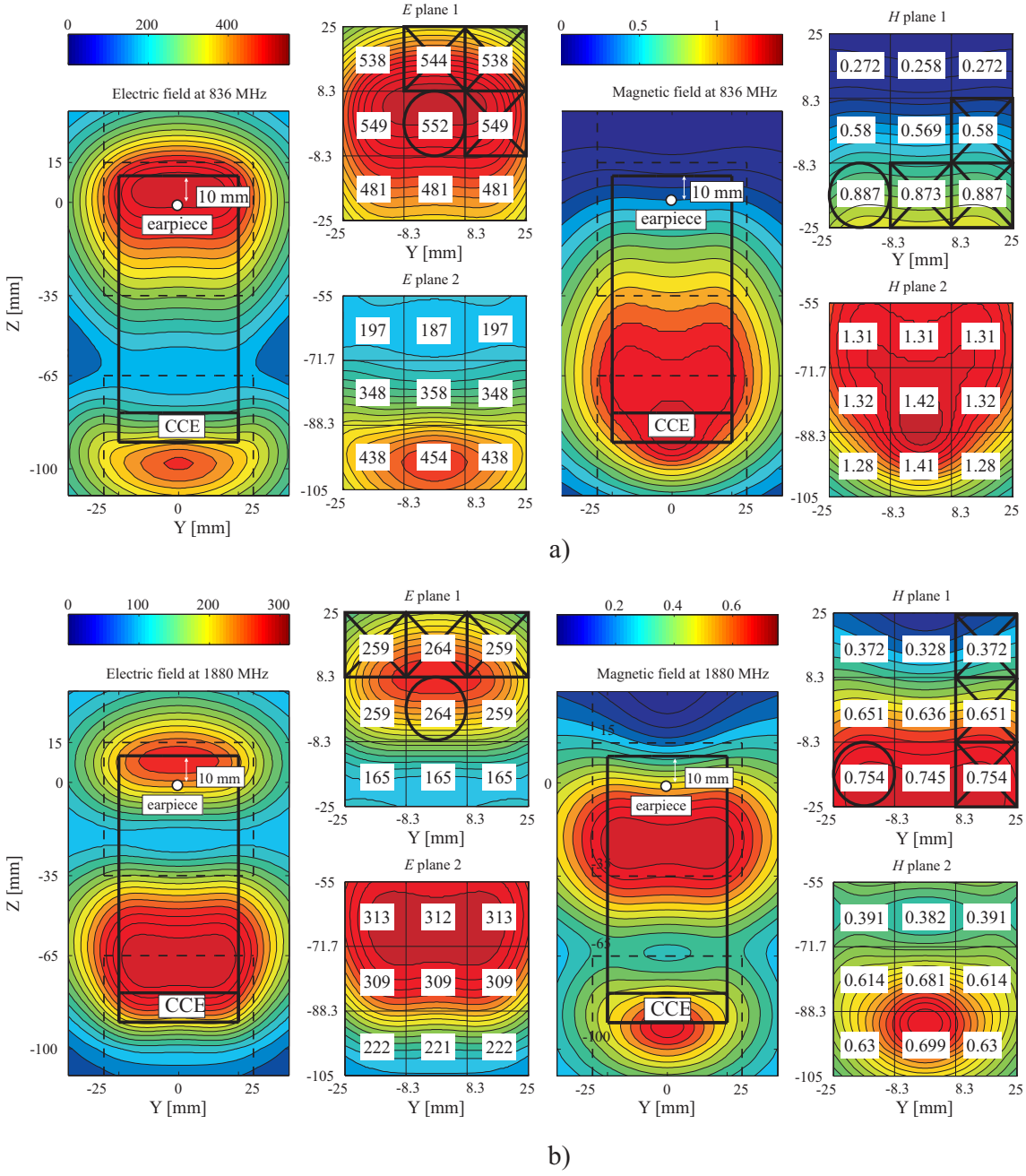

Figure 4.8: a) Electric and magnetic fields of the reference antenna on the HAC plane at 836 MHz, and b) electric and magnetic fields on the HAC plane at 1880 MHz.

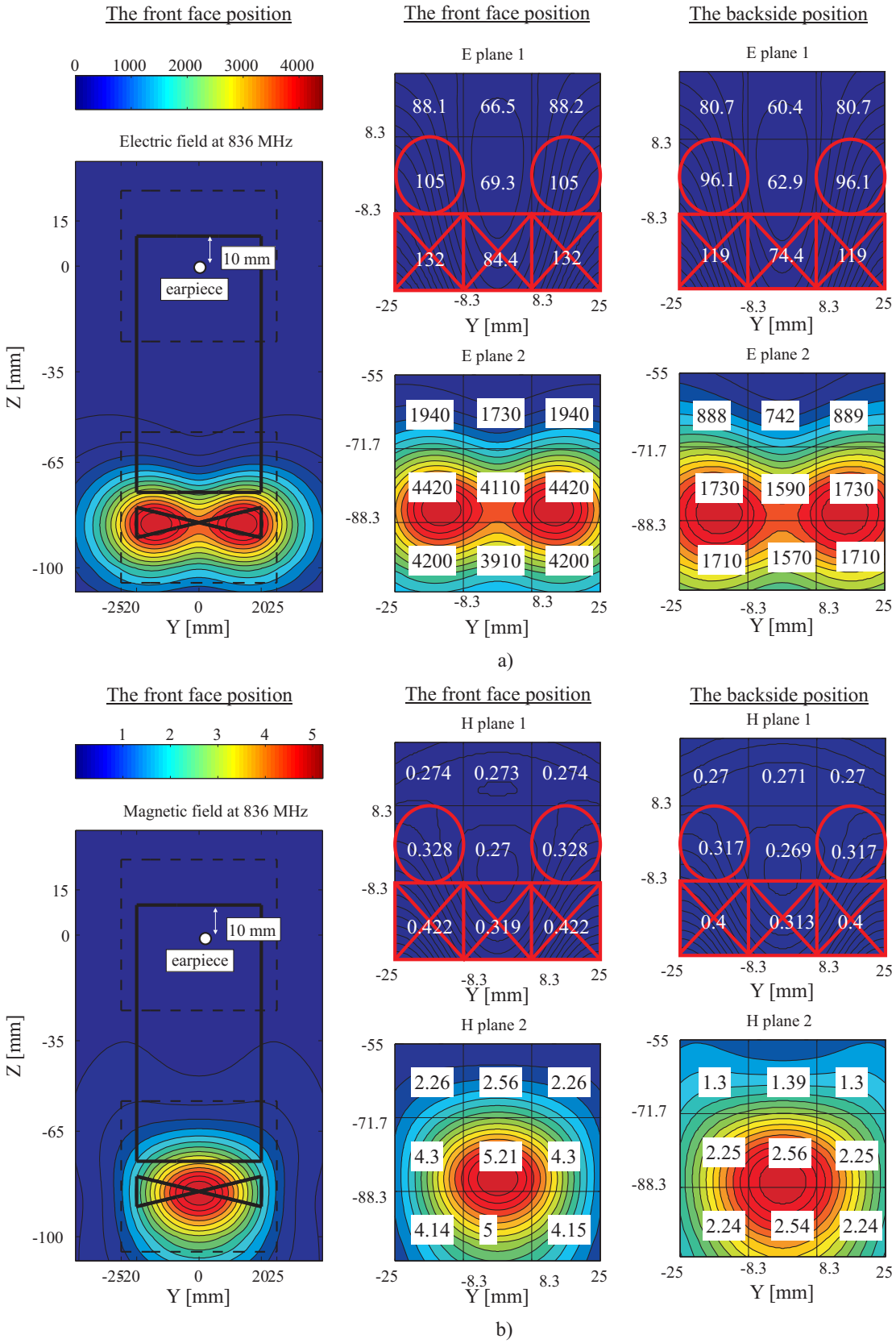

Figure 4.9: a) Electric field of the small bow-tie case #1 on the HAC plane at 836 MHz, and b) magnetic fields on the HAC plane at 836 MHz.

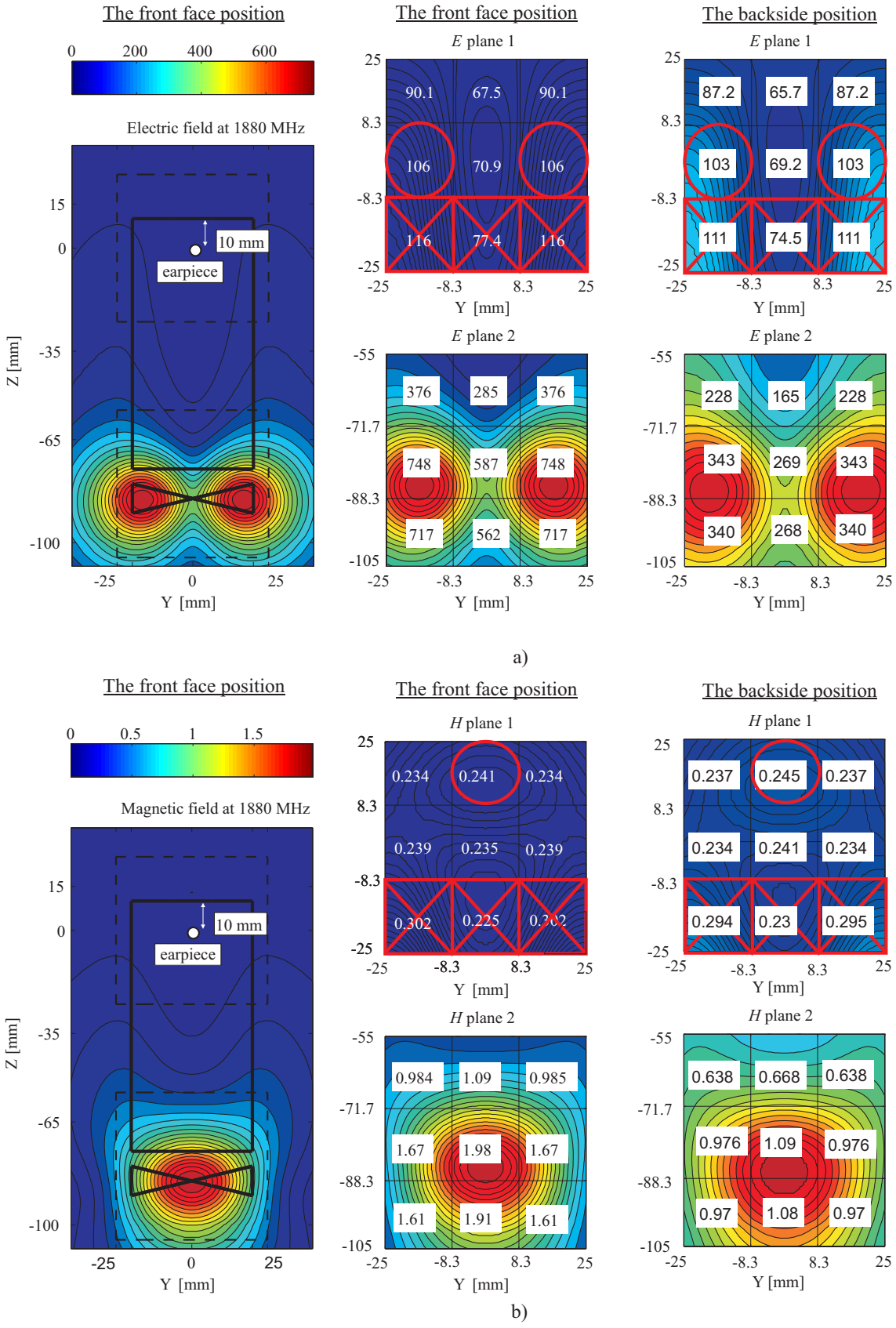

Figure 4.10: a) Electric field of the small bow-tie case #1 on the HAC plane at 1880 MHz, and b) magnetic fields on the HAC plane at 1880 MHz.

CHAPTER 5

Summary and conclusions

The feasibility of isolated antenna structures in mobile terminal use was studied in this master's thesis with the main emphasis on the available bandwidth potential. Isolated antenna structures have many promising features compared to the traditional antenna structures; large and solid chassis is not required and thus the design of the mobile terminal can be done more freely. Isolated antenna structures might have reduced effect of the user and thus also the effect of the user on matching and radiation efficiency as well as specific absorption rate (SAR) and hearing-aid compatibility (HAC) of the isolated antenna structures were investigated in this thesis.

First, some background of small antennas and some antenna parameters was studied. Definition of a small antenna was examined starting from the resonator theory and the definition of the quality factor. The small antenna has a strong correlation between the antenna size, efficiency and impedance bandwidth and it is not possible to maximize all of them at the same time. In this work the quality factor has a very significant role since when dealing with small antennas the quality factor defines the bandwidth of an antenna, and thus a comprehensive study has been made. A historical recap and some today's methods to approximate the quality factor were discussed. In this work two different methods to estimate the impedance bandwidth were studied: 1) calculating first the quality factor of the antenna structure to get the bandwidth potential and 2) calculating all possible matching circuit topologies with a single resonant LC-circuit to get the bandwidth potential directly. It was found reasonable to use both of them in the same time. In this work the bandwidth of ca. 2% was found to be a feasible bandwidth requirement for the isolated antenna structures since it gives a good compromize between the size of the antenna and the feasibility of the tuning circuit.

Different isolated structures were introduced and investigated. Main part of this thesis were the balanced antenna structures and the following balanced structures were introduced and studied: wire, loop, helical, and bow-tie antennas. The main theory and

some basic equations to estimate the radiation resistance of those balanced antennas were presented. Also some galvanically isolated antenna structures were studied. Different coupling mechanisms of the galvanically isolated antennas were studied and a study of the effect of the gap between the antenna structure and the chassis was made. It was found that increasing the gap between the chassis and the antenna structure is not a very efficient way to increase the isolation.

Next the achievable bandwidth potentials of the isolated antenna structures were investigated to study the feasibility in the mobile terminal environment. The simulation results indicate that at lower UHF frequencies, below 1 GHz, there are two potential ways to achieve the fixed bandwidth requirement of 2% of this work: 1) Using a meandered antenna structure that has a self-resonance near the operating frequency. These structures can be made very small-sized (10 mm x 40 mm [length x width]) but the functional operating band is restricted only near the self-resonance. 2) Using a large-sized antenna structure (40 mm x 40 mm [length x width]) that has a self-resonance at much higher frequencies (from 1.4 GHz to 2 GHz). These large-sized antenna structures are wideband. At higher frequencies, near 1.8 GHz or above, the size of the antenna structure can be very small and still fulfill the banwidth requirement. Also radiation patterns of the isolated antenna structures were simulated and it was noticed that the chassis distorts only a little the radiation pattern and thus the interaction between the chassis and antenna structure is very small. The radiation pattern corresponds a 'doughnut' shape. The minimum of the radiation pattern is achieved in y-axis which correspond the width of the antenna. The cross-polar component increases at higher frequencies and thus the effect of the chassis is getting more significant though it is still much smaller than in the reference antenna case.

Performance of the isolated antenna structures was investigated by studying the effect of the user as well as the values of the specific absorption rate (SAR) and hearing-aid compatibility (HAC). The studies were performed using SEMCAD X simulator. The simulation results of large antenna structures show that the matching is very sensitive to the user's hand when the finger is located close to the antenna. Small-sized antenna structures are on the contrary quite robust to the effect of the user even if the hand of the user is close. The top located antenna structures give better radiation efficiency compared to the reference antenna and the bottom located antennas. The bottom located antenna structures have almost constant radiation efficiencies at both frequencies.

The SAR simulations show that the balanced antenna structures have high SAR at the lower 900 MHz frequency. This is because the balanced antenna structures have very high near field values close to the antenna structure. At the higher 1800 MHz frequency the SAR values are notably lower (about half of the SAR values at 900 MHz). On the contrary, the near field values are very small in the vicinity of the chassis because the antenna structure is isolated from the chassis. Hence the isolated antenna structures can

be used to control the near field values on the HAC plane.

In this thesis some promising isolated antenna structures, like the small bow-tie and helix, have been found. Simulation results show that isolated antenna structures suit best for higher UHF frequencies, over 1.8 GHz, where the 2% bandwidth is easy to achieve and isolated antenna structures have low SAR values. Small-sized top located isolated structures are shown to increase the radiation efficiency compared to the traditional antenna structures and in these structures the user effect on matching is very small. When the antenna is bottom located the performance is deteriorated; the performance of the bottom located isolated antenna is similar to the reference antenna. The bottom located isolated antenna structures can also be used to decrease the near field values on the HAC plane and therefore can be used to fulfill the HAC specifications. The drawbacks of the isolated antenna structures are associated with lower GSM frequencies; large antenna structure is needed if the wideband operation is required and high SAR values are common.

Since a basic research of the feasibility of the isolated antenna structures in mobile terminals was the main purpose of this thesis, the manufacturing and measuring of the prototype antennas were not done. The next logical step would be the user effect measurements with the prototypes of the most promising antenna structures. Further studies concerning the most promising antenna structures at higher 1800-3600 MHz frequencies having already sufficient system bandwidth should be done. Another important subject would be to study the chassis characteristic modes that might deteriorate the isolation between the chassis and the antenna structure at higher, over 1800 MHz frequencies.

Bibliography

[1] P. Vainikainen, J. Ollikainen, O. Kivekäs, and I. Kelander, "Resonator-based analysis of the combination of mobile handset antenna and chassis," *IEEE Transactions on Antennas and Propagation*, vol. 50, no. 10, pp. 1433–1444, Oct. 2002.

[2] C. A. Balanis, *Antenna Theory: Analysis and Design*, 2nd ed. New York: John Wiley & Sons, 1997.

[3] J. D. Kraus, *Antennas*, 2nd ed. New York: McGraw-Hill Companies, 1988.

[4] I. Lindell and K. Nikoskinen, *Antenniteoria (Antenna Theory, in Finnish)*, 4th ed. Helsinki: Otatieto, 1995.

[5] H. A. Wheeler, "Fundamental limitations of small antennas," *Proceedings of the IRE*, vol. 35, pp. 1479–1484, Dec. 1947.

[6] R. E. Collin, "Minimum Q of small antennas," *Journal of Electromagnetic Waves and Applications*, vol. 12, pp. 1369–1393, Dec. 1998.

[7] A. Räisänen and A. Lehto, *Radiotekniikan perusteet (Fundamentals of Radio Engineering, in Finnish)*, 11th ed. Espoo: Otatieto, 2003.

[8] K. Fujimoto, A. Henderson, K. Hirasawa, and J. R. James, *Small antennas*. New York: Research Studies Press Ltd., 1987.

[9] H. Pues and A. V. de Capelle, "An impedance-matching technique for increasing the bandwidth of microstrip antennas," *IEEE Transactions on Antennas and Propagation*, vol. 37, no. 11, pp. 1345–1354, Nov. 1989.

[10] J. Ollikainen, "*Design and Implementation Techniques of Wideband Mobile Communications Antennas*," doctoral thesis, Helsinki University of Technology, Radio laboratory, Espoo, Finland, Nov. 2004.

[11] IEEE, *IEEE Standard Definitions of Terms for Antennas*. IEEE STD-145, Mar. 1993.

[12] L. J. Chu, "Physical limitations of omni-directional antennas," *Journal of Applied Physics*, vol. 19, pp. 1163–1175, Dec. 1948.

[13] R. F. Harrington, "Effect of antenna size on gain, bandwidth, and efficiency," *IEEE Transactions on Antennas and Propagation*, vol. 64-D, no. 1, pp. 1–12, Jan. 1960.

[14] R. E. Collin and S. Rothschild, "Evaluation of antenna Q," *IEEE Transactions on Antennas and Propagation*, vol. AP-12, no. 1, pp. 23–27, Jan. 1964.

[15] J. S. Mclean, "A re-examination of the fundamental limits on the radiation Q of electrically small antennas," *IEEE Transactions on Antennas and Propagation*, vol. 44, no. 5, pp. 672–676, May 1996.

[16] G. A. Thiele, P. L. Detweiler, and R. P. Penno, "On the lower bound of the radiation Q for electrically small antennas," *IEEE Transactions on Antennas and Propagation*, vol. 51, no. 6, pp. 1263–1269, Jun. 2003.

[17] W. Geyi, "A method for the evaluation of small antenna Q," *IEEE Transactions on Antennas and Propagation*, vol. 51, no. 8, pp. 2124–2129, Aug. 2003.

[18] W. Geyi and P. Jarmuszewski, "The foster reactance theorem for antennas and radiation Q," *IEEE Transactions on Antennas and Propagation*, vol. 48, no. 3, pp. 401–408, Mar. 2000.

[19] A. D. Yaghjian and S. R. Best, "Impedance, bandwidth, and Q of antennas." *IEEE AP-S International Symposium*, Columbus, USA, Jun. 22-27 2003, pp. 501–504.

[20] ——, "Impedance, bandwidth, and Q of antennas," *IEEE Transactions on Antennas and Propagation*, vol. 53, no. 4, pp. 1298–1324, Apr. 2005.

[21] A. D. Yaghjian, "Internal energy, Q-energy, poynting's theorem, and the stress dyadic in dispersive material," *IEEE Transactions on Antennas and Propagation*, vol. 55, no. 6, pp. 1495–1505, Jun. 2007.

[22] S. R. Best, "A discussion on the quality factor of impedance matched electrically small wire antennas," *IEEE Transactions on Antennas and Propagation*, vol. 53, no. 1, pp. 502–508, Jan. 2005.

[23] H. R. Stuart, S. R. Best, and A. D. Yaghjian, "Limitations in relating quality factor to bandwidth in a double resonance small antenna," *IEEE Antennas and Wireless Propagation Letters (AWPL)*, vol. 6, pp. 460–463, 2007.

[24] S. R. Best, "Low Q electrically small linear and elliptical polarized spherical dipole antenna," *IEEE Transactions on Antennas and Propagation*, vol. 53, no. 3, pp. 1047–1053, Mar. 2005.

[25] IE3D, a MoM-based electromagnetic simulator, version 14.10, Zeland Software Inc, California, USA. [Online]. Available: http://www.zeland.com(CitedMarch10,2009).

[26] J. Rahola, "Bandwidth potential and electromagnetic isolation: tools for analysing the impedance behaviour of antenna systems." *The 3rd European Conference on Antennas and Propagation (EuCAP09)*, Berlin, Germany, Mar. 23-27 2009, pp. 944–948.

[27] H. Bode, *Network Analysis and Feedback Amplifier Design*. New York: Van Nostrad, 1945.

[28] R. M. Fano, "Theoretical limitation on the broad-band matching of arbitrary impedances," *Journal of the Franklin Institute*, vol. 249, pp. 57–83, January 1950, and pp. 139-154, Feb. 1950.

[29] D. M. Pozar, *Microwave Engineering*, 2nd ed. New York: John Wiley & Sons, 1998.

[30] G. Wang, *RF MEMS switches with novel materials and micromachining techniques for Soc/SoP RF front ends*. Ph.D. Dissertation, Atlanta, Georgia Institute of Technology, 2006.

[31] P. Grant and M. Denhoff, "A comparison between RF MEMS switches and semiconductor switches." *Proceedings of the 2004 International Conference on MEMS, NANO and Smart Systems (ICMENS04)*, Alberta, Canada, Aug. 25-27 2004, pp. 515–521.

[32] S. R. Best, "A discussion on the performance properties of electrically small self-resonant wire antennas," *IEEE Antennas and Propagation Magazine*, vol. 46, no. 6, pp. 9–22, Dec. 2004.

[33] C. A. Balanis, *Modern Antenna Handbook*. John Wiley & Sons, 2008.

[34] K. L. Wong and J. S. Kuo, "Bandwidth enhancement of bow-tie microstrip antenna using integrated reactive loading," *Microwave Optical Technology Letters*, vol. 22, no. 1, pp. 69–71, Jul. 1999.

[35] A. A. Lestari, A. G. Yarovoy, and L. P. Ligthart, "RC-loaded bow-tie antenna for improved pulse radiation," *IEEE Transactions on Antennas and Propagation*, vol. 52, no. 10, pp. 2555–2563, Oct. 2004.

[36] J. Anguera, C. Puente, C. Borja, R. Montero, and J. Soler, "Small and high-directivity bow-tie patch antenna based on the sierpinski fractal," *Microwave Optical Technology Letters*, vol. 31, no. 3, pp. 239–241, Nov. 2001.

[37] S. R. Best and J. D. Morrow, "On the significance of current vector alignment in establishing the resonant frequency of small space-filling wire antennas," *IEEE Antennas and Wireless Propagation Letters*, vol. 2, pp. 201–204, Dec. 2003.

[38] Z. Guangping, "A non-uniform pitch dual band helix antenna." *Antennas and Propagation Society International Symposium*, Salt Lake City, USA, Jul. 16-21 2000, pp. 274–277.

[39] SEMCAD-X, a FDTD-based electromagnetic simulator, version 13.4 Bernina, Schmid & Partner Engineering AG, Zurich, Switzerland. [Online]. Available: http://www.semcad.com(citedMay20,2009).

[40] C. Gabriel, "Tissue equivalent material for hand phantoms," *Physics in Medicine and Biology*, vol. 52, pp. 4205–4210, 2007.

[41] M. Foegelle, K. Li, A. Pavacic, and P. Moller, "Developing a Standard Hand Phantom for Wireless Testing," Wireless Design and Development, 2008. [Online]. Available: http://www.wirelessdesignmag.com(citedAug17,2009).

[42] APLAC, circuit simulator, version 8.21, AWR, California, USA. [Online]. Available: http://web.awrcorp.com/Usa/Products/APLAC/(citedJun24,2009).

[43] *IEEE Standard for Safety Levels with Respect to Human Exposure to Radio Frequency Electromagnetic Fields, 3 kHz to 300 GHz* (ANSI / IEEE C95.1-2005), IEEE Standards Coordinating Committee Std., 2006.

[44] P. Wainwright, "Thermal effects of radiation from cellular telephones," *Phys. Med. Biol.*, vol. 45, pp. 2363–2372, 2000.

[45] R. Nylund and D. Leszczynski, "Proteomics analysis of human endothelial cell line EA.hy926 after exposure to GSM 900 radiation," *Proteomics*, pp. 1359 – 1365, Mar. 2004.

[46] L. Salford, A. Brun, J. Eberhardt, L. Malmgren, and B. Persson, "Nerve cell damage in mammalian brain after exposure to microwaves from gsm mobile phones," *Environmental Health Perspectives*, vol. 111, no. 7, pp. 881–883, Jan. 2003.

[47] *IEEE Standard for Safety Levels with Respect to Human Exposure to Radio Frequency Electromagnetic Fields, 3 kHz to 300 GHz* (ANSI / IEEE C95.1-1999), IEEE Standards Coordinating Committee Std., 1999.

[48] "Guidelines for limiting exposure to time-varying electric, magnetic, and electromagnetic fields (up to 300 GHz)," International Commission on Non-Ionizing Radiation Protection (ICNIRP), pp. 494–522, Apr. 1998.

[49] *IEEE Recommended Practice for Determining the Peak Spatial-Average Specific Absorption Rate (SAR) in the Human Head from Wireless Communications Devices: Measurement Techniques* (IEEE Std 1528-2003), IEEE Standards Coordinating Committee Std., 2003.

[50] *American National Standard for Method of Measurements of Compatibility between Wireless Communication Devices and Hearing Aids* (ANSI C63.19-2007), American National Standards Institute Std., 2007.

[51] J. Holopainen, J. Ilvonen, O. Kivekäs, R. Valkonen, C. Icheln, and P. Vainikainen, "Near field control of handset antennas based on inverted top wavetraps: Focus on hearing-aid compatibility," *Antennas and Wireless Propagation Letters (AWPL)*, vol. 8, pp. 592–595, 2009.

APPENDIX A

Radiation patterns

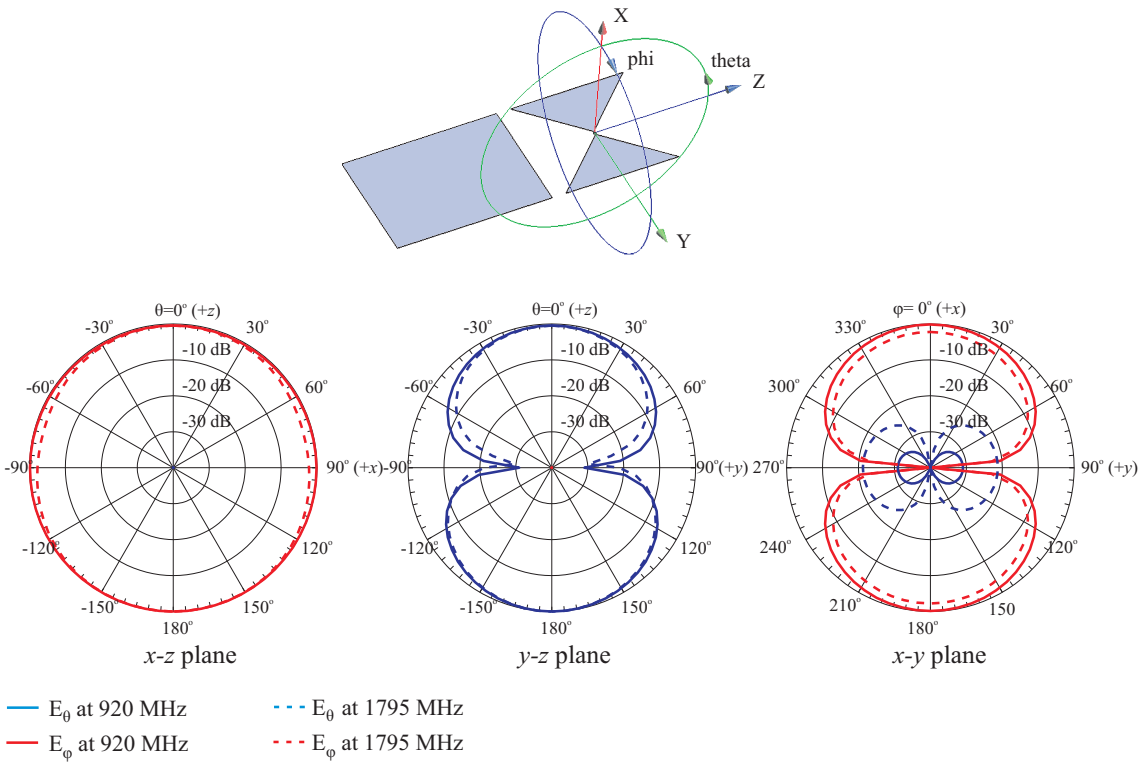

Figure A.1: Simulated radiation patterns at 920 MHz and 1795 MHz of the large bow-tie #2 with the chassis.

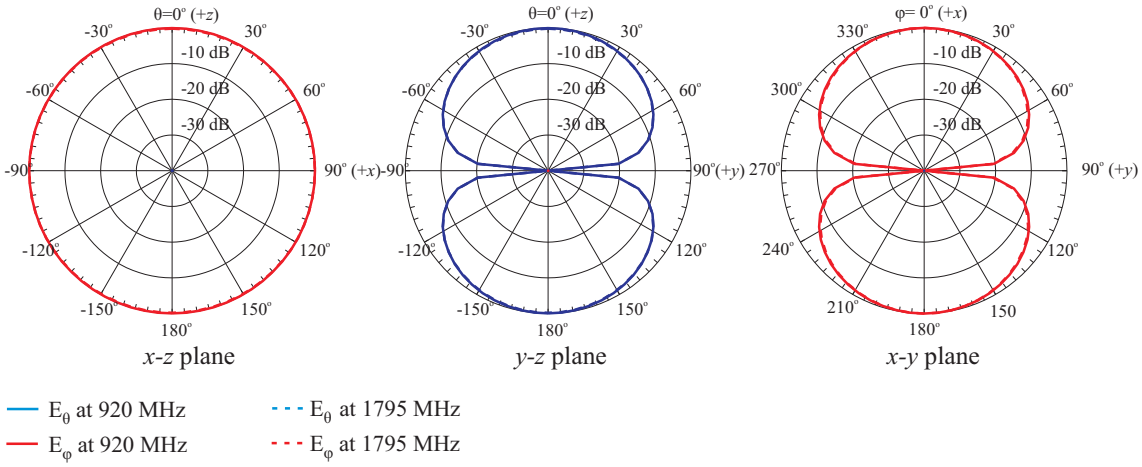

Figure A.2: Simulated radiation patterns at 920 MHz and 1795 MHz of the large bow-tie #2 without the chassis.

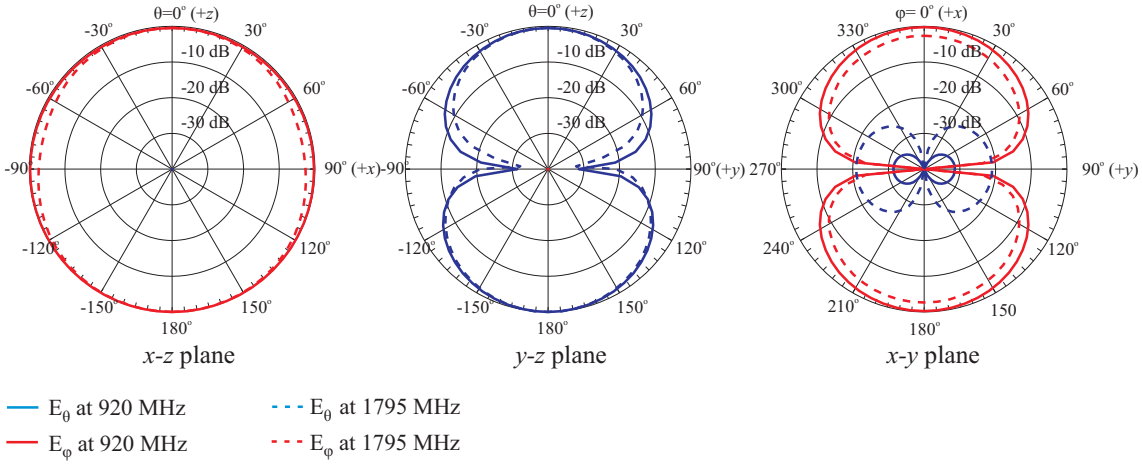

Figure A.3: Simulated radiation patterns at 920 MHz and 1795 MHz of the periodically loaded dipole with the chassis.

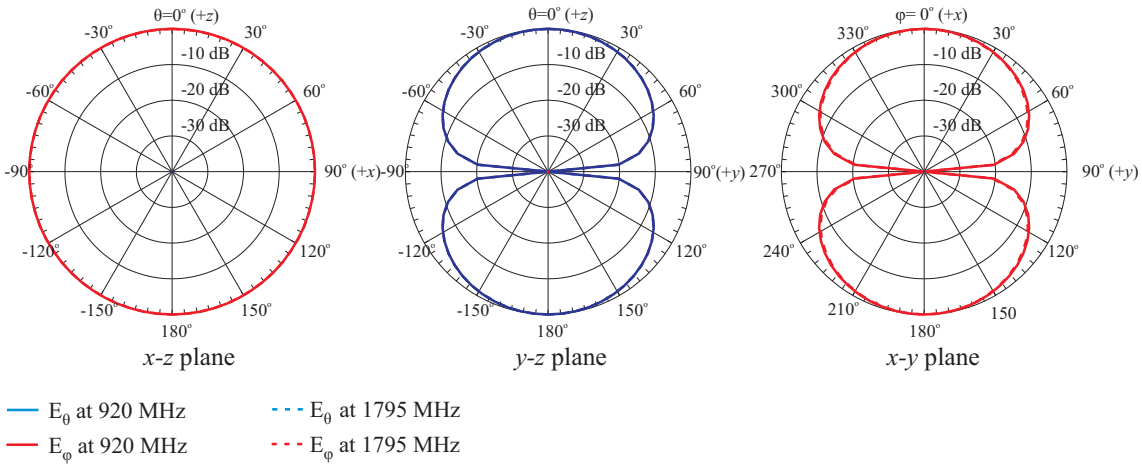

Figure A.4: Simulated radiation patterns at 920 MHz and 1795 MHz of the periodically loaded dipole without the chassis.

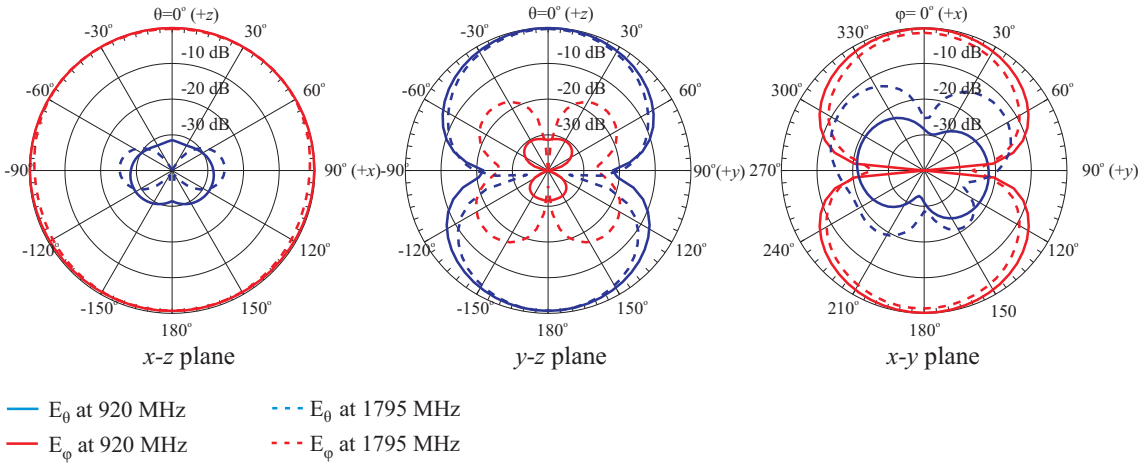

Figure A.5: Simulated radiation patterns at 920 MHz and 1795 MHz of the helix with the chassis.

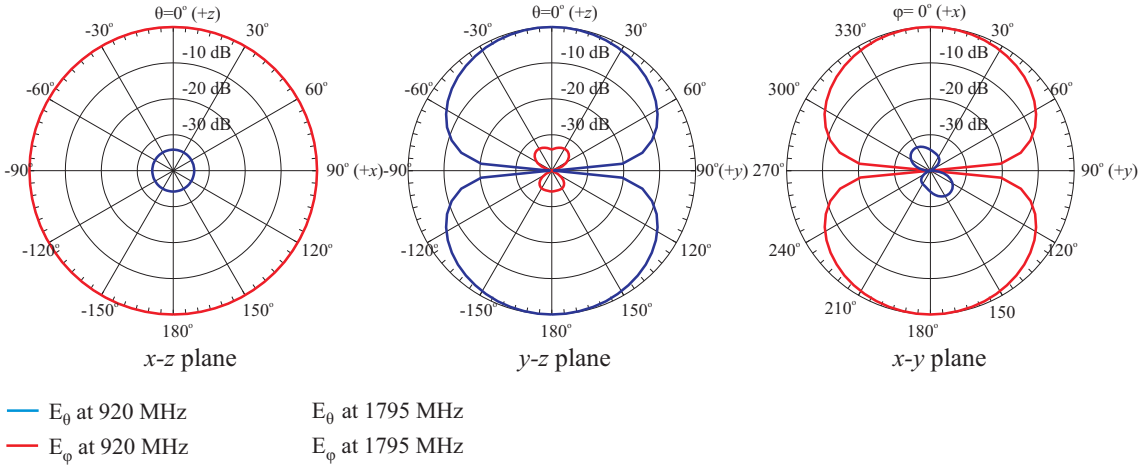

Figure A.6: Simulated radiation patterns at 920 MHz and 1795 MHz of the helix without the chassis.

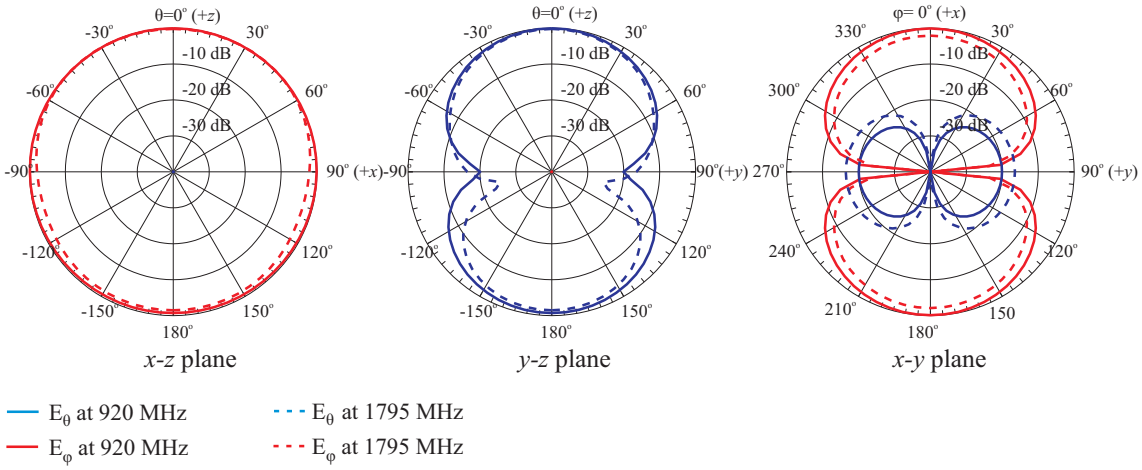

Figure A.7: Simulated radiation patterns at 920 MHz and 1795 MHz of the meandered wire dipole with the chassis.

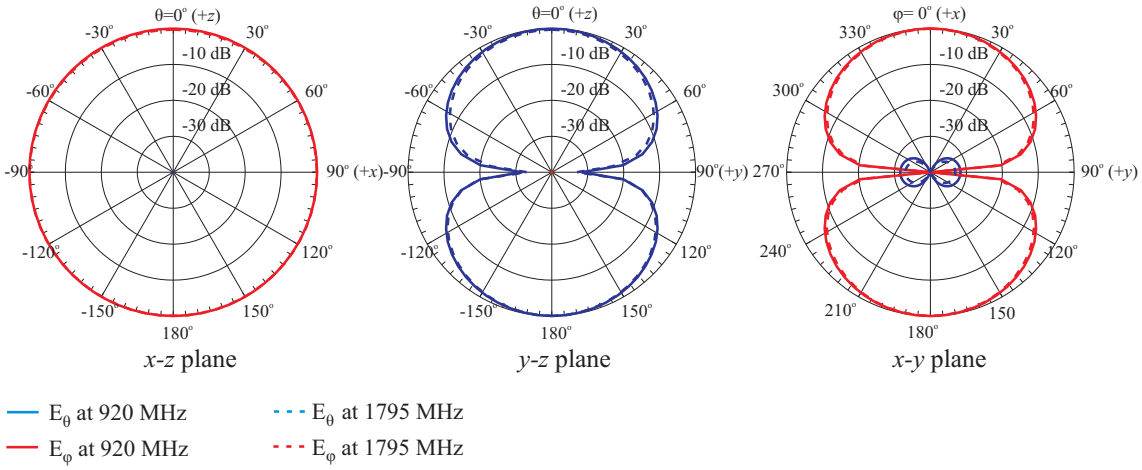

Figure A.8: Simulated radiation patterns at 920 MHz and 1795 MHz of the meandered wire dipole without the chassis.

APPENDIX B

SAM HEAD PHANTOM

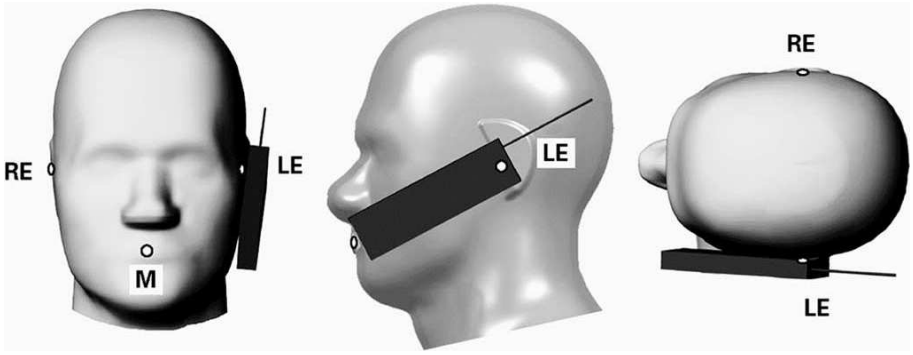

Figure B.1: Specific Anthropomorphic Mannequin (SAM) with cell phone in cheek/touch position on the left side. RE = Right Ear, LE = Left Ear, and M = Mouth [49].

APPENDIX C

NEAR FIELDS ON THE HAC PLANE

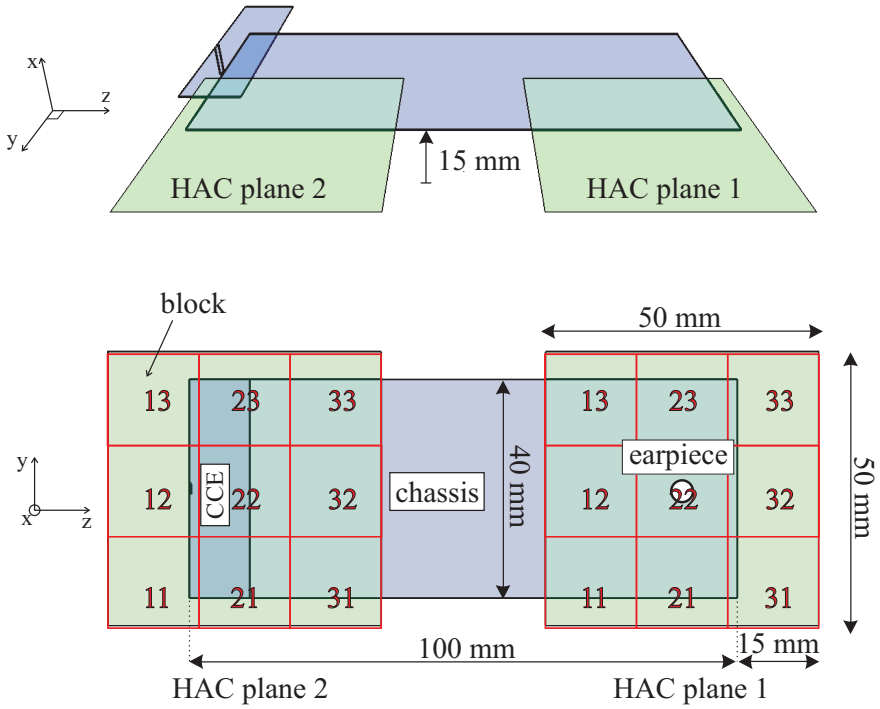

HAC category M3 limits (*AWF* = -5 dB)	Telephone RF parameters	
	< 960 MHz	> 960 MHz
Maximum electric field (rms)	188.2 V/m	59.5 V/m
Maximum magnetic field (rms)	0.57 A/m	0.18 A/m

Figure C.1: Simulation setup of the hearing aid compatibility.

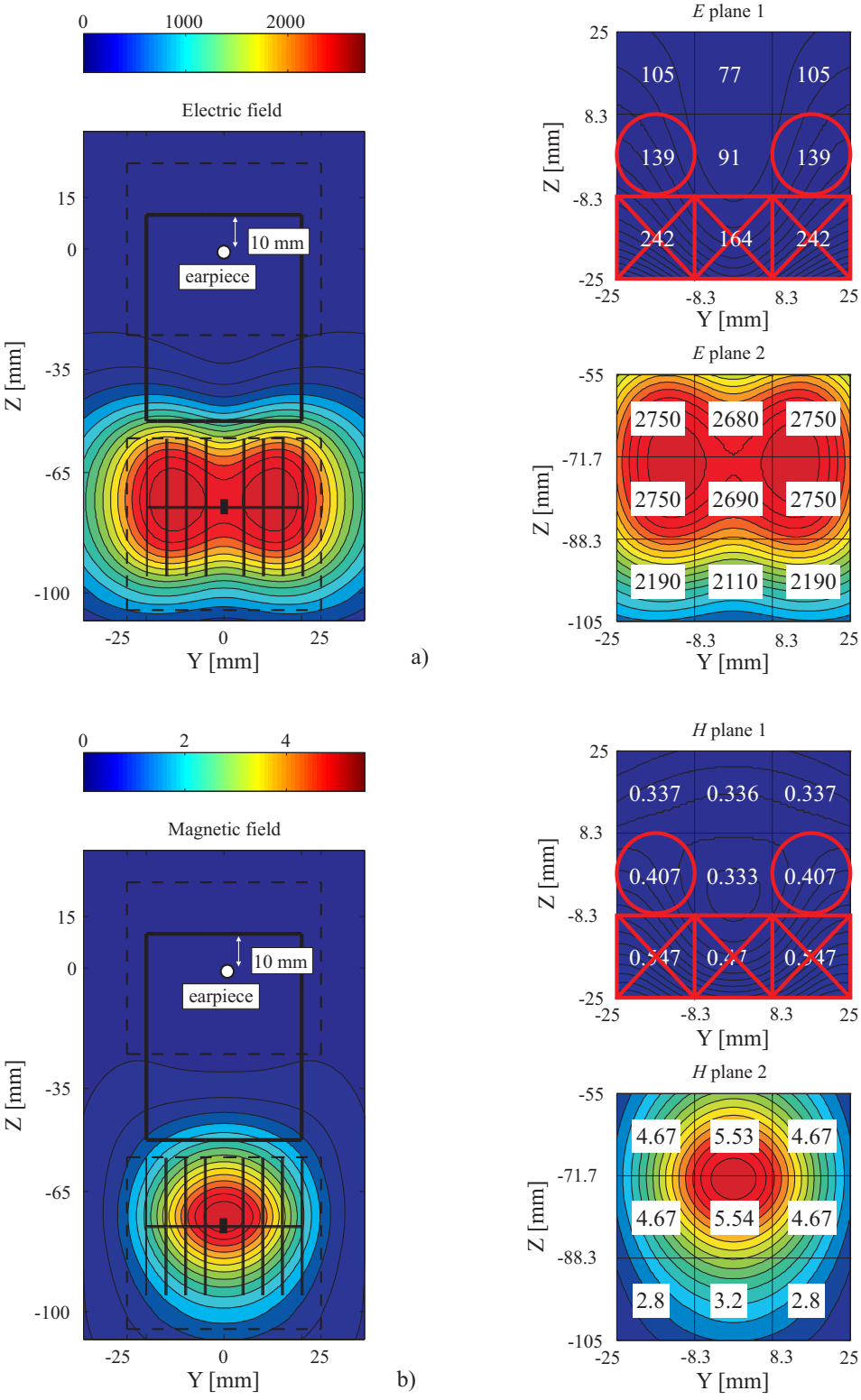

Figure C.2: a) Electric and b) magnetic fields on the HAC plane. The periodically loaded wire dipole case #3 at 836 MHz.

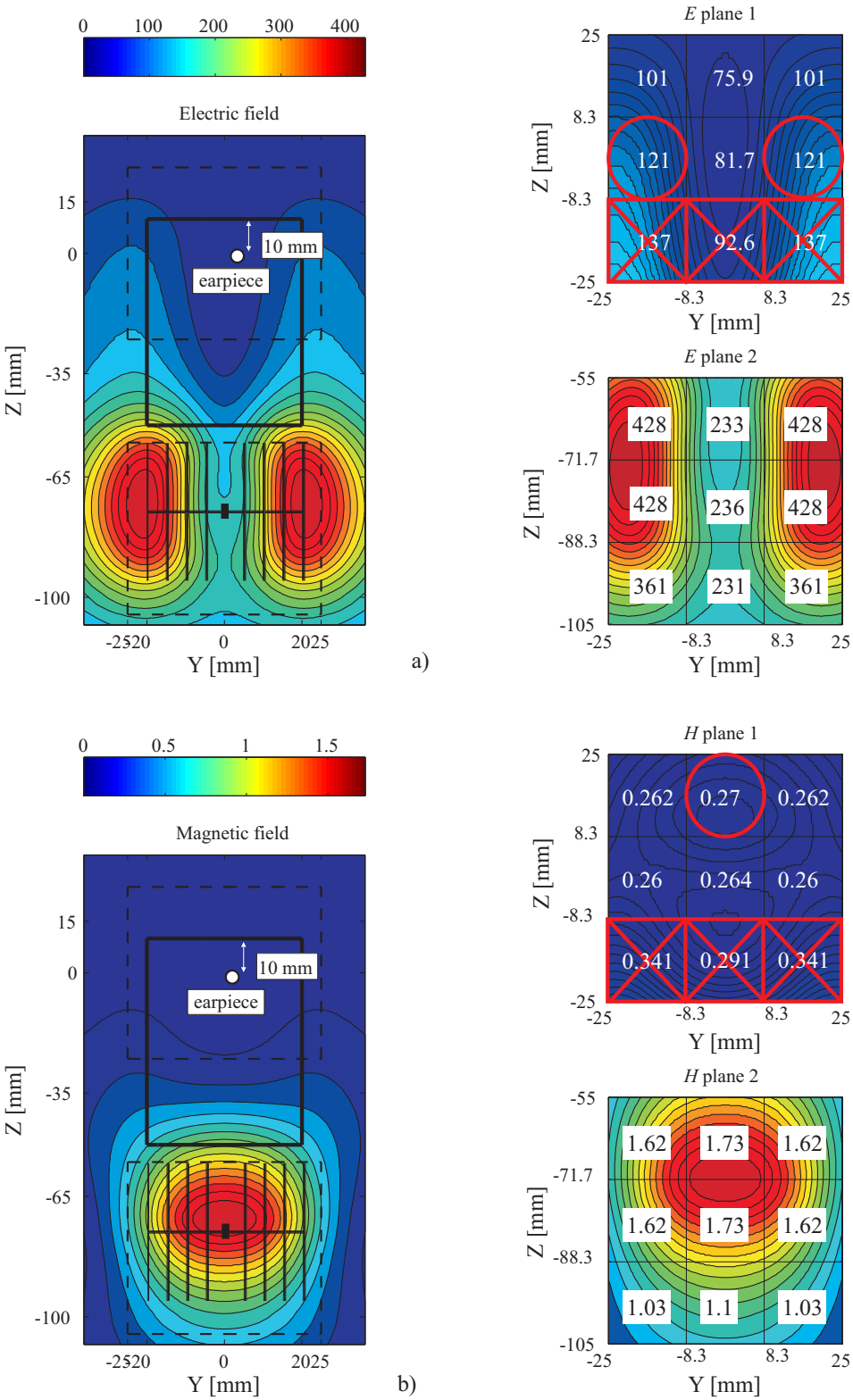

Figure C.3: a) Electric and b) magnetic fields on the HAC plane. The periodically loaded wire dipole case #3 at 1880 MHz.

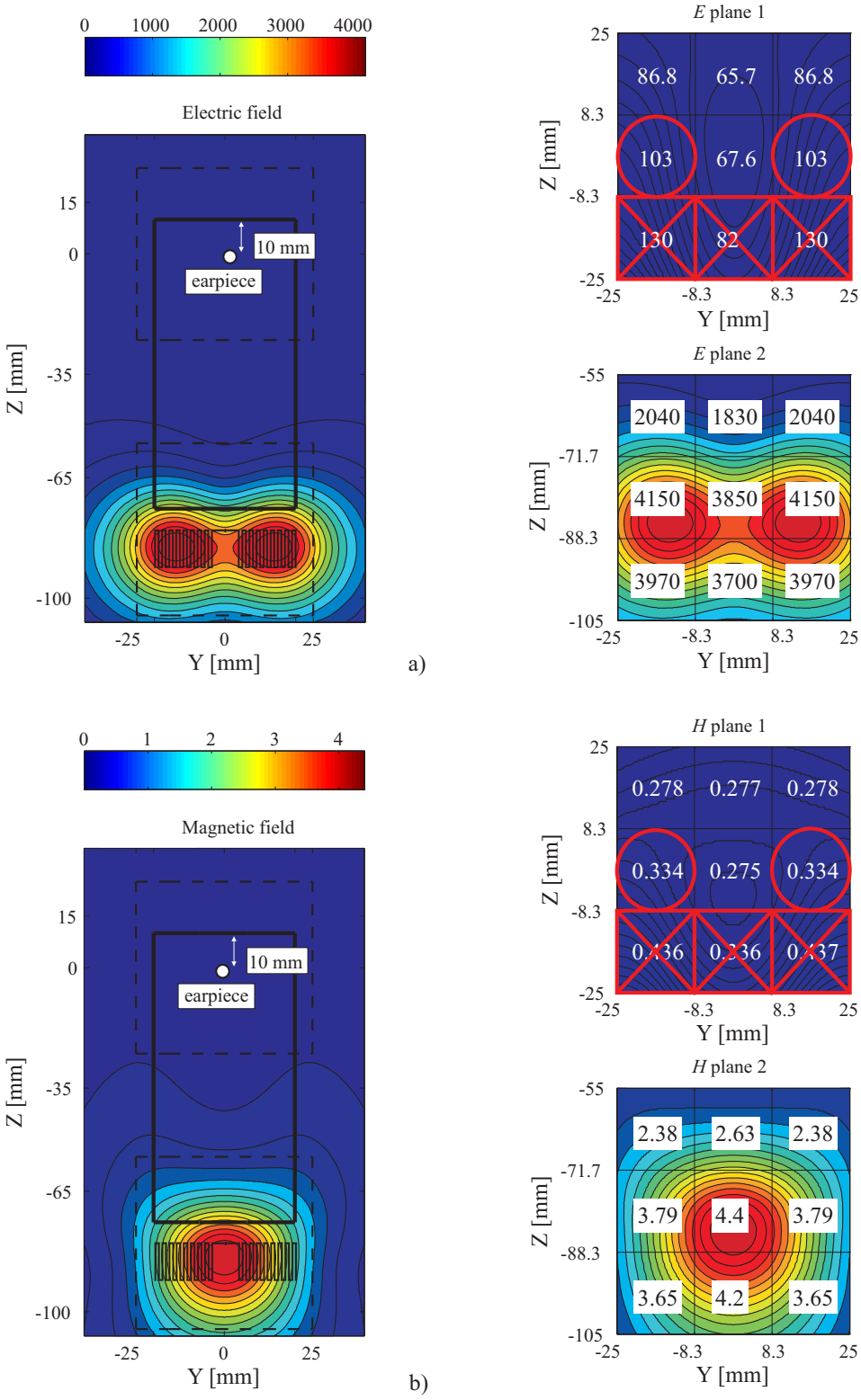

Figure C.4: a) Electric and b) magnetic fields on the HAC plane. The meandered wire dipole case #5 at 836 MHz.

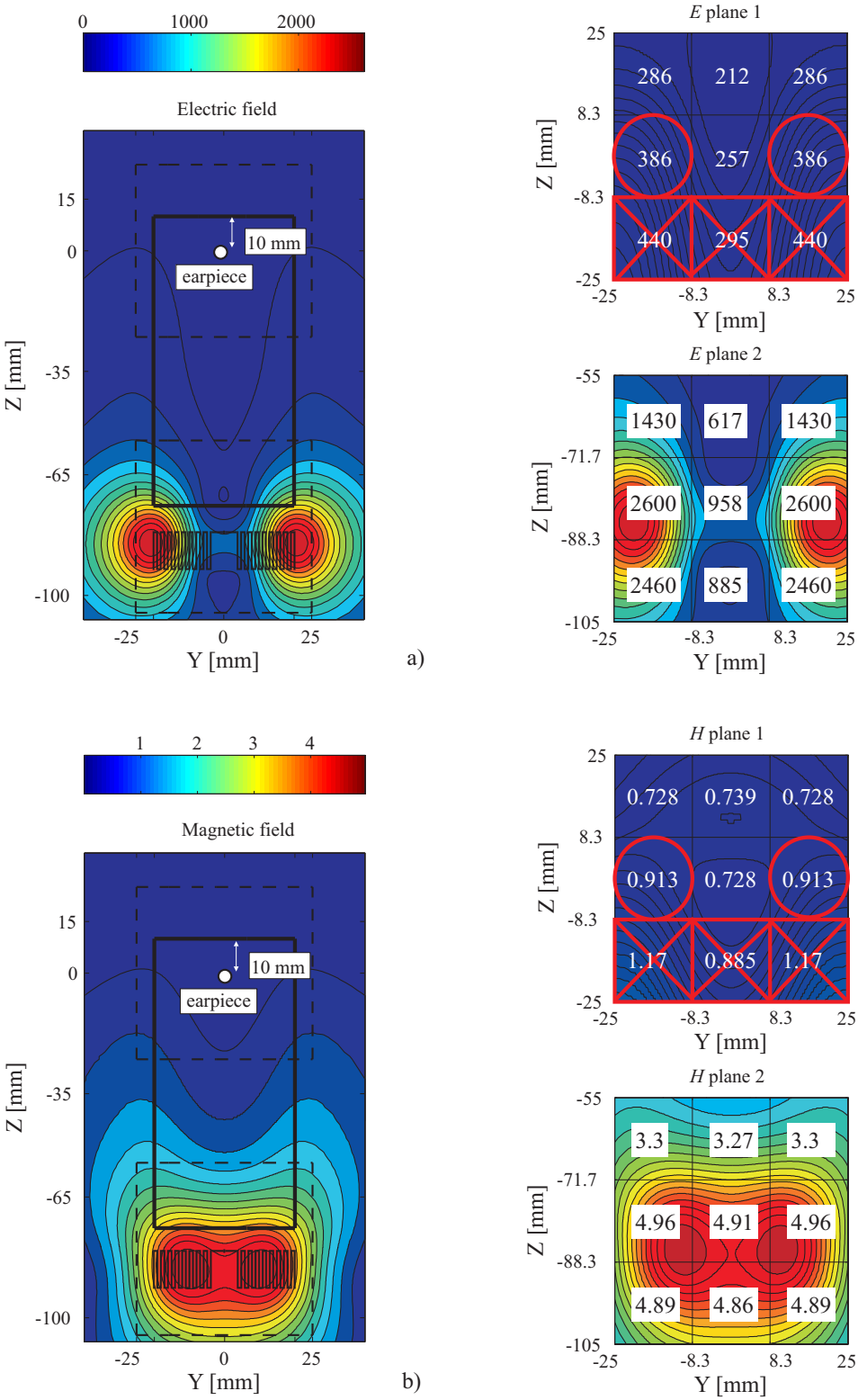

Figure C.5: a) Electric and b) magnetic fields on the HAC plane. The meandered wire dipole case #5 at 1880 MHz.

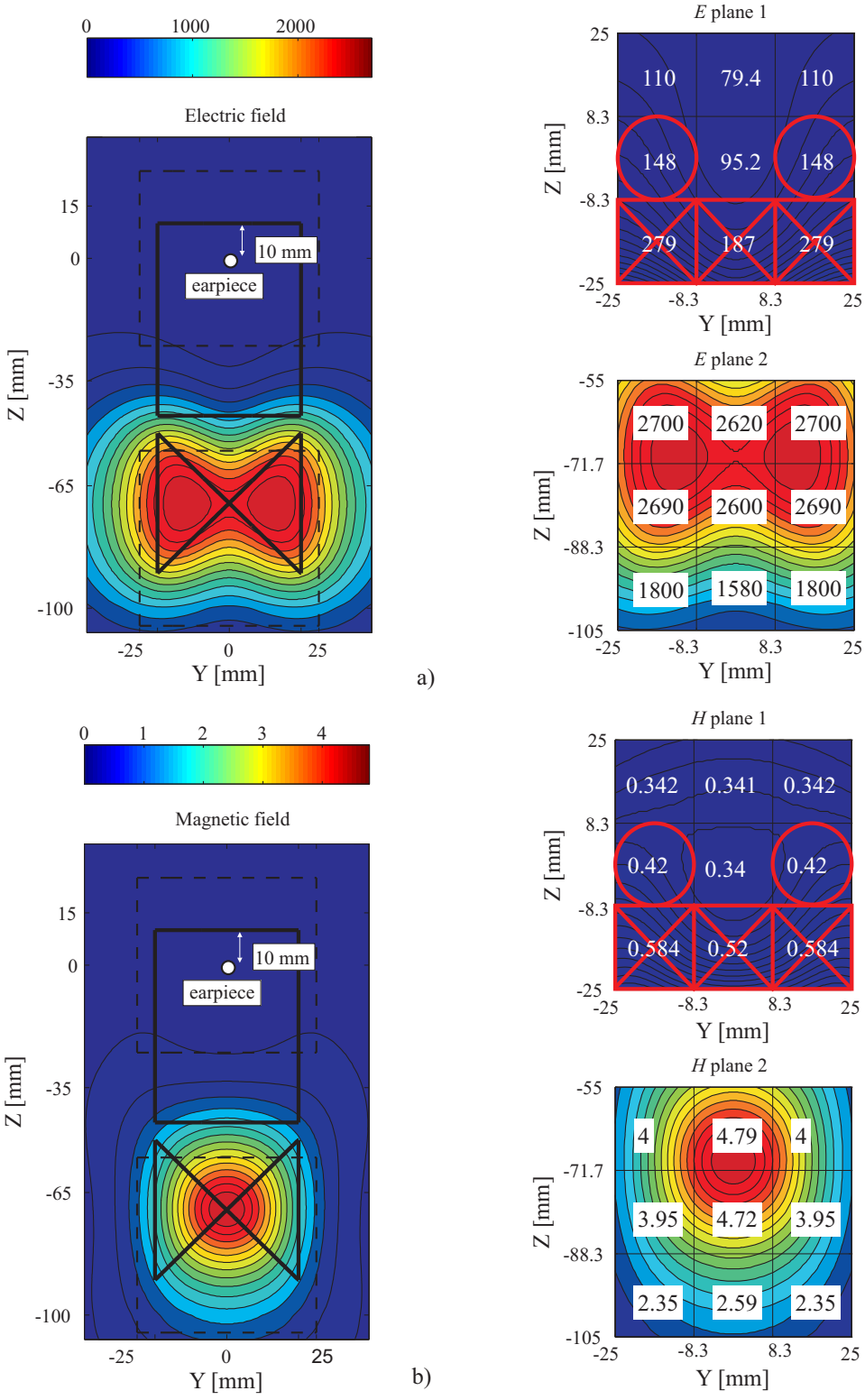

Figure C.6: a) Electric and b) magnetic fields on the HAC plane. The bow-tie case #1 at 836 MHz.

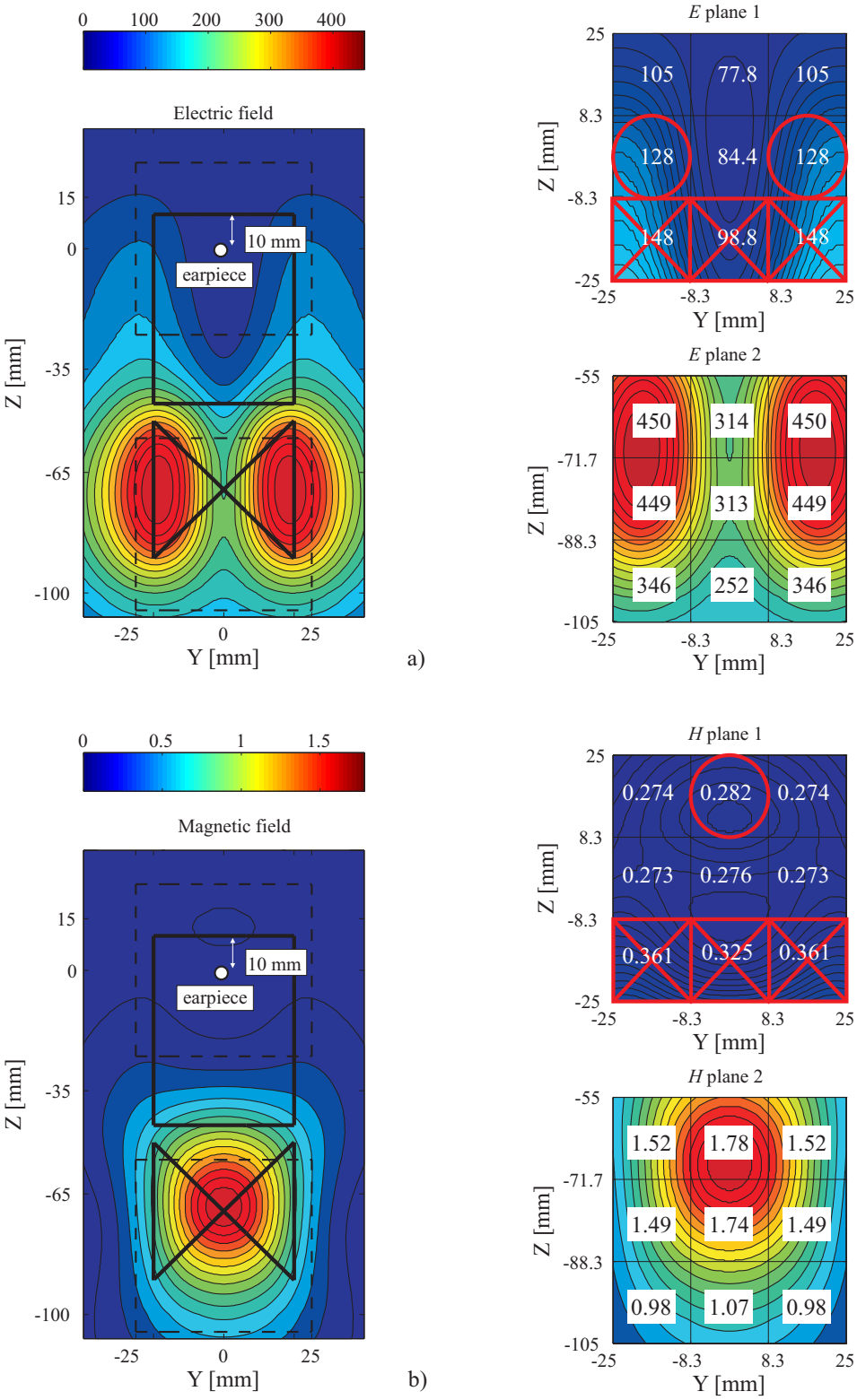

Figure C.7: a) Electric and b) magnetic fields on the HAC plane. The bow-tie case #1 at 1880 MHz.

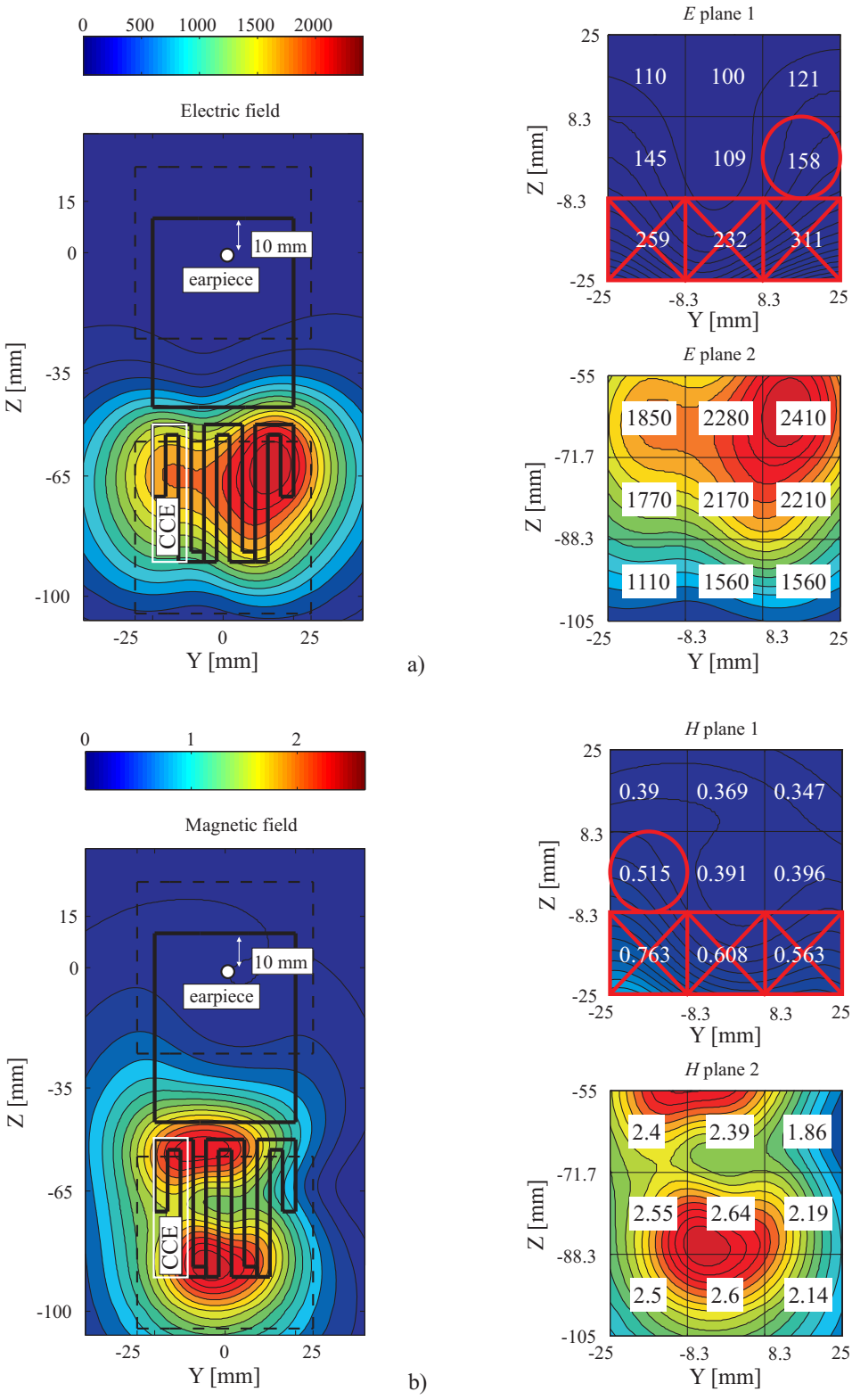

Figure C.8: a) Electric and b) magnetic fields on the HAC plane. The CCE with meandered ground plane side loaded at 836 MHz.

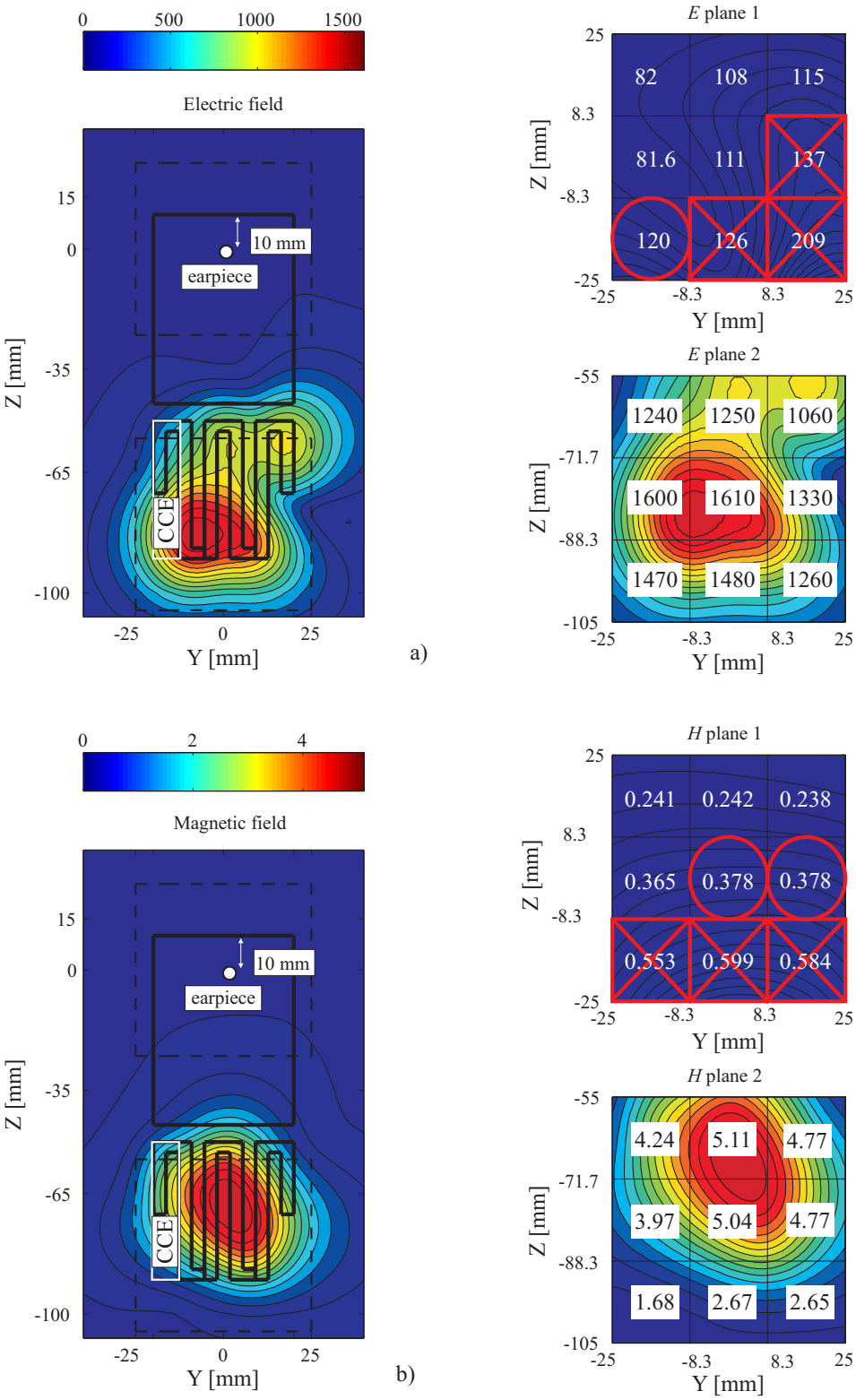

Figure C.9: a) Electric and b) magnetic fields on the HAC plane. The CCE with meandered ground plane side loaded at 1880 MHz.

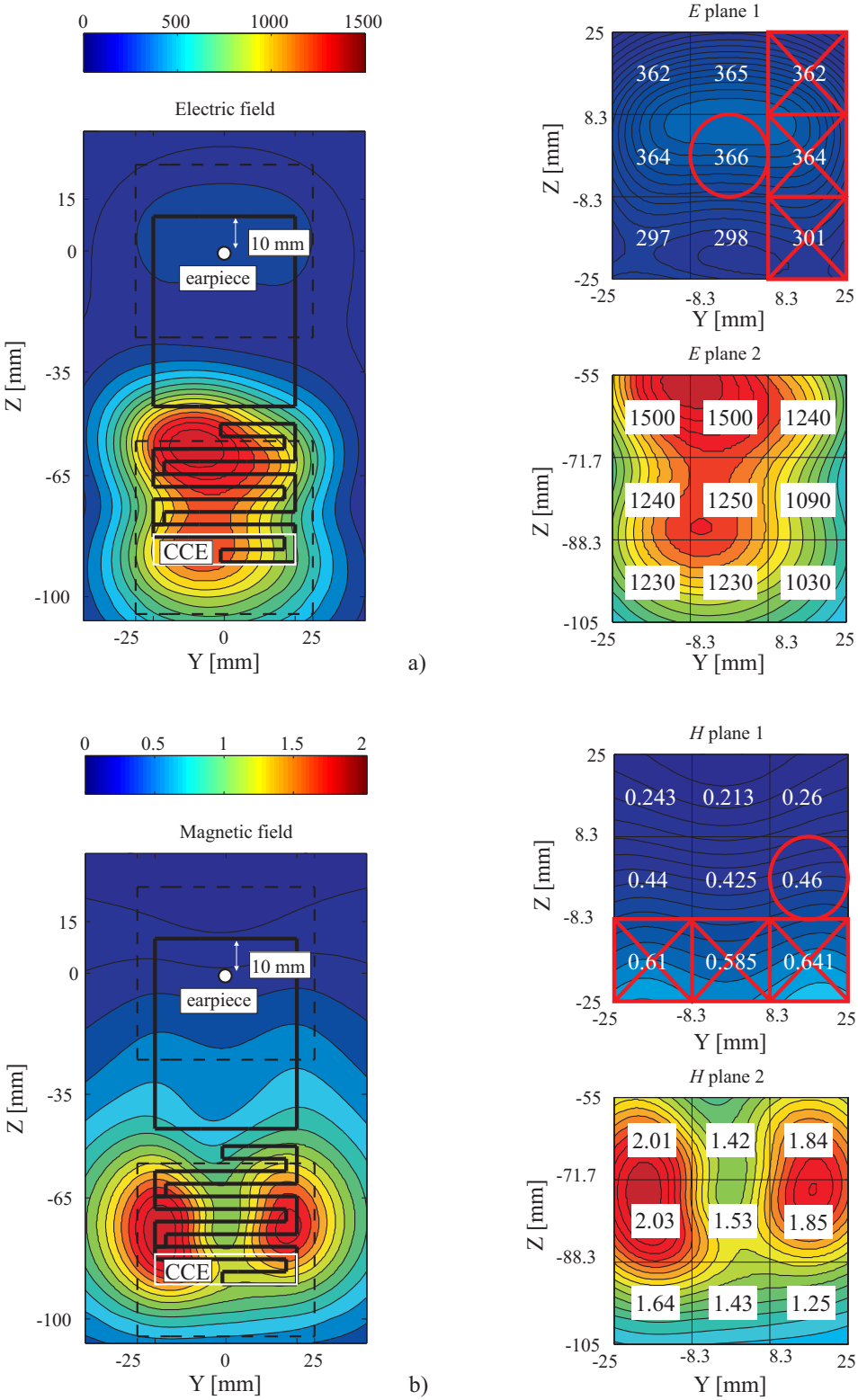

Figure C.10: a) Electric and b) magnetic fields on the HAC plane. The CCE with meandered ground plane top loaded at 836 MHz.

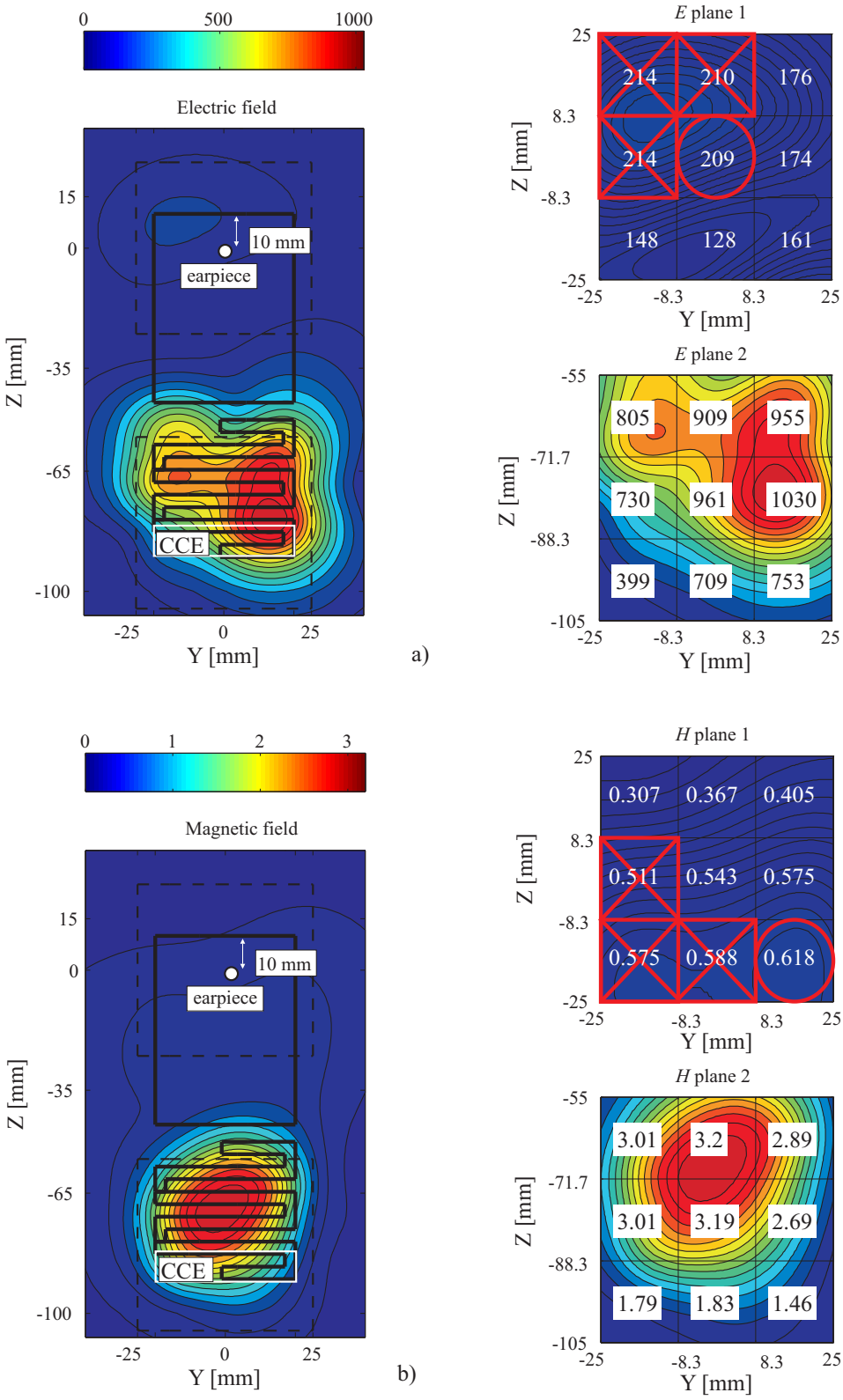

Figure C.11: a) Electric and b) magnetic fields on the HAC plane. The CCE with meandered ground plane top loaded at 1880 MHz.